THEORETICAL AND EXPERIMENTAL CHARACTERIZATION OF THE FIRST HYPERPOLARIZABILITY

By

Javier Pérez-Moreno

A dissertation submitted in partial fulfillment
of the requirements for the degree of

DOCTOR IN PHILOSOPHY

WASHINGTON STATE UNIVERSITY

Department of Physics and Astronomy

May 2007

To the Faculty of Washington State University:

The members of the Committee appointed to examine the dissertation of Javier Pérez-Moreno find it satisfactory and recommend that it be accepted.

_____

(Chair)

_____

_____

ACKNOWLEDGEMENT

First, I would like to acknowledge the unconditional support from my relatives. Thanks also to all the friends that have become my second family through the PhD years. I am very grateful to Maria Diaz for introducing me into the world of nonlinear optics. Thanks to the Department of Physics in Washington State University, faculty, peers and staff members. Thank you for making me feel part of a wonderful team.

Special thanks to my two promotors: Mark G. Kuzyk in Washington State Univesity and Koen Clays in KULeuven. Thank you for your immense patience, your unconditional help and all the excitement that you have brought into my life.

Thanks to the members of the Chemistry Department here in Leuven, specially to the Division of Molecular and Nanomaterials group, which have also made me feel part of a great team and - together with Jeff, Lupo and Sensei - have helped me to think of Leuven as my home.

During my years in Pullman, the Department of Physics and Astronomy provided primary financial support with partial funding through E.P.R.I., Wright Patterson Air Force and the Army Research Office.

Here in Leuven, the research in the Department of Chemistry was funded by Doctoral Scolarhsip for advanced EU doctoral students, profile BDB-B, from the Research Council of the Katholieke Universiteit Leuven.

Finally, I would like to thank the members of my defense Committee for all their dedication and patience.

THEORETICAL AND EXPERIMENTAL CHARACTERIZATION OF THE FIRST HYPERPOLARIZABILITY

Abstract

by Javier Pérez-Moreno
Washington State University
May 2007

Chair: Mark G. Kuzyk

We present a theoretical and experimental study of the molecular susceptibilities. The generalized Thomas-Kuhn sum rules are used to characterize the nonlinear response of organic chromophores in terms of fundamental parameters. The nonlinear optical performance of real molecules is evaluated from the calculation of the quantum limits and Hyper-Rayleigh scattering measurements. Different strategies for the enhancement of nonlinear behavior at the molecular and supramolecular level are evaluated and new paradigms for de design of more efficient nonlinear molecules are proposed.

Contents

List of Figures

List of Tables

Chapter 1

Preface

The field of nonlinear optics and nonlinear optical applications has become one of the fastest growing areas of research for the last four decades, impacting upon many other disciplines, such as medicine, signal processing, communications, computing, etc. Although the Kerr-effect was discovered in 1875, the birth of modern nonlinear optics should be associated to the first observation of second harmonic generation by *Franken et al.* in 1961, [1] soon after the invention of the laser in 1960. [2]

Although the first nonlinear optical effects were observed in crystalline structures, they were soon extended to organic materials and later to solid state heterostructures. In particular, the area of *organic* nonlinear optics has been extremely active in the past two decades.

Organic materials might be preferred for many reasons. First, the origin of the nonlinear optical response in organic system lies in the electronic polarizability of the electrons at the molecular level.[3] The intrinsically electronic nature of the response implies a very fast response for non resonant optical excitations, a great advantage for organic photonic devices over some of the inorganic analogues. Organic materials are also easier to produce, more versatile and potentially cheaper.

Yet, the biggest advantage of organic materials is the virtually infinite number of organic molecules that can be synthesized.[4, 5] The great versatility of organic synthesis means that a wealth of potential strategies for the optimiza-

tion of the nonlinear response are available. The number of medium size organic molecular structures is immense.[6, 4, 5] A recent study showed that the number of organic structures that could be considered as drug candidates is greater than Avogadro's number.[5] There is a strong need for a theoretical and experimental framework that provides clear guidance in the search for optimal structures.

The quantum limit analysis, originally used to show how the quantum sum rules impose limits on the first and second hyperpolarizabilities, [7, 8, 9, 10, 11], became the first step towards the development of such a theoretical and experimental framework. By establishing the existence of the quantum limits, it became possible to determine the performance of a molecular design motif. In this work, we present further results that extend the use of the quantum limits to provide a better understanding of the molecular nonlinear response.

Part of this work was originally presented in my Master's dissertation,[12] and was the result of my first years of doctoral program in Washington State University, becoming part of my Ph.D. research.

An overview of the theory of nonlinear optical response is presented in Chapters 2, 3 and 4. The theory of the nonlinear optical response is based on the work of *Butcher and Cotter* [13], and the qualitative approach reviews the treatment of *Boyd* [14], after *Owyoung* [15], while the calculations of the local field follows the description of *Kuzyk* [16]. The expressions for the molecular polarizations were first obtained by *Orr and Ward* [17], using quantum perturbation theory, and are used to express the molecular susceptibilities in terms of quantum mechanical quantities.

Hyper-Rayleigh scattering, the experimental technique that was used to characterize most of the molecular compounds included in this study, is presented in Chapter 5.

The generalized Thomas-Kuhn sum rules[18] are introduced in Chapter 6, in the same manner they were presented in my Master's dissertation.[12].

The dipole-free expressions for the first and second hyperpolarizability are introduced in Chapter 7. The dipole-free expression for the first hyperpolarizability was originally developed by Mark G. Kuzyk,[19] and here the dipole-free expression for the second hyperpolarizability is presented for the first time.

In Chapter 8 the off-resonance quantum limits for the first hyperpolarizability are derived, and the existence of a gap between the fundamental limit and measurements is studied. The results of this work were first published in [20], as well as the contents of Chapter 10 and 9 were two different hypothesis that could explain the existence of the quantum gap are analyzed. The results are presented in Chapters 11 and 12.

In Chapter 11 we present the results of a study of ionic chromphores, a material that has been published in the *Journal of Chemical Physics.*[22]

In Chapter 12 the quantum limits analysis are extended to study the third-order nonlinear response of organic molecules, using the same structure as in its publication format.[21]

In Chapter 16 we summarize and discuss our results, while some of the perspectives are presented in Chapter 14

Finally, for completeness, the results of our most recent publication are presented as an epilogue in Chapter 15.[23]

Bibliography

[1] P. A. Franken, A. E. Hill, C. W. Peters and G. Weinreich, Phys. Rev. Lett. **7**, 118 (1961).

[2] T. H. Maiman, Nature **187**, 493 (1960).

[3] D. S. Chemla and J. Zyss, Eds. "Nonlinear Optical Properties of Organic Molecules and Crystals." Vol 1. "Quantum electronics. Principles and Applications." (Y. -H. Pao, P. F. Liao, and P. Kelley, Eds.) Academic Press, Orlando, Fl, (1987).

[4] C. Lipinski and C. Hopkins, Nature **432**, 855, (2004).

[5] P. Ertl, J. Chem. Inf. Comput. Sci. **43**, 374 (2003).

[6] M. Wang, X. Hu, D. Beratan and W. Yang, J. Am. Chem. Soc. **128**, 3228 (2006).

[7] M. G. Kuzyk, Phys. Rev. Lett. **85**, 1218, (2000).

[8] M. G. Kuzyk, Opt. Lett. **25**, 1183, (2000).

[9] M. G. Kuzyk, Phys. Rev. Lett. **90**, 39902, (2003).

[10] M. G. Kuzyk, Opt. Lett. **28**, 135, (2003).

[11] M. G. Kuzyk, IEEE J. Select. Topics Quantum Electron. **7**, 774, (2001).

[12] J. Pérez-Moreno, "Quantum limits of the nonlinear optical response", *M.S. Thesis*, Washington State University, Department of Physics. August 2004.

[13] P. N. Butcher and D. Cotter, *The Elements of Nonlinear Optics*, Cambridge University Press, New York, (1990).

[14] R. W. Boyd, *Nonlinear Optics*, Academic Press, San Diego, (1992).

[15] A. Owyoung, *The Origins of nonlinear Refractive Indices of Liquids and Glasses*, Ph.D. dissertation, California Institute of Technology, (1971).

[16] *Characterization techniques and tabulations for organic nonlinear optical materials*, Edited by M. G. Kuzyk and C. W. Dirk, Marcel Dekker, Inc., (1998).

[17] B. J. Orr and J. F. Ward, Mol. Phys. **20**, 513 (1971).

[18] H. A. Bethe E. E. and Salpeter, *Quantum Mechanics of One and Two Electron Atoms*, Plenum, New York, (1997).

[19] M. G. Kuzyk, Phys. Rev. A **72**, 53819 (2005).

[20] K. Tripathy, J. Pérez-Moreno, M. G. Kuzyk, B. Coe, K. Clays and A. M. Kelley, J. Chem. Phys. **121**, 7932 (2004).

[21] J. Pérez-Moreno and M. G. Kuzyk, J Chem Phys. **123**, 194101 (2005).

[22] J. Pérez-Moreno et al. J. Chem. Phys. **126**, 74705 (2007).

[23] J. Pérez-Moreno, Y. Zhao, K. Clays and M. G. Kuzyk, Opt. Lett. **32**, 59 (2007).

Chapter 2

Introduction

The field of Optics studies the interaction between matter and light, and investigates how the optical properties of a material change and how the changes can be quantified and manipulated. Nonlinear Optics is the branch of Optics that focuses on the regime where the response of the material is nonlinearly related to the electric field.

In this chapter we present an overview of the principles of nonlinear optics, setting up the notations and conventions that will be used throughout the rest of this dissertation.

The harmonic and anharmonic oscillator analogies are also introduced. The original calculations for the nonlinear susceptibility on a classical anharmonic oscillator were derived by *Boyd* [1], after *Owyoung* [2].

2.1 The linear regime

In the absence of external fields, the electromagnetic forces between the positive and the negative charges inside of the material are usually in equilibrium, and the material is electrically neutral. However, when a beam of light is applied to the material, the electromagnetic forces inside the material are perturbed. In reaction to the external electric field, the charge distribution in the material changes and the material gets polarized. The polarization of the material is the

macroscopic manifestation of electric dipoles induced at the microscopic level.

In the optical linear regime, the polarization of the medium ($\vec{P}$) defined as *the electric dipole moment per unit of volume* is directly proportional to the applied electric field ($\vec{E}$):

$$\vec{P} = \chi \vec{E}, \tag{2.1}$$

with χ being a constant of proportionality called the electric susceptibility of the material. The electric susceptibility is a property of the material that measures how the polarization is changed in response to an electric field.

The harmonic oscillator analogy

J. D. Jackson describes two different ways in which the polarization of a collection of molecules or atoms can change:[3]

- The charge distribution is distorted by the applied field.
- The initially randomly oriented permanent dipole moment of the molecules are aligned in response to the field.

The harmonic oscillator analogy provides some insight on how the polarization is induced by the external electric field. We assume that the electrons are bound to the positive sites through a harmonic restoring force. When displaced from the equilibrium position, the electron feels a force that is proportional to the displacement x:

$$F_{harmonic} = -kx, \tag{2.2}$$

where k is a positive constant.

When an electric field is applied, the electron feels a force that is proportional to the field:

$$F_{electric} = -eE, \tag{2.3}$$

where $-e$ is the electron charge and E is the magnitude of the electric field.

The new equilibrium is reached when the sum of the two forces is zero:

$$-eE - kx = 0. \tag{2.4}$$

The resulting induced dipole moment is then proportional to the electric field:

$$p = ex = \frac{e^2 E}{k} \equiv \alpha E, \tag{2.5}$$

where p is the magnitude of the induce dipole moment. The linear polarizability of the harmonic oscillator is given by:

$$\alpha = \frac{e^2}{k}. \tag{2.6}$$

Since e^2 is a constant, in this simple model, as the force constant increases (stronger binding force) the linear polarizability decreases. This is in agreement with our intuition. When the binding force is increased the electron is less influenced by the external field.

2.2 The nonlinear regime

As the applied becomes intense, reaching values of the order of $10^8 V/m$ the nonlinearities become measurable and the domain of nonlinear optics is entered[1]. No direct proportionality exists between the polarization of the medium and the electric field. Instead, the polarization of the medium is expanded as a series in the electric field $\vec{E}$:

$$\vec{P} = \chi^{(1)}\vec{E} + \chi^{(2)}(\vec{E})^2 + \chi^{(3)}(\vec{E})^3 + \chi^{(4)}(\vec{E})^4 + \cdots \tag{2.7}$$

Eq. (2.7) is a short hand to express the dependence of $\vec{P}$ in different powers of $\vec{E}$. More rigorously, the *ith* component of $\vec{P}$ is related with the components of the electric field through:

$$P_i = \sum_j \chi^{(1)}_{ij} E_j + \sum_{jk} \chi^{(2)}_{ijk} E_j E_k + \sum_{jkl} \chi^{(3)}_{ijkl} E_j E_k E_l + \cdots \tag{2.8}$$

The *nth* term of the expansion is proportional to the *nth* power of the electric field $\vec{E}$, and for the expansion to converge, each successive term must be smaller than the previous one, so $\vec{E}$ must be smaller than the internal atomic and molecular fields, which are typically on the order of $10^{11} V/m$. That is why usually the linear effects dominate the optical response at low light intensities.

[1]For comparison, the intensity of sunlight hitting the earth surface is of the order of $10^2 V/m$.

2.2.1 The anharmonic oscillator analogy

While a weak oscillating electric field is applied, the electrons are slightly perturbed from equilibrium and the restoring force is linear in the electronic displacement. This is because in most cases the real restoring force can be approximated by a harmonic oscillator for a sufficiently small domain around the equilibrium position.

However, as the intensity of the optical applied electric field increases, the higher order terms in the restoring force become more relevant, and the motion of the electron is no longer directly proportional to the field. When this happens, the system shows a nonlinear response and higher terms must be included in order to properly describe the polarization of the material.

This can be illustrated by including the next term in the Taylor expansion for the restoring force:

$$F_{harmonic} = -kx - k'x^2 \equiv -m\omega_0^2 x - mbx^2, , \tag{2.9}$$

where k' (b) is a constant that characterizes the strength of the anharmonic contribution to the restoring force and m is the mass of the electron. We allow for a damping force that is proportional to the speed of the electron, v:

$$F_{damping} = 2m\gamma v, \tag{2.10}$$

where γ is the damping coefficient.

The equation of motion is now expressed as:

$$\frac{d^2x}{dt^2} + 2\gamma\frac{dx}{dt}\omega_0^2 x + bx^2 = -e\frac{E}{m}. \tag{2.11}$$

If we assume that the electric field is oscillates at frequency ω_1,

$$E(t) = E_1(e^{-i\omega_1 t} + e^{i\omega_1 t}), \tag{2.12}$$

we can solve for x using perturbation theory:

$$x = x^{(1)} + x^{(2)} + x^{(3)} + \cdots, \tag{2.13}$$

where $x^{(1)}$ proportional to the small parameter $(\frac{e}{m}E)$, $x^{(2)}$ is quadratically dependent on $(\frac{e}{m}E)$, and so on.

The first term in the expansion of x (Eq. 2.13) is the linear solution:

$$x^{(1)} = \frac{(e/m)E}{\omega_0^2 - \omega_1^2 - i\omega_1\gamma}(e^{-i\omega_1 t} + e^{+i\omega_1 t}). \tag{2.14}$$

However, the next terms in the expansion of x are quadratically in the electric field and therefore oscillates at frequency $(2\omega_1)$ or (0):

$$x^{(2)}(\omega \pm \omega) = \frac{-2b(e/m)^2 E^2}{(\omega_0^2 - \omega_1^2 - i\omega_1\gamma)(\omega_0^2 - \omega_1^2 \pm i\omega_1\gamma)} e^{-i(\omega_1 \pm \omega_1)t}. \tag{2.15}$$

Clearly, the introduction of an anharmonic term in the restoring force has generated a nonlinear dependence on the electric field for the position of the electron. The second-order nonlinear polarizability of this model is given by:

$$\beta(\omega_1 \pm \omega_1) = \frac{-2b(e/m)^2 e}{(\omega_0^2 - \omega_1^2 - i\omega_1\gamma)(\omega_0^2 - \omega_1^2 \pm i\omega_1\gamma)}. \tag{2.16}$$

2.3 Description of the nonlinear optical response

In general the polarization is a function of time, t, and the spatial coordinates, $\vec{r}$:

$$\vec{P} = \vec{P}(\vec{r}, t). \tag{2.17}$$

However, we will adopt the "electric dipole approximation", by assuming that the wavelength of the applied light beam is much larger than the dimensions of the molecules responsible for the nonlinear optical response. At any given time, the electric field is uniform through the entire molecule and we can neglect the spatial dependence of the polarization: $\vec{P}(t, \vec{r}) = \vec{P}(t)$.

It is convenient to express the polarization as a sum over ascending orders:

$$\vec{P}(t) = \vec{P}^{(0)}(t) + \vec{P}^{(1)}(t) + \vec{P}^{(2)}(t) + \cdots + \vec{P}^{(n)}(t) + \cdots \tag{2.18}$$

where $\vec{P}^{(0)}(t)$ is the static polarization independent of the external electric field $\vec{E}(t)$, $\vec{P}^{(1)}(t)$ is linear in $\vec{E}(t)$, $\vec{P}^{(2)}(t)$ is quadratic in $\vec{E}(t)$, $\vec{P}^{(3)}(t)$ is cubic in

$\vec{E}(t)$, and so on.

2.3.1 The frequency domain

Until now we have been considering quantities in the time domain. However, in practice it is common to express the nonlinear quantities in the frequency domain.

The time-dependent electric field of the applied beam of light $\vec{E}(t)$ can be Fourier decomposed into different frequency contributions:

$$\vec{E}(t) = \int_{-\infty}^{\infty} d\omega \vec{E}(\omega) \exp(-i\omega t) \Longleftrightarrow \vec{E}(\omega) = \frac{1}{2\pi} \int_{-\infty}^{\infty} dt \vec{E}(t) \exp(i\omega t). \quad (2.19)$$

In the same manner, the Fourier Transform relates the polarization in the time domain, $\vec{P}(t)$, with the polarization in the frequency domain, $\vec{P}(\omega)$:

$$\vec{P}(t) = \int_{-\infty}^{\infty} d\omega \vec{P}(\omega) \exp(-i\omega t) \Longleftrightarrow \vec{P}(\omega) = \frac{1}{2\pi} \int_{-\infty}^{\infty} dt \vec{P}(t) \exp(i\omega t), \quad (2.20)$$

or, using the sum over ascending expansion of the polarization (Eq. 2.18), the *ith* component of the *nth* order polarization $\vec{P}^{(n)}(t)$ can be written in terms of its Fourier counterparts:

$$P_i^{(n)}(t) = \int_{-\infty}^{\infty} d\omega P_i^{(n)}(\omega) \exp(-i\omega t) \Longleftrightarrow P_i^{(n)}(\omega) = \frac{1}{2\pi} \int_{-\infty}^{\infty} dt P_i^{(n)}(t) \exp(i\omega t). \quad (2.21)$$

When the applied and radiated light is monochromatic, the electric field can be expressed as the discrete superposition of different frequencies, ω_k,

$$\vec{E}(t) = \frac{1}{2} \sum_{\omega_k \geq 0} \left[\vec{E}^{\omega_k} e^{-i\omega_k t} + \vec{E}^{-\omega_k} e^{+i\omega_k t} \right] \quad (2.22)$$

where $\vec{E}^{\omega_k}$ is the amplitude of the electric field oscillating at frequency ω_k and the sum is only over the positive frequency components. Also, since the fields

are real, $(\vec{E}^{\omega_k})^* = \vec{E}^{-\omega_k}$.

If the electric field contains only discrete frequencies, the induced polarization will also be the sum of discrete frequencies:

$$\vec{P}^{(n)}(t) = \frac{1}{2} \sum_{\omega_k \geq 0} \left[\vec{P}^{(n)^{\omega_k}} e^{-i\omega_k t} + \vec{P}^{(n)^{-\omega_k}} e^{+i\omega_k t} \right], \tag{2.23}$$

with $(\vec{P}^{(n)^{\omega_k}})^* = \vec{P}^{(n)^{-\omega_k}}$.

Working in the frequency domain is very convenient because the relationship between the electric fields and the induced polarization takes a simple form:

$$P_i^{(n)^{\omega_\sigma}} = K(\omega_\sigma; \omega_1, \omega_2, \cdots, \omega_n) \sum_{\alpha_1, \cdots, \alpha_n} \chi^{(n)}_{i\alpha_1 \cdots \alpha_n}(-\omega_\sigma; \omega_1, \cdots, \omega_n) E_{\alpha_1}^{\omega_1} \cdots E_{\alpha_n}^{\omega_n}, \tag{2.24}$$

where $\chi^{(n)}_{i\alpha_1 \cdots \alpha_n}(-\omega_\sigma; \omega_1, \cdots, \omega_n)$ are the tensorial components of the *nth*-order electric susceptibility and $K(\omega_\sigma; \omega_1, \omega_2, \cdots, \omega_n)$ is a numerical factor that is determined by the $\frac{1}{2}$ factors of the Fourier expansions (Eqs. 2.22 and 2.23) and the multinomial expansion coeffiecients. Notice that in contrast with Eqs. 2.22 and 2.23 in Eq. 2.24, $\omega_1, \omega_2, \cdots, \omega_n$ can be either positive, negative or zero, representing incident and outgoing fields, respectively.

The *nth*-order electric susceptibility is a property of the optical material that tells us how *"easily"* the material gets polarized in response to the fields.

The following general relationships hold for all the electric susceptibilities:

1. $$\chi^{(n)}_{i\alpha_1 \cdots \alpha_n}(-\omega_\sigma; \omega_1, \cdots, \omega_n) = \chi^{(n)}_{i\alpha_1 \cdots \alpha_n}(\omega_\sigma; -\omega_1, \cdots, -\omega_n). \tag{2.25}$$

   This is a consequence of the reality of the fields.

2. $$\chi^{(n)}_{i\alpha_1 \cdots \alpha_n}(-\omega_\sigma; \omega_1, \cdots, \omega_n) = 0, \textbf{ unless } \omega_\sigma = \omega_1 + \omega_2 + \cdots + \omega_n. \tag{2.26}$$

   This is a consequence of energy conservation.

3.

$$\chi^{(n)}_{i\alpha_1\cdots\mathbf{j}\cdots\mathbf{k}\cdots\alpha_n}(-\omega_\sigma;\omega_1,\cdots,\omega_\mathbf{j},\cdots,\omega_\mathbf{k},\cdots\omega_n) = \chi^{(n)}_{i\alpha_1\cdots\mathbf{k}\cdots\mathbf{j}\cdots\alpha_n}(-\omega_\sigma;\omega_1,\cdots,\omega_\mathbf{k},\cdots,\omega_\mathbf{j},\cdots\omega_n). \tag{2.27}$$

(Any two indices can be permuted as long as the associated frequencies are also permuted.)

This is known as intrinsic permutation symmetry.

The numerical coefficients $K(\omega_\sigma;\omega_1,\omega_2,\cdots,\omega_n)$ depend on the presence of zero frequencies and repeated frequencies in the following manner (as defined in [4]):

$$K(\omega_\sigma;\omega_1,\omega_2,\cdots,\omega_n) = \frac{D}{2^{q-p}}\,, \tag{2.28}$$

where

- q is the number on non-zero input frequencies in the set $(\omega_1,\omega_2,\cdots,\omega_n)$.
- p is equal to 0 when $\omega_\sigma = 0$ and 1 otherwise.
- D is the number of different distinguishable orderings in the input frequencies $(\omega_1,\omega_2,\cdots,\omega_n)$.

Bibliography

[1] R. W. Boyd, *Nonlinear Optics*, Academic Press, San Diego, (1992).

[2] A. Owyoung, *The Origins of nonlinear Refractive Indices of Liquids and Glasses*, Ph.D. dissertation, California Institute of Technology, (1971).

[3] J. D. Jackson, *Classical Electrodynamics*, **3rd Edition**, John Wiley & Sons Canada, Ltd, (1998).

[4] B. J. Orr and J. F. Ward, Mol. Phys. **20**, 513 (1971).

Chapter 3

The molecular susceptibilities

The electric susceptibility tensors relate the applied electric fields to the polarization of the material, as it was expressed in Eq. 2.24:

$$P_i^{(n)^{\omega_\sigma}} = K(\omega_\sigma;\omega_1,\omega_2,\cdots,\omega_n)\sum_{\alpha_1,\cdots,\alpha_n}\chi^{(n)}_{i\alpha_1\cdots\alpha_n}(-\omega_\sigma;\omega_1,\cdots,\omega_n)E^{\omega_1}_{\alpha_1}\cdots E^{\omega_n}_{\alpha_n}. \tag{3.1}$$

Substituting Eq. 2.24 into the frequency domain version of Eq. 2.18, the general expression for the *ith* component of the polarization as a function of the electric fields is obtained:

$$\begin{aligned} P_i^{\omega_\sigma} &= \delta_{\omega_\sigma,0}P_i + \sum_j K(-\omega_\sigma;\omega)\chi^{(1)}_{ij}(-\omega_\sigma;\omega)E^{\omega}_j \\ &+ \sum_{jk} K(-\omega_\sigma;\omega_1,\omega_2)\chi^{(2)}_{ijk}(-\omega_\sigma;\omega_1,\omega_2)E^{\omega_1}_j E^{\omega_2}_k \\ &+ \sum_{jkl} K(-\omega_\sigma;\omega_1,\omega_2,\omega_3)\chi^{(3)}_{ijkl}(-\omega_\sigma;\omega_1,\omega_2,\omega_3)E^{\omega_1}_j E^{\omega_2}_k E^{\omega_3}_l\cdots \end{aligned} \tag{3.2}$$

where the material is allowed to have permanent polarization P_i that is independent of the applied electric fields and $\delta_{\omega_\sigma,0}$ is the kronecker delta.

The electric susceptibility is a property of the material and is a macroscopic manifestation of its electromagnetic structure. For example, if a material is centrosymmetric even-order nonlinear response is not allowed as we shall now

illustrate.

A system is centrosymmetric when its radiating charges have a symmetrical arrangement around a central point. In other words, a system is centrosymmetric when a system of cartesian coordinates can be found such as that the distribution of the charges is left invariant under the transformation $(x, y, z) \to (-x, -y, -z)$.

If the system is centrosymmetric we could apply electric fields in the directions $\hat{x}, \hat{y}, \cdots, \hat{z}$, indexed by $j, k, \cdots, l$ and measure the resultant polarization in the $\hat{w}$ direction, with index i:

$$P_i^{(n)}(\omega_\sigma) = \sum \chi_{ijk\cdots l}^{(n)} E_j^{\omega_1} E_k^{\omega_2} \cdots E_l^{\omega_n}. \tag{3.3}$$

On the other hand, we could also apply the same electric fields in the opposite directions $(-\hat{x}, -\hat{y}, -\cdots, -\hat{z})$ and since the material is centrosymmetric we should observe a polarization in the $-\hat{w}$ direction that has the same magnitude as $P_i^{(n)}$:

$$\begin{aligned} -P_i^{(n)}(\omega_\sigma) &= \sum \chi_{ijk\cdots l}^{(n)} (-E_j^{\omega_1})(-E_k^{\omega_2}) \cdots (-E_l^{\omega_n}) \\ &= \sum \chi_{ijk\cdots l}^{(n)} (-1)^n E_j^{\omega_1} E_k^{\omega_2} \cdots E_l^{\omega_n} \\ &= (-1)^n P_i^{(n)}. \end{aligned} \tag{3.4}$$

When n is even:

$$-P_i^{(n)}(\omega_\sigma) = P_i^{(n)}(\omega_\sigma) \Longrightarrow P_i^{(n)}(\omega_\sigma) = 0, \tag{3.5}$$

which proves that no even-order polarization can be observed in a centrosymmetric system.

As previously discussed, for the expansion of the induced polarization in terms of the electric fields to converge (Eq. 2.18), each successive term must be smaller than the previous one. In practice, this means that most of the nonlinear optical phenomena that is observed is either a second- or a third-order process. Thus, materials with high values of $\chi_{ijk}^{(2)}$ and $\chi_{ijkl}^{(3)}$ are needed in order to explore the nonlinear regime and realize nonlinear optical technology.

As an example, we could consider the problem of producing a frequency doubling system. The system would take an input beam at frequency ω and

radiate an output beam at frequency 2ω. This can be achieved through a second-order nonlinear optical material such as:

$$P_x^{2\omega} = K(-2\omega;\omega,\omega)\chi^{(2)}_{xxx}(-2\omega;\omega,\omega)\left(E_x^{\omega}\right)^2 = \frac{1}{2}\chi^{(2)}_{xxx}(-2\omega;\omega,\omega)\left(E_x^{\omega}\right)^2, \quad (3.6)$$

where we have arbitrarily chosen all the fields to be in the $\hat{x}$ direction. The time-varying induced polarization oscillating at frequency 2ω would radiate an electromagnetic field oscillating at 2ω.

In order to increase the output power of the device, we could either increase the intensity of the input beam or find a material with a high $\chi^{(2)}_{xxx}(-2\omega;\omega,\omega)$ value. The most efficient choice would be to find the best material, so less input energy is required to produce the same output.

Consequently, great efforts have been put applied towards the realization of materials with high nonlinear electric susceptibilities. Since we want to investigate the nonlinear response at the molecular level, we need to introduce the molecular equivalent of the bulk electric susceptibilities.

3.1 Molecular susceptibilities

In the same manner as the macroscopic polarization was expressed in terms of the components of the electric field (Eq. 3.2), we wish now to expand the induced dipole of a molecule $\vec{p}$. However, at the molecular level, the applied electric field $\vec{E}$ is modified by the presence of dielectric material around the molecule. Therefore, the ith component of the induced dipole of the molecule, p_i is expanded in terms of the local field, $\vec{f}$, which is the actual electric field that acts on the molecule resulting from the combination of the external electric field and the electric field generated by the environment.

The local field and the induced dipole of the molecule are related through the microscopic molecular susceptibilities,

$$\begin{aligned} p_i^{\omega_\sigma} &= \delta_{\omega_\sigma,0}\mu_i + \sum_j K(-\omega_\sigma;\omega)\alpha_{ij}(-\omega_\sigma;\omega)f_j^{\omega} \\ &+ \sum_{jk} K(-\omega_\sigma;\omega_1,\omega_2)\beta_{ijk}(-\omega_\sigma;\omega_1,\omega_2)f_j^{\omega_1}f_k^{\omega_2} \end{aligned} \quad (3.7)$$

$$+ \quad \sum_{jkl} K(-\omega_\sigma;\omega_1,\omega_2,\omega_3)\gamma_{ijkl}(-\omega_\sigma;\omega_1,\omega_2,\omega_3)f_j^{\omega_1}f_k^{\omega_2}f_l^{\omega_3}\cdots$$

where again we have allowed for the possibility of the molecule having a permanent dipole moment $\vec{\mu}$ that does not depend on the local fields, $\alpha_{ij}(-\omega_\sigma;\omega)$ is the molecular linear polarizability, $\beta_{ijk}(-\omega_\sigma;\omega_1,\omega_2)$ is the molecular second order susceptibility, and $\gamma_{ijkl}(-\omega_\sigma;\omega_1,\omega_2,\omega_3)$ is the molecular third order susceptibility and so on.

The molecular second order susceptibility is also known as the *first hyperpolarizability* while the molecular third order susceptibility is also denominated as the *second hyperpolarizability*. In the same manner as the electric susceptibilities are a property of the material, the first and second hyperpolarizabilities are properties of the molecule, which depends on its structure.

Bibliography

[1] R. W. Boyd, *Nonlinear Optics*, Academic Press, San Diego, (1992).

[2] *Characterization techniques and tabulations for organic nonlinear optical materials*, Edited by M. G. Kuzyk and C. W. Dirk, Marcel Dekker, Inc., (1998).

[3] B. J. Orr and J. F. Ward, Mol. Phys. **20**, 513 (1971).

Chapter 4

Quantum mechanical expressions for the molecular susceptibilities

In this chapter, the quantum mechanical expressions for the molecular susceptibilities as derived from time-dependent quantum perturbation theory by Orr and Ward are introduced.[1] The expressions apply to effects produced by changes in the electronic configuration of the nonlinear system. The picture will be completed later in Chapter 10 where the effects of vibrational contributions are considered.

The expressions for the vacuum molecular susceptibilities are derived under the electric dipole approximation (See section 2.1) and it is based in the Bogoliubov and Mitroplsky [2] method of averages. It assumes that the state wave function of the molecule interacting with light has a slowly varying component and a rapidly varying component and its initially in the ground state. When the molecule is perturbed by the oscillating electric field, its wave function changes from the ground state to a superposition of ground and excited states. The new wave function is calculated as a function of the unperturbed wave functions assuming that the ground state component changes slowly in time in comparison with the rate of change of the excited states components.

4.1 Description of the problem

If $H(t)$ denotes the time-dependent Hamiltonian of the system, the time-dependent Schrödinger equation for the state vector of the molecule, $|\Psi(t)\rangle$, is given by:

$$i\hbar\frac{\partial}{\partial t}|\Psi(t)\rangle = H(t)|\Psi(t)\rangle. \tag{4.1}$$

It is assumed that the solutions of the unperturbed hamiltonian of the molecule, $H(0)$ are known:

$$H(0)|n\rangle = \hbar\Omega_n|n\rangle, \tag{4.2}$$

where spontaneous decay is introduced in a non rigorous standard way by defining:

$$\Omega_n = \omega_n - i\Gamma_n/2, \tag{4.3}$$

where ω_n and Γ_n are real, $\hbar\omega_n = E_n$ and Γ_n is the inverse radiative lifetime of the state $|n\rangle$.

At an initial time, $t = 0$, the molecule is in the unperturbed state, and after that, the local field interacts with the molecule. The time-dependent Hamiltonian of the molecule can be expressed as:

$$H(t) = H(0) + \epsilon H'(t), \tag{4.4}$$

where $\epsilon H'(t)$ is the explicitly time-dependent Hamiltonian associated with the perturbing local electric field.

The expressions for the molecular polarization obtained through this method are accurate for any applied field frequencies and also work in the presence of resonances as long as excited-state populations remain insignificant in comparison with the ground-state population. Mathematically, this condition is expressed as:

$$\frac{2\langle\epsilon\bar{H}'\rangle_{nm}}{\hbar\Gamma_n} \ll 1, \tag{4.5}$$

if neither n or m are equal to the ground state.

In this notation, $\langle A\rangle_{ij}$ denotes the matrix element $\langle i|A|j\rangle$ of the quantum operator A and the barred operator is defined as:

$$\bar{A} = A - \langle A\rangle_{gg}. \tag{4.6}$$

Within the electric dipole approximation and using semiclassical radiation theory,[3] the time-dependent Hamiltonian is given by:

$$\epsilon H'(t) = -\vec{\mu}.\vec{f}(t) = e\vec{f}(t).\vec{r}, \tag{4.7}$$

where $\vec{f}(t)$ is the perturbing local field, and the dipole moment operator is given by:

$$\vec{\mu} = -e\vec{r}, \tag{4.8}$$

where $-e$ is the charge of an electron, and $\vec{r}$ is the electronic position operator. For a molecule with N-electrons that contribute to the molecular polarization the position operator is defined as:

$$\vec{r} \equiv \vec{r}^{\,1} + \vec{r}^{\,2} + \cdots + \vec{r}^{\,N}, \tag{4.9}$$

where $\vec{r}^{\,i}$ is the position operator of the i^{th} electron.

4.2 Expressions for the molecular susceptibilities in the frequency domain

Again, we focus on the action of monochromatic fields and summarize the expressions for the molecular susceptibilities in the frequency domain:[1, 4, 5]

- The linear molecular electric susceptibility is a second-rank tensor with components:

$$\alpha_{ij}(-\omega;\omega) = (\hbar)^{-1}e^2{\sum_n}' \left\{ \frac{\langle r_i\rangle_{gn}\langle r_j\rangle_{ng}}{(\Omega_{ng}-\omega)} + \frac{\langle r_j\rangle_{gn}\langle r_i\rangle_{ng}}{(\Omega^*_{ng}+\omega)} \right\}. \tag{4.10}$$

- The first hyperpolarizability is a third-order rank tensor with components:

$$\begin{aligned}
&\beta_{ijk}(-\omega_\sigma;\omega_1,\omega_2) = \\
&-(\hbar)^{-2}e^3 I_{1,2}{\sum_{m,n}}' \left\{ \frac{\langle r_i\rangle_{gm}\langle \bar{r}_k\rangle_{mn}\langle r_j\rangle_{ng}}{(\Omega_{mg}-\omega_\sigma)(\Omega_{ng}-\omega_1)} + \right. \\
&\left. + \frac{\langle r_k\rangle_{gm}\langle \bar{r}_j\rangle_{mn}\langle r_i\rangle_{ng}}{(\Omega^*_{mg}+\omega_2)(\Omega^*_{ng}-\omega_\sigma)} + \frac{\langle r_k\rangle_{gm}\langle \bar{r}_i\rangle_{mn}\langle r_j\rangle_{ng}}{(\Omega^*_{mg}+\omega_2)(\Omega_{ng}-\omega_1)} \right\},
\end{aligned} \tag{4.11}$$

  where $I_{1,2}$ indicates that the average over all terms generated by pairwise permutations of (i,ω_1) and (j,ω_2) should be taken on the expression. Intrinsic permutation symmetry is insured by the presence of the operator

$I_{1,2}$.

- The second hyperpolarizability is a fourth-order rank tensor with components:

$$
\begin{aligned}
&\gamma_{ijkl}(-\omega_\sigma;\omega_1,\omega_2,\omega_3) = (\hbar)^{-3}e^4 I_{1,2,3} \\
&\times\Bigg[\sum_{lmn}{}'\Bigg\{\frac{\langle r_i\rangle_{gl}\langle\bar{r}_l\rangle_{lm}\langle\bar{r}_k\rangle_{mn}\langle r_j\rangle_{ng}}{(\Omega_{lg}-\omega_\sigma)(\Omega_{mg}-\omega_1-\omega_2)(\Omega_{ng}-\omega_1)}+ \\
&+\frac{\langle r_l\rangle_{gl}\langle\bar{r}_i\rangle_{lm}\langle\bar{r}_k\rangle_{mn}\langle r_j\rangle_{ng}}{(\Omega^*_{lg}+\omega_3)(\Omega_{mg}-\omega_1-\omega_2)(\Omega_{ng}-\omega_1)}+ \\
&+\frac{\langle r_j\rangle_{gl}\langle\bar{r}_k\rangle_{lm}\langle\bar{r}_i\rangle_{mn}\langle r_l\rangle_{ng}}{(\Omega^*_{lg}+\omega_1)(\Omega^*_{mg}+\omega_1+\omega_2)(\Omega_{ng}-\omega_3)}+ \\
&+\frac{\langle r_j\rangle_{gl}\langle\bar{r}_k\rangle_{lm}\langle\bar{r}_l\rangle_{mn}\langle r_i\rangle_{ng}}{(\Omega^*_{lg}+\omega_1)(\Omega^*_{mg}+\omega_1+\omega_2)(\Omega^*_{ng}+\omega_\sigma)}\Bigg\}+ \\
&-\sum_{mn}{}'\Bigg\{\frac{\langle r_i\rangle_{gm}\langle r_l\rangle_{mg}\langle r_k\rangle_{gn}\langle r_j\rangle_{ng}}{(\Omega_{mg}-\omega_\sigma)(\Omega_{mg}-\omega_3)(\Omega_{ng}-\omega_1)}+ \\
&+\frac{\langle r_i\rangle_{gm}\langle r_l\rangle_{mg}\langle r^{\omega_j}\rangle_{gn}\langle r_j\rangle_{ng}}{(\Omega_{mg}-\omega_3)(\Omega^*_{ng}+\omega_2)(\Omega_{ng}-\omega_1)}+ \\
&+\frac{\langle r_l\rangle_{gm}\langle r_i\rangle_{mg}\langle r_j\rangle_{gn}\langle r^{\omega_j}\rangle_{ng}}{(\Omega^*_{mg}+\omega_\sigma)(\Omega^*_{mg}+\omega_3)(\Omega^*_{ng}+\omega_1)}+ \\
&+\frac{\langle r_l\rangle_{gm}\langle r_i\rangle_{mg}\langle r_j\rangle_{gn}\langle r_k\rangle_{ng}}{(\Omega^*_{mg}+\omega_3)(\Omega_{ng}-\omega_2)(\Omega^*_{ng}+\omega_1)}\Bigg\}\Bigg],
\end{aligned}
\tag{4.12}
$$

where $I_{1,2,3}$ denotes the average over all terms generated by generating pairwise permutations of (i,ω_1), (j,ω_2) and (k,ω_3).

The same general properties that must be obeyed for the bulk electric susceptibilities are obeyed by the molecular susceptibilities (Eqs. 2.25, 2.26 and 2.27).

Bibliography

[1] B. J. Orr and J. F. Ward, Mol. Phys. **20**, 513 (1971).

[2] N. N. Bogliubov and Y. A. Mitropolsky, *Assymptotic Methods in the Theory of Non-Linear Oscillations* (Gordon & Breach), translated from Rusian, (1961).

[3] J. D. Jackson, *Classical Electrodynamics*, **3rd Edition**, John Wiley & Sons Canada, Ltd, (1998).

[4] R. W. Boyd, *Nonlinear Optics*, Academic Press, San Diego, (1992).

[5] *Characterization techniques and tabulations for organic nonlinear optical materials*, Edited by M. G. Kuzyk and C. W. Dirk, Marcel Dekker, Inc., (1998).

Chapter 5

Experimental characterization of the first hyperpolarizability: Hyper-Rayleigh scattering

The accurate experimental characterization of the molecular susceptibilities is a fundamental step in the study of nonlinear optical phenomena. The characterization of the first hyperpolarizability of most of the organic chromophores studied in this work was achieved using Hyper-Rayleigh scattering experiments in the Department of Chemistry at KULeuven.

In this chapter we will describe the physical principles that allow the realization of Hyper-Rayleigh scattering and overview the principles of operation used in our laboratory. We will also compare the incoherent Hyper-Rayleigh scattering technique with a coherent experimental technique: Electric-Field-Induced Second-Harmonic Generation. Both the Hyper-Rayleigh (HRS) technique, and Electric-Field-Induced-Harmonic Generation (EFISHG) can be employed to characterize the first hyperpolarizability of molecules (chromophores) in solution.

The description of the Hyper-Rayleigh scattering technique is based on a review article by Clays and Persoons.[1] The experimental Hyper-Rayleigh scattering set-up section overviews an article recently published by our group,[2] and the description of the local fields is based in the work of Mark G. Kuzyk.[3]

5.1 Incoherent and coherent nonlinear characterization

Coherent techniques take advantage of temporarily induced or macroscopic "ordering" of the molecules to generate a signal where the contributions of each chromophore add coherently. In this manner, the relatively small nonlinear behavior of the molecules can be characterized by measuring the overall coherent signal and relating the macroscopic measurements to the molecular properties. However, some fundamental assumptions about the nature of the molecules have to be made in order to relate the macroscopic quantities to the molecular properties.

EFISHG is the coherent technique that allows one to measure the response of chromophores in solution. In the EFISHG technique the centrosymmetry of the solution is broken by applying a DC electric field. This field induces an average orientation of the molecules that results in coherent second-harmonic signal.

Unlike EFISHG, Hyper-Rayleigh scattering is a non-coherent technique and the efficiencies are low, which means that the detection system will have to detect small signals which can sometimes be difficult if there is background noise. A high intensity input beam is also desirable in order to increase the intensity of the small signal and get a better ratio between signal and noise.

However, with Hyper-Rayleigh scattering, the macroscopic results are related to the microscopic susceptibilities through relationships that are simpler and that rely on more general assumptions than the coherent counterparts. Also, in contrast to the EFISHG technique, Hyper-Rayleigh scattering allows to measure ionic compounds in solution, like the ones we will study in Chapter 11.

5.2 Rayleigh scattering

The linear equivalent of Hyper-Rayleigh Scattering is Rayleigh scattering, where the scattered light originates from the oscillation of the induced dipole moment $\mu_{ind,i}$ as a consequence of the linear interaction with the electromagnetic field oscillating at frequency ω and with Fourier components $E_i^{(\omega)}$:

$$\mu_{ind,i}(\omega) \propto \sum_j \alpha(-\omega;\omega) E_i^{(\omega)}. \tag{5.1}$$

.

The intensity of the linearly scattered light is derived by taking the second derivative with respect to time of the expression for the oscillating dipole and then taking the square to give an expression for the i^{th} component of the scattered light intensity, $\vec{I}^{(\omega)}$ as a function of the components of the incident light intensity, $\vec{I}_0$:[1]

$$I_i^{(\omega)} = C \sum_j \omega^4 \alpha^2(-\omega;\omega) I_{j,0} = \frac{C'}{\lambda^4} \sum_j \alpha^2(-\omega;\omega) I_{j,0}. \tag{5.2}$$

The constants of proportionality C and C' are related to the distance and positions of the observer and the scattering particles. Aside from the frequency dependence of the linear molecular susceptibility, $\alpha(-\omega;\omega)$, the intensity is proportional to the fourth power of the frequency, or equivalently, inversely proportional to the fourth power of the wavelength, λ. If the light is scattered from a collection of molecules, the total intensity of the scattered light is directly related to the number of scattering particles. The nature of the scattering particles is reflected by the linear molecular susceptibility (the polarizability) of the molecule $\alpha(-\omega;\omega)$ which is related to the allowed electron motions due to the molecular structure. For example, an organic compound with only single carbon-carbon bonds, which inhibit the motion of electrons, has a smaller polarizability than the same unsaturated structure with conjugated carbon-carbon double bonds.

The inverse relationship between the fourth power of the wavelength and the scattered intensity is responsible for the blue color of the sky. Blue light has a shorter wavelength than the rest of the colors coming from the sun and therefore it gets more scattered through the atmosphere in all directions. However, if the distribution of scattering particles in the atmosphere was perfectly homogeneous, we would not see the blue scattered light. This is because for every scatterer that scatters light into the direction of the observer, there would be another scatterer that scatters light into the same direction but with opposite phase, resulting in destructive interference. We see the sky blue because locally,

the scattering particles fluctuate in position, which causes fluctuations in phase, and results into fluctuating scattered light intensities.

5.3 Hyper-Rayleigh Scattering

Hyper-Rayleigh Scattering is the non-linear equivalent of Rayleigh Scattering where the nonlinear terms in the molecular response function are introduced:

$$\begin{aligned} I_i^{(2\omega)} &= C\omega^4 \sum_j \beta_{ijj}^2(-2\omega;\omega,\omega)(I_j^{(\omega)})^2 = \\ &= \frac{C'}{\lambda^4} \sum_j \beta_{ijj}^2(-2\omega;\omega,\omega)(I_{j,0})^2, \end{aligned} \tag{5.3}$$

and

$$\begin{aligned} I_i^{(3\omega)} &= C\omega^4 \sum_j \gamma_{ijjj}^2(-3\omega;\omega,\omega,\omega)(I_j^{(\omega)})^3 = \\ &= \frac{C'}{\lambda^4} \sum_j \gamma_{ijjj}^2(-3\omega;\omega,\omega,\omega)(I_{j,0})^3. \end{aligned} \tag{5.4}$$

Only noncentrosymmetrical molecules show even-order scattering, so it is possible to dissolve noncentrosymmetric molecules in centrosymmetrical solvents and measure only the intensity of the second-order scattered light generated by the dissolved molecules. For odd-order scattering, the solvent molecules also contribute to the scattering, and as they outnumber the solute molecules by several orders of magnitude, they dominate the response.

As in the case of linear Rayleigh Scattering, fluctuations play a fundamental role in the detection of second-order nonlinear light scattering.[4] Rather than translational, due to symmetry requirements, the second-order nonlinear scattering is caused by rotational. The rotational fluctuations destroy the average isotropy in the solution locally in time and space. Spatial and temporal orientational fluctuations result in detectable Hyper-Rayleigh Scattering signal. [5]

Hyper-Rayleigh scattering has several advantages over the EFISHG technique:

- No knowledge of the dipole moment of the molecule is required in order to interpret the results and obtain the first hyperpolaralizability.

- The first hyperpolarizability of ionic chromophores which are electrically conducting in solution can be measured because there is no need to apply an electric field to align the molecules.
- Since alignment is not necessary, the first hyperpolarizability of octupolar molecules can also be characterized. Octupolar molecules can not be measured through EFISHG because it is not possible to align the molecules in solution by applying an external field.
- Additionally, the depolarization ratio between the different components of the scattered light can be used to determine the tensorial character of the molecules.

Hyper-Rayleigh scattering also has some disadvantages. First, because it is a non-coherent technique the second-order efficiencies are low. Secondly, the incoherent scattering that is collected can have multi-photon fluorescence contributions and harmonic Hyper-Rayleigh signal,[6, 7, 8], which can result in an overestimation of the first hyperpolarizability. In principle three-photon fluorescence (3PF) can be detected due to the cubic dependence of the fundamental intensity, but in practice it is difficult to distinguish between a quadratic dependence and a quadratic dependence with a small contribution of cubic dependence.[9] Two-photon fluorescence (2PF) is also quadratically dependent on the fundamental intensity, and therefore, the discrimination between two-photon fluorescence and harmonic Hyper-Rayleigh signal can not be based solely on intensity dependence. In most cases, two-photon absorption fluorescence shows a Stokes shift which can allow discrimination between Hyper-Rayleigh scattering and two-photon fluorescence by using a narrow interference filter. However, anti-stokes 2PF has also been reported.[8, 10] In this case, an optical filter has little use. Since there is a difference in spectral width (the Hyper-Rayleigh scattering signal is a small sharp peak while two-photon fluorescence is a broad background peak) it is possible to discriminate between both contributions by detecting the signal at different wavelengths. This technique has been reported but is very time-consuming.[8]

The solution we use is to discriminate by the time difference between the time-delayed multi-photon fluorescence and the instantaneous Hyper-Rayleigh signal.[9] Since typical fluorescence lifetimes of organic chromophores are in the nanosecond scale, a picosecond or femtosecond pulsed laser is required to perform the experiments. The Fourier transform of this technique in the frequency domain has been implemented in our group,[11] which is experimentally easier to achieve than the time-domain approach. The principle of this set-up will be explained later after the introduction to Hyper-Rayleigh scattering and the experimental details of a classical nanosecond Hyper-Rayleigh scattering set-up.

A Hyper-Rayleigh scattering experiment is performed by measuring the intensity of the incoherently scattered frequency-doubled light generated by an intense laser beam from an isotropic solution.[12, 5] The scattered intensity of a single molecule at the harmonic wavelength can be calculated by performing an orientational average over β_{HRS}:

$$I_{2\omega} = \frac{32\pi^2}{\epsilon_0^3 \lambda^4 r^2} \langle \beta_{HRS}^2 \rangle I_\omega^2, \tag{5.5}$$

where the brackets indicate the orientational averaging, λ is the fundamental wavelength and r is the distance to the scattering molecule. We have used MKS units, so c the speed of light in vacuum ($c = 2.998 \times 10^8 m/s$) and ϵ_0 is the permittivity of free space ($\epsilon_0 = 8.85 \times 10^{-12} F/m$). Assuming the molecules in the scattering volume are independent, the total intensity is proportional to the sum of the intensity scattered by the individual molecules:

$$I_{2\omega} = \frac{32\pi^2}{c\epsilon_0^3 \lambda^4 r^2} N (f_\omega)^4 (f_{2\omega})^2 \langle \beta_{HRS}^2 \rangle I_\omega^2, \tag{5.6}$$

where N is the concentration of chromophores, and f_ω, $f_{2\omega}$ are the local field factors that take into account the dielectric effects of the environment around the molecules and will be described in section 5.5. The experimental evidence shows that, so far, individual molecules in solution are well treated as uncorrelated scatterers.

The scattering geometry and the polarization state of both the fundamental and the harmonic light beams determines the relationship between β_{HRS} and the molecular tensor components β_{ijk}. In classical Hyper-Rayleigh scattering experiments the 90^o angle geometry is mainly used. The set-up is built in such a way that the fundamental light beam is propagating in the $\hat{X}$-direction and polarized in the $\hat{Z}$-direction, and the scattered light is collected in the $\hat{Y}$-direction (see Fig. 5.1). We distinguish between the laboratory coordinate system of reference $(\hat{X}, \hat{Y}, \hat{Z})$, and the molecular coordinate system of reference $(\hat{x}, \hat{y}, \hat{z})$. With this measuring geometry the relation between the orientationally averaged tensor components and the molecular tensor components can be expressed as:

$$\langle \beta_{ZZZ}^2 \rangle = \frac{1}{7} \sum_i \beta_{iii}^2 + \frac{6}{35} \sum_{i \neq j} \beta_{iii} \beta_{ijj} + \frac{9}{35} \sum_{i \neq j} \beta_{iij}^2 + \frac{6}{35} \sum_{ijk, cyclic} \beta_{iij} \beta_{jkk} + \frac{12}{35} \beta_{ijk}^2. \tag{5.7}$$

$$\langle \beta_{XZZ}^2 \rangle = \frac{1}{35} \sum_i \beta_{iii}^2 - \frac{2}{105} \sum_{i \neq j} \beta_{iii} \beta_{ijj} + \frac{11}{105} \sum_{i \neq j} \beta_{iij}^2 - \frac{2}{105} \sum_{ijk, cyclic} \beta_{iij} \beta_{jkk} + \frac{8}{35} \beta_{ijk}^2. \tag{5.8}$$

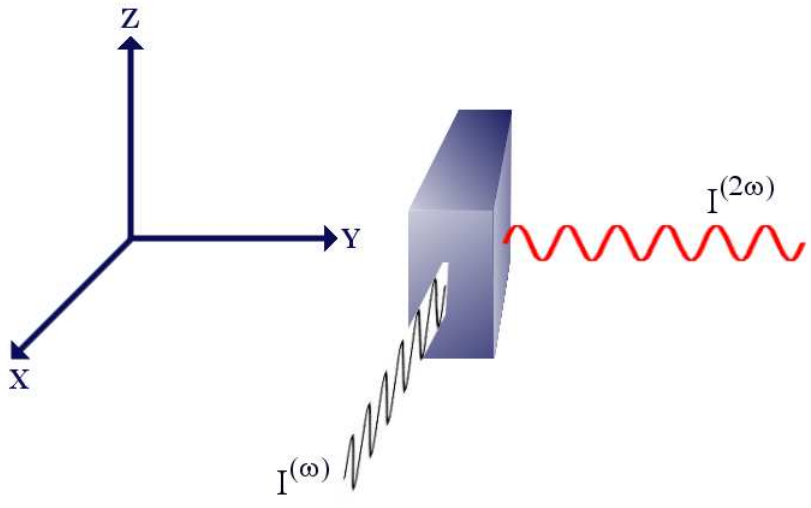

Fig. 5.1: Schematic view of the classical 90^o angle Hyper-Rayleigh scattering geometry. An intense laser beam ($I^{(\omega)}$) is brought to focus through a cell containing the isotropic solution and the frequency-doubled light, $I^{(2\omega)}$, is collected and detected at 90^o with respect to the direction of propagation of the fundamental beam.

The first subscript (X or Z) refers to the polarization state of the frequency doubled light (in the laboratory coordinate system). Since both polarizations are detected with equal sensitivity, and the fundamental light beam is polarized vertically, the orientational average over β is the sum of both contributions:

$$\langle\beta^2_{HRS}\rangle = \langle\beta^2_{ZZZ}\rangle + \langle\beta^2_{XZZ}\rangle. \tag{5.9}$$

The orientational averaged hyperpolarizability squared $\langle\beta_{HRS}\rangle$ is related to the molecular hyperpolarizability tensor components according to Eqs. 5.7 and 5.8. For a molecule of $C_{\infty,v}$ symmetry, or equivalently, when the conjugated path of the molecule is one-dimensional, these equations reduce to:

$$\langle\beta^2_{ZZZ}\rangle = \frac{1}{7}\beta^2_{zzz} + \frac{6}{35}\beta_{zzz}\beta_{zyy} + \frac{9}{35}\beta^2_{zyy} \approx \frac{1}{7}\beta^2_{zzz}, \tag{5.10}$$

and

$$\langle\beta^2_{XZZ}\rangle = \frac{1}{35}\beta^2_{zzz} - \frac{2}{105}\beta_{zzz}\beta_{zyy} + \frac{11}{105}\beta^2_{zyy} \approx \frac{1}{35}\beta^2_{zzz}. \tag{5.11}$$

Therefore, for a molecule of $C_{\infty,v}$ symmetry the square root of the orienta-

tional averaged hyperpolarizability reduces to:

$$\sqrt{\langle\beta^2_{HRS}\rangle} = \sqrt{\langle\beta^2_{XZZ}\rangle + \langle\beta^2_{ZZZ}\rangle} \approx \sqrt{(\frac{1}{7} + \frac{1}{35})\beta^2_{zzz}} = \sqrt{\frac{6}{35}}\beta_{zzz}. \qquad (5.12)$$

On the other hand, for an octupolar molecule (with D_{3h} symmetry) only 4 equal tensor components are not zero: $\beta_{zzz} = -\beta_{zzx} = -\beta_{xzx} = -\beta_{xxz}$ and Eqs. 5.10 and 5.11 reduce to:

$$\langle\beta^2_{ZZZ}\rangle = \frac{1}{7}\beta^2_{zzz} + \frac{6}{35}\beta_{zzz}(-\beta_{zxx}) + \frac{9}{35}\beta^2_{zxx} \approx \frac{8}{35}\beta^2_{zzz}, \qquad (5.13)$$

and

$$\langle\beta^2_{XZZ}\rangle = \frac{1}{35}\beta^2_{zzz} - \frac{2}{105}\beta_{zzz}(-\beta_{zxx}) + \frac{11}{105}\beta^2_{zxx} \approx \frac{16}{105}\beta^2_{zzz}. \qquad (5.14)$$

Therefore for an octupolar molecule (with D_{3h} symmetry):

$$\langle\beta^2_{HRS}\rangle = \frac{8}{21}\beta^2_{zzz}. \qquad (5.15)$$

These two cases illustrate how the orientational averaged hyperpolarizability is dependent on the symmetry of the molecule investigated and different relations to the molecular tensor elements have to be used. The molecules studied in this work have $C_{\infty,0}$ symmetry so the first hyperpolarizability is obtained from Hyper-Rayleigh scattering measurements through Eq. 5.12.

5.4 The experimental Hyper-Rayleigh scattering set-up

Since Hyper-Rayleigh scattering is a forbidden process in isotropic solution, the efficiency is very low as the output arises from rotational fluctuations. As a consequence, optical fields with high optical power-density are needed together with an efficient collection system to detect the Hyper-Rayleigh scattering signal. The fundamental light beam is passed between two crossed polarizers. A half-wave plate is placed in between the two polarizers to control the intensity of the fundamental beam. Then the fundamental beam is focused in the cell. Part of the intensity is split off and detected by a photodiode which will related the fundamental signal I_ω. The collection system consists of a concave mirror, an aspherical lens, a planoconvex lens and a photomultiplier. Separation

of the fundamental and harmonic light is achieved by an interference filter. A schematic view of the set-up is shown in Figure 5.2.

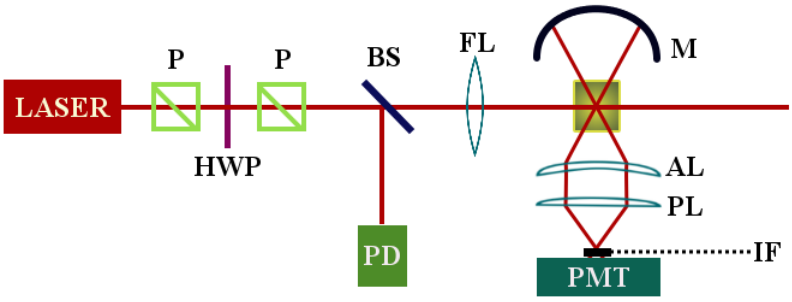

Fig. 5.2: Schematic view of the experimental Hyper-Rayleigh scattering set-up. The fundamental beam from the laser passes between two crossed polarizers (P), and the intensity is controlled through a half-wave plate (HWP). Part of the intensity is split off by a beam-splitter (BS) and detected by a photodiode (PD). The fundamental beam is focused to the sample through a focusing lens (FL). The second-harmonic signal is then collected and focused to a photomultiplier (PMT). The collection system consist of a concave mirror (M), an aspheric lens (AL) and a planoconvex lens (PL). An interference filter (IF) separates the harmonic signal from the fundamental light.

For a solution of two components (solvent and solute), the harmonic intensity $I_{2\omega}$ is given by:

$$I_{2\omega} = G(N_s\langle\beta^2_{HRS}\rangle_s + N_x\langle\beta^2_{HRS}\rangle_x)I^2_\omega = q.c. \times I^2_\omega, \tag{5.16}$$

where we have defined the quadratic coefficient:

$$q.c. \equiv G(N_s\langle\beta^2_{HRS}\rangle_s + N_x\langle\beta^2_{HRS}\rangle_x), \tag{5.17}$$

G includes all experimental factors and the subscripts s and x refer to the solvent (s) and the chromophores (x).

To take advantage of the linear dependence on the chromophores concentration (N_x), a series of different concentrations (usually five) are prepared. The quadratic coefficient for each concentration, $q.c.$ is then obtained. If $\langle\beta^2_{HRS}\rangle_s$ is known and the experimental conditions are well characterized, $\langle\beta^2_{HRS}\rangle_x$ can be obtained by calculating the slope of the quadratic coefficients as a function of concentration. This is referred as the internal reference method.

Alternatively, the external reference method can be used to eliminate the need for precise characterization of the experimental set-up. The variations in experimental conditions are eliminated by measuring a concentration series of a reference compound with known hyperpolarizability at the same time as the measurements for the unknown sample are performed. The slopes of the quadratic coefficients as a function of concentration are calculated. The ratio of the slopes provides $\langle\beta^2_{HRS}\rangle_x$.

In a classical Hyper-Rayleigh scattering experiment a nanosecond pulsed laser (often Nd^{3+} YAG laser with a fundamental light beam of 1064 nm) is used. Because of the low repetition rate of the laser pulses, gated integrators are used to measure the intensity of the Hyper-Rayleigh signal. The measurement is computer controlled and I_ω and $I_{2\omega}$ are recorded. From these data β_{HRS} of the compounds is then determined. This type of setup, however, does not allow one to separate between genuine Hyper-Rayleigh signal contribution and multi-photon fluorescence,[7, 8] that can result in an overestimation of $\langle\beta^2_{HRS}\rangle$.[9]

Therefore, in our lab, the original Hyper-Rayleigh experiment has been modified in order to eliminate multi-photon contributions.

A femtosecond pulsed laser (Millennia X + Tsunami with a lock-to-clock system that ensures a $80MHz$ pulsed output) at fundamental wavelength $\lambda = 800nm$ is used in conjugation with a low frequency lock-in-amplifier and a signal generator.

The principle of discriminating between immediate HRS and time-delayed fluorescence is based on the phase shift φ and the demodulation $M = \frac{M_f}{M_r}$ (ratio between the intensity of fluorescence, M_f , and the intensity of excitation M_r) that the fluorescence acquires versus the excitation light at a particular amplitude modulation frequency $\omega = 2\pi f$. The normalized magnitude M and the phase φ of the fluorescence at a particular frequency are experimentally observable in the time domain and in the real and imaginary part of the Fourier transform. The frequency dependence of φ and M is determined by the fluorescence decay parameters, which are the fluorescence lifetime and its respective amplitude. In the frequency domain the phase shift φ of the fluorescence tends to 90^o and the normalized magnitude M tends to zero for long lifetimes τ and/or high modulation frequencies. The fluorescence is "out-of-phase" and completely "demodulated" with the excitation.

The fluorescence-suppression scheme takes advantage of this demodulation

(lowering in amplitude) of the on average time-delayed fluorescence for high amplitude-modulation (AM) frequencies. These AM frequencies are obtained as the higher harmonics of the 80 MHz repetition rate of a femtosecond Titanium-sapphire laser. The output is comprised of a train of laser pulses, each approximately 130 femtoseconds in duration, 12.5 nanoseconds apart, at 800 nm.[11] The presence of a multi-photon fluorescence contribution to the Hyper-Rayleigh scattering signal is detected by measuring the apparent value for the first hyperpolarizability as a function of AM frequency. If no demodulation is observed, the apparent hyperpolarizability does not change for increasing AM frequencies, and there is no overestimation due to multi-photon fluorescence. An accurate average hyperpolarizability value can be obtained from the values at the different AM frequencies. If demodulation is present, the apparent hyperpolarizability decreases towards the fluorescence-free value as the AM frequency increases. Thus, by taking the high-frequency limit, where fluorescence can no longer contribute, the fluorescence-free first hyperpolarizability is obtained.

5.5 The local fields

In section 5.4 the local field factors - that take into account the dielectric effects of the environment around the molecules - were introduced. Here we will describe this effects and how to account for them, following the work of M. G Kuzyk, [3] as it was described in my Master's dissertation.[13]

When a molecule is in vacuum, the incident electric field $\vec{E}^{\omega}$ and the local field felt by the molecule, $\vec{f}^{\omega}$ are the same; but molecules are generally embedded in a material. The local electric field at a molecular location is the superposition of the internal electric field generated by the rest of the material and the external applied electric field. While the macroscopic susceptibilities relate the polarization of the material to the external electric field, the microscopic susceptibilities relate the molecular polarization to the local electric field.

The surrounding material might contribute to the local field in different ways:[3]

- The surrounding material gets polarized in response to the external electric field, adding to the field that is felt by the molecule.
- Although the bulk material is neutral, the fluctuations in the electric field do not cancel around the molecule, so the material generates an electric field even in the absence of an applied one.

- When a molecule has a dipole moment in its ground state, it surrounding material gets polarized and affects the field around the molecule.
- The external field polarizes first the molecule and then the polarization of the molecule polarizes the surrounding material which in turns affects the molecule.

Accounting for all these effects in the calculation of the local field at a molecule location is extremely difficult and requires a detailed knowledge of the dielectric properties of the medium. We will use a simplified version, the Lorentz-Lorenz model [14] to find the relationship between the external electric field, $\vec{E}$, and the local field, $\vec{f}$. The Lorentz-Lorenz model applies to non-dipolar homogeneous liquids and solids. This model produces results that are accurate enough within the experimental uncertainties that are expected in nonlinear optical measurements.

To calculate the local field in the Lorentz-Lorenz model, we treat the material (usually a liquid, dye-doped polymer or a molecular organic crystal) as a continuum. The molecules inside the material are colliding with each other, but we assume that the time scales used to observe the system are much longer than the average time between collisions, so the system is well approximated as a continuous ensemble of molecules.

Let us consider a volume of the material small enough so the applied external field is constant throughout the volume, but sufficiently big to contain enough molecules for the continuous assumption to hold. When a constant electric field, $\vec{E}$, is applied to a dielectric medium, its time averaged polarization is given by[1][3]:

$$\vec{P} = \chi^{(1)}\vec{E} = \left(\frac{\epsilon - 1}{4\pi}\right)\vec{E}, \tag{5.18}$$

where ϵ is the dielectric function of the material.

To calculate the local field at a molecular site we will now consider the molecule as a dielectric sphere. The polarization of the dielectric sphere that represents the molecule is due to the local field, $\vec{f}$. The induced dipole, $\vec{p}$, of a dielectric sphere with dielectric constant ϵ in vacuum under the influence of a constant external field, $\vec{f}$ is given by [3]:

$$\vec{p} = \left(\frac{\epsilon - 1}{\epsilon + 2}\right) a^3 \vec{f}, \tag{5.19}$$

[1]Note that we consider only the linear effect, since it dominates the local fields.

where a is the radius of the sphere. The polarization of the sphere, $\vec{P}$, defined as the dipole moment per unit volume, is given by:

$$\vec{P} = \frac{\vec{p}}{\frac{4}{3}\pi a^3} = \frac{3}{4\pi}\left(\frac{\epsilon - 1}{\epsilon + 2}\right)\vec{f}. \tag{5.20}$$

Comparing Eq. (5.20) with Eq. (5.18)we get:

$$(\epsilon - 1)\vec{E} = 3\left(\frac{\epsilon - 1}{\epsilon + 2}\right)\vec{f}, \tag{5.21}$$

or

$$\vec{f} = \left(\frac{\epsilon + 2}{3}\right)\vec{E}. \tag{5.22}$$

This is the Lorentz-Lorenz local field model. The local field factor is defined as:

$$f_\omega = \left(\frac{\epsilon(\omega) + 2}{3}\right), \tag{5.23}$$

so that the local field is proportional to the externally applied field,

$$\vec{f}^{(\omega)} = f_\omega \vec{E}^{(\omega)}. \tag{5.24}$$

Bibliography

[1] K. Clays and A. Persoons, "Hyper-Rayleigh scattering: opportunities for molecular, supramolecular, and device characterization by incoherent second-order nonlinear scattering" *Handbook of Advanced electronic and photonic materials devices*, Edited by H. S. Nawla, Vol 9, Academic Press (2001).

[2] I. Asselberghs, J. Pérez-Moreno and K. Clays "Characterization techniques of nonlinear optical materials: An introduction to experimental nonlinear optical techniques", *Non-Linear Optical Properties of Matter*, Edited by M.G. Papadopoulos et al. Springer (2006).

[3] *Characterization techniques and tabulations for organic nonlinear optical materials*, Edited by M. G. Kuzyk and C. W. Dirk, Marcel Dekker, Inc., (1998).

[4] K. Clays, A. Persoons and L. De Maeyer, in "Modern Nonlinear Optics." Advances in Chemical Physics, Vol 85 (I. Prigogine and S. A. rice, Eds.), Part 3, 455. Wyley, New York, (1994).

[5] K. Clays and A. Persoons, Phys. Rev. Lett. **66** 2980 (1991).

[6] M. C. Flipse, R. de Jonge, R. H. Woudenberg, A. W. Marsman, C. A. van Walree and L. W. Jenneskens, Chem. Phys. Lett. **245**, 297 (1995).

[7] I. D. Morrison, R. G. Denning, W. M. Laidlaw, and M. A. Stammers, Rev. Sci. Instrum. **67**, 1445 (1996).

[8] N. W. Song, T. I- Kang, S. C. Jeoung, S. -J. Joen, B. R. Cho and D. Kim, Chem. Phys. Lett. **261**, 307, (1996).

[9] O. F. J. Noordman and N. F. van Hulst, Chem. Phys. Lett. **253**, 145 (1996).

[10] S. F. Hubbard, R. G. Petschek and K. D. Singer, Opt. Lett. **21**, 1774 (1996).

[11] G. Olbrechts, R. Strobbe, K. Clays, and A. Persoons, Rev. Sci. Instrum. **69**, 2233 (1998).

[12] E. Hendrickx, K. Clays and A. Persoons, Acc. Chem. Res. **31**, 675 (1998).

[13] J. Pérez-Moreno, "Quantum limits of the nonlinear optical response",*M.S. Thesis*, Washington State University, Department of Physics. August 2004.

[14] J. D. Jackson, *Classical Electrodynamics*, **3rd Edition**, John Wiley & Sons Canada, Ltd, (1998).

Chapter 6

The Thomas-Kuhn sum rules

Calculation of the molecular susceptibilities requires the evaluation of matrix elements of the position operator, $\vec{r}$, and the energies of the unperturbed quantum states of the system. However, these parameters are not independent. They are related to each other as a consequence of quantum mechanics. The use of the Thomas-Kuhn sum rules [1] leads to simplifications in the expressions of the molecular susceptibilities.

In this chapter we deduce the generalized Thomas-Kuhn sum rules in a rigorous way that highlights the assumptions made in the derivation, in the way it was presented in my Master's dissertation.[2]

6.1 Definitions

We assume that the (unperturbed) molecule is a quantum mechanical system possessing N-electrons that contribute to the molecular polarization. The electronic coordinate of the ith electron is given by $\vec{r}^{\,i}$ and its momentum is given by $\vec{p}^{\,i}$. In cartesian coordinates:

$$\vec{r}^{\,i} = r_x^i\ \hat{x} + r_y^i\ \hat{y} + r_z^i\ \hat{z}, \tag{6.1}$$

and

$$\vec{p}^{\,i} = p_x^i\ \hat{x} + p_y^i\ \hat{y} + p_z^i\ \hat{z}. \tag{6.2}$$

To calculate the dipole moment of the molecule, we need to sum over all the contributions from the different electrons,

$$\vec{\mu} = -e\vec{r}^{\,1} - e\vec{r}^{\,2} + \cdots - e\vec{r}^{\,N} \equiv -e\vec{r}, \tag{6.3}$$

where we have defined

$$\vec{r} \equiv \sum_{i=1}^{N} \vec{r}^{\,i} = \sum_{i=1}^{N} (r_x^i\ \hat{x} + r_y^i\ \hat{y} + r_z^i\ \hat{z}). \tag{6.4}$$

Similarly we define

$$\vec{p} = \sum_{i=1}^{N} \vec{p}^{\,i} = \sum_{i=1}^{N} (p_x^i\ \hat{x} + p_y^i\ \hat{y} + p_z^i\ \hat{z}). \tag{6.5}$$

We assume that the (unperturbed) system is conservative. The (unperturbed) Hamiltonian is given by:

$$H = \sum_{i}^{N} \frac{(\vec{p}^{\,i})^2}{2m} + V(\vec{r}^{\,1}, \vec{r}^{\,2}, \cdots, \vec{r}^{\,N}), \tag{6.6}$$

where m is the mass of the electron and

$$\frac{(\vec{p}^{\,i})^2}{2m} = \frac{(p_x^i)^2 + (p_y^i)^2 + (p_z^i)^2}{2m}, \tag{6.7}$$

is the total kinetic energy of the k-th electron.

The eigenstates, $|k\rangle$, of the unperturbed system are known,

$$H|k\rangle = E_k|k\rangle. \tag{6.8}$$

We define the following matrix elements

$$\vec{r}_{kl} = \langle k|\vec{r}|l\rangle = \langle k|r_x|l\rangle\ \hat{x} + \langle k|r_y|l\rangle\ \hat{y} + \langle k|r_z|l\rangle\ \hat{z}, \tag{6.9}$$

and

$$\vec{p}_{kl} = \langle k|\vec{p}|l\rangle = \langle k|p_x|l\rangle\ \hat{x} + \langle k|p_y|l\rangle\ \hat{y} + \langle k|p_z|l\rangle\ \hat{z}. \tag{6.10}$$

6.2 The generalized Thomas-Kuhn sum rules

Now we are ready to calculate the generalized Thomas-Kuhn sum rules. The ground state sum rules were first formulated by Thomas[3] and Kuhn[4] using a semiclassical approach. Heisenberg derived the rules using the laws of quantum mechanics[5] and they were generalized by Bethe et al.[1]. We will use the generalized sum rules as derived by M. G. Kuzyk.[6, 7, 8].

We begin by calculating the commutator $[r_x, H]$:

$$\begin{aligned}
[r_x, H] &= \left[\sum_{l=1}^{N} r_x^l, \left\{\sum_k^N \frac{(\vec{p}^{\,k})^2}{2m} + V(\vec{r}^{\,1}, \vec{r}^{\,2}, \cdots, \vec{r}^{\,N})\right\}\right] \\
&= \left[\sum_{l=1}^{N} r_x^l, \sum_{k=1}^{N} \frac{(p_x^k)^2}{2m}\right] = \sum_{kl} \frac{1}{2m}[r_x^l, (p_x^k)^2] \\
&= \sum_{kl} \frac{2}{2m} i\hbar p_x^k \delta_{kl} = \frac{i\hbar}{m}\sum_k p_x^k.
\end{aligned} \tag{6.11}$$

Now we evaluate the commutator $[[r_x, H], r_x]$:

$$[[r_x, H], r_x] = \left[\frac{i\hbar}{m}\sum_k p_x^k, \sum_{l=1}^{N} r_x^l\right] = \frac{i\hbar}{m}\sum_{lk}[p_x^k, r_x^l] = \frac{i\hbar}{m}\sum_{lk}^{N} -i\hbar\delta_{kl} = \frac{\hbar^2 N}{m}. \tag{6.12}$$

Bracketing Eq. (6.12) between $\langle k|$ and $|l\rangle$ we find:

$$\begin{aligned}
&\langle k|\,[[r_x, H], r_x]\,|l\rangle = \langle k|[r_x, H]r_x - r_x[r_x, H]|l\rangle \\
=\ &\langle k|r_x H r_x - H r_x r_x - r_x r_x H + r_x H r_x|l\rangle = \langle k|2r_x H r_x - H r_x r_x - r_x r_x H|l\rangle \\
=\ &\sum_n \{2\langle k|r_x|n\rangle\langle n|H r_x|l\rangle - \langle k|H r_x|n\rangle\langle n|r_x|l\rangle - \langle k|r_x|n\rangle\langle n|r_x H|l\rangle \\
=\ &\sum_n \{2\langle r_x\rangle_{kn} E_n \langle r_x\rangle_{nl} - E_k\langle r_x\rangle_{kn}\langle r_x\rangle_{nl} - \langle r_x\rangle_{kn}\langle r_x\rangle_{nl} E_l\},
\end{aligned} \tag{6.13}$$

where we have used completeness. Substituting Eq. (6.12) into (6.13) we obtain the generalized Thomas-Kuhn sum rule for the $\hat{x}$-cartesian coordinate:

$$\sum_n (2E_n - E_k - E_l)\langle r_x\rangle_{kn}\langle r_x\rangle_{nl} = \frac{\hbar^2 N}{m}\delta_{kl}. \tag{6.14}$$

Similarly we can find the equivalent equations for the $\hat{y}$ and $\hat{z}$-cartesian coordinates,

$$\sum_n (2E_n - E_k - E_l)\langle r_y\rangle_{kn}\langle r_y\rangle_{nl} = \frac{\hbar^2 N}{m}\delta_{kl}, \tag{6.15}$$

and

$$\sum_n (2E_n - E_k - E_l)\langle r_z\rangle_{kn}\langle r_z\rangle_{nl} = \frac{\hbar^2 N}{m}\delta_{kl}. \tag{6.16}$$

It must be emphasized that in the derivation of the generalized Thomas-Kuhn sum rules we have not made any assumption about the particular behavior of the system. Therefore the results obtained by applying the Thomas-Kuhn sum rule in the calculation of susceptibilities are valid for any quantum system for which $V = V(\vec{r}^{\,1}, \cdots, \vec{r}^{\,N})$, regardless of how exactly the potential depends on the position of the charged particles.

Bibliography

[1] H. A. Bethe and E. E. Salpeter, *Quantum Mechanics of One and Two Electron Atoms*, Plenum, New York, (1997).

[2] J. Pérez-Moreno, "Quantum limits of the nonlinear optical response", *M.S. Thesis* Washington State University, Department of Physics. August 2004.

[3] W. Thomas, Naturwissenschaften **13**, 627 (1925).

[4] W. Kuhn, Z. Phys., **33** 408 (1925).

[5] W. Heisenberg, Z. Phys. **33**, 879 (1925).

[6] M. G. Kuzyk, Opt. Lett. **25**, 1183 (2000).

[7] M. G. Kuzyk, Phys. Rev. Lett. **85** No. 6, 1218 (2000).

[8] M. G. Kuzyk, IEEE Journal on Selected Topics on Quantum Electrocnics **7**, 774 (2001).

[9] J. J. Sakurai. *Modern Quantum Mechanics. Revised Edition.* Addison-Wesley Publishing Company, 1993.

Chapter 7

The dipole-free molecular susceptibilities

The Thomas-Kuhn sum rules derived in Chapter 6 can be applied to the expressions for the first and second hyperpolarizabilities (Eqs. 4.11 and 4.12). The expressions are simplified by the elimination of the explicit dependence on the dipolar terms. The dipole-free expression for the first hyperpolarizability was first derived by M. G. Kuzyk,[1] and his derivation is summarize here. After that a new dipole-free expression for the second hyperpolarizability is presented for the first time.

7.1 The dipole-free first hyperpolarizability

We begin by writing down the expression for the first hyperpolarizability that was introduced in chapter 4:

$$\begin{aligned}\beta_{ijk}(-\omega_\sigma;\omega_1,\omega_2) &= -(\hbar)^{-2}e^3 I_{1,2}\sum_{m,n}{}' \left\{ \frac{\langle r_i\rangle_{gm}\langle \bar{r}_k\rangle_{mn}\langle r_j\rangle_{ng}}{(\Omega_{mg}-\omega_\sigma)(\Omega_{ng}-\omega_1)} \right. \\ &+ \left. \frac{\langle r_k\rangle_{gm}\langle \bar{r}_j\rangle_{mn}\langle r_i\rangle_{ng}}{(\Omega^*_{mg}+\omega_2)(\Omega^*_{ng}-\omega_\sigma)} + \frac{\langle r_k\rangle_{gm}\langle \bar{r}_i\rangle_{mn}\langle r_j\rangle_{ng}}{(\Omega^*_{mg}+\omega_2)(\Omega_{ng}-\omega_1)} \right\},\end{aligned} \tag{7.1}$$

where, as a reminder, the operator $I_{1,2}$ which denotes the average over all terms generated by pairwise permutations of (i,ω_1) and (j,ω_2). For example, when

$I_{1,2}$ acts on the first term we get:

$$\begin{aligned} I_{1,2}\left(\frac{\langle r_i\rangle_{gm}\langle\bar{r}_k\rangle_{mn}\langle r_j\rangle_{ng}}{(\Omega_{mg}-\omega_\sigma)(\Omega_{ng}-\omega_1)}\right) &= \\ \frac{1}{2}\left(\frac{\langle r_i\rangle_{gm}\langle\bar{r}_k\rangle_{mn}\langle r_j\rangle_{ng}}{(\Omega_{mg}-\omega_\sigma)(\Omega_{ng}-\omega_1)}\right. &+ \left.\frac{\langle r_j\rangle_{gm}\langle\bar{r}_k\rangle_{mn}\langle r_i\rangle_{ng}}{(\Omega_{mg}-\omega_\sigma)(\Omega_{ng}-\omega_2)}\right). \end{aligned} \tag{7.2}$$

For clarity, we will focus on the diagonal component of the first hyperpolarizability, $\beta_{xxx}(-\omega_\sigma;\omega_1,\omega_2)$. The procedure can be used to obtain the expression for other components. Also, for simplicity, since $r_i = r_j = r_k = r_x$ we will define:

$$x_{ij} = \langle r_x\rangle_{ij} \tag{7.3}$$

Using this notation we can write:

$$\beta_{xxx}(\omega_\sigma;\omega_1,\omega_2) = -e^3{\sum_{m,n}}' x_{gm}\bar{x}_{mn}x_{ng}D_{nm}, \tag{7.4}$$

where we have defined:

$$\begin{aligned} D_{nm} &= \Big[\frac{1}{2\hbar^2}\left\{\frac{1}{(\omega_{n0}-\omega_1-\omega_2)(\omega_{m0}-\omega_1)}+\right. \\ &+ \left.\frac{1}{(\omega^*_{n0}+\omega_2)(\omega_{m0}-\omega_1)}+\frac{1}{(\omega^*_{n0}+\omega_2)(\omega^*_{m0}+\omega_1+\omega_2)}\right\} \\ &+ \text{Permutations of } (\omega_1\leftrightarrow\omega_2) \text{ in the above expression}\Big], \end{aligned} \tag{7.5}$$

with

$$\omega_{m0} = \omega^0_{m0} - i\gamma_{m0}, \tag{7.6}$$

$$\hbar\omega^0_{m0} = E_{m0}, \tag{7.7}$$

$$\gamma_{m0} = \frac{\Gamma_{m0}}{2}. \tag{7.8}$$

Now we recall the definition of the barred operator:

$$\bar{x}_{mn} = \langle x\rangle_{mn} - \langle x\rangle_{gg}\langle m|n\rangle, \tag{7.9}$$

which implies that $\bar{x}_{nn}$ is directly related to the dipole moment change of the molecule between the state n and the ground state,

$$\bar{x}_{nn} = x_{nn} - x_{gg} \equiv \Delta x_{n0}, \tag{7.10}$$

and $\bar{x}_{mn} = x_{mn}$ if $n \neq m$.

Next, we will separate the contributions into explicitly dipolar terms and non explicitly dipolar terms:

$$\beta_{xxx}(\omega_\sigma;\omega_1,\omega_2) = -e^3 {\sum_n}' \frac{|x_{n0}|^2 \Delta x_{n0}}{D^{-1}_{nn}(\omega_1,\omega_2)} + {\sum_n}' {\sum_{m\neq n}}' \frac{x_{0n}x_{nm}x_{m0}}{D^{-1}_{nm}(\omega_1,\omega_2)}. \tag{7.11}$$

Now we can use the generalized Thomas-Kuhn sum rule for the $\hat{x}$-cartesian coordinate (Eq. 6.14):

$$\sum_n (2E_n - E_k - E_l)\langle r_x\rangle_{kn}\langle r_x\rangle_{nl} = \frac{\hbar^2 N}{m}\delta_{kl}. \tag{7.12}$$

Considering the case where $k \neq l$ Eq. 7.12 can be written as:

$$\sum_{n=0}^{\infty}\left(\frac{E_{nk}}{2} + \frac{E_{nl}}{2}\right) x_{kn}x_{nl} = 0 \Rightarrow \sum_{n=0}^{\infty}\left(E_{nk} + E_{nl}\right) x_{kn}x_{nl} = 0, \tag{7.13}$$

which can be rewritten as:

$$\left\{\sum_{n\neq l, n\neq k}(E_{nk}+E_{nl})x_{kn}x_{nl})\right\} + E_{kl}x_{kk}x_{kl} + E_{lk}x_{kl}x_{ll} =$$
$$\left\{\sum_{n\neq l, n\neq k}(E_{nk}+E_{nl})x_{kn}x_{nl})\right\} + E_{kl}x_{kl}(x_{ll} - x_{kk}) = 0, \tag{7.14}$$

where we have used the fact that $E_{kl} = -E_{lk}$.

If we now set $l = 0$ in Eq. 7.14 we obtain:

$$\left\{\sum_{n\neq 0, n\neq k}(E_{nk}+E_{n0})x_{kn}x_{n0})\right\} + E_{k0}x_{k0}\Delta x_{k0} = 0. \tag{7.15}$$

From Eq. 7.15 we can isolate $|x_{k0}|^2\Delta x_{k0}$:

$$|x_{k0}|^2 \Delta x_{k0} = -{\sum_{n\neq k}}' \frac{(E_{nk}+E_{n0})}{E_{k0}} x_{0k}x_{kn}x_{n0}, \tag{7.16}$$

which can be substituted into Eq. 7.11 to obtain the dipole-free expression for the diagonal term of the first hyperpolarizability:

$$\begin{aligned} \beta_{xxx}(\omega_\sigma;\omega_1,\omega_2) &= \\ -e^3 {\sum_n}' {\sum_{m\neq n}}' \frac{x_{0n}x_{nm}x_{m0}}{D^{-1}_{nm}(\omega_1,\omega_2)} \Big(1 &- \frac{D^{-1}_{nm}(\omega_1,\omega_2)}{D^{-1}_{nn}(\omega_1,\omega_2)} \frac{(E_{mn}+E_{m0})}{E_{n0}} \Big) = \\ -e^3 {\sum_n}' {\sum_{m\neq n}}' \frac{x_{0n}x_{nm}x_{m0}}{D^{-1}_{nm}(\omega_1,\omega_2)} \Big(1 &- \frac{D^{-1}_{nm}(\omega_1,\omega_2)}{D^{-1}_{nn}(\omega_1,\omega_2)} \left\{ 2\frac{E_{m0}}{E_{n0}} - 1 \right\} \Big). \end{aligned} \tag{7.17}$$

7.2 The dipole-free second hyperpolarizability

Again, for clarity, we will focus on the diagonal component of the second hyperpolarizability, which was introduced in chapter 4:

$$\begin{aligned} \gamma_{xxxx}(-\omega_\sigma;\omega_1,\omega_2,\omega_3) &= \\ e^4 \left({\sum_{lmn}^{\infty}}' \frac{x_{0l}\bar{x}_{lm}\bar{x}_{mn}x_{n0}}{D^{-1}_{lmn}(\omega_1,\omega_2,\omega_3)} \right. &- \left. {\sum_{mn}^{\infty}}' \frac{x_{0m}x_{m0}x_{0n}x_{n0}}{D^{-1}_{mn}(\omega_1,\omega_2,\omega_3)} \right), \end{aligned} \tag{7.18}$$

where the dispersion of γ is given by the $D^{-1}_{lmn}(\omega_1,\omega_2,\omega_3)$ and $D^{-1}_{mn}(\omega_1,\omega_2,\omega_3)$ and are defined as follows:

$$\begin{aligned} D_{lmn}(\omega_1,\omega_2,\omega_3) &= \frac{1}{6} \times \\ \Big\{ & \frac{1}{(\hbar\Omega_{lg}-\hbar\omega_\sigma)(\hbar\Omega_{mg}-\hbar\omega_1-\hbar\omega_2)(\hbar\Omega_{ng}-\hbar\omega_1)} \\ + & \frac{1}{(\hbar\Omega^*_{lg}+\hbar\omega_3)(\hbar\Omega_{mg}-\hbar\omega_1-\hbar\omega_2)(\hbar\Omega_{ng}-\hbar\omega_1)} \\ + & \frac{1}{(\hbar\Omega^*_{lg}+\hbar\omega_1)(\hbar\Omega^*_{mg}+\hbar\omega_1+\hbar\omega_2)(\hbar\Omega_{ng}-\hbar\omega_3)} \\ + & \frac{1}{(\hbar\Omega^*_{lg}+\hbar\omega_1)(\hbar\Omega^*_{mg}+\hbar\omega_1+\hbar\omega_2)(\hbar\Omega^*_{ng}+\hbar\omega_\sigma)} \\ + & \text{ Permutations of } (\omega_1,\omega_2,\omega_3) \text{ for the above terms} \Big\}. \end{aligned} \tag{7.19}$$

$$
\begin{aligned}
&D_{mn}(\omega_1,\omega_2,\omega_3) = \frac{1}{6} \times \\
&\Bigg\{ \frac{1}{(\hbar\Omega_{mg} - \hbar\omega_\sigma)(\hbar\Omega_{mg} - \hbar\omega_3)(\hbar\Omega_{ng} - \hbar\omega_1)} \\
&+ \frac{1}{(\hbar\Omega_{mg} - \hbar\omega_3)(\hbar\Omega^*_{ng} + \hbar\omega_2)(\hbar\Omega_{ng} - \hbar\omega_1)} \\
&+ \frac{1}{(\hbar\Omega^*_{mg} + \hbar\omega_\sigma)(\hbar\Omega^*_{mg} + \hbar\omega_3)(\hbar\Omega^*_{ng} + \hbar\omega_1)} \\
&+ \frac{1}{(\hbar\Omega^*_{mg} + \hbar\omega_3)(\hbar\Omega_{ng} - \hbar\omega_2)(\hbar\Omega^*_{ng} + \hbar\omega_1)} \\
&+ \text{Permutations of } (\omega_1,\omega_2,\omega_3) \text{ for the above terms} \Bigg\} . \qquad (7.20)
\end{aligned}
$$

To transform Eq. 7.18 into a dipole-free expression we only need to rework the first term in the equation since the second term is already dipole-free:

$$
\begin{aligned}
&\sum_{lmn}^{\infty\ \prime} \frac{x_{0l}\bar{x}_{lm}\bar{x}_{mn}x_{n0}}{D^{-1}_{lmn}} = \\
&\sum_{n}^{\infty\ \prime}\sum_{m}^{\infty\ \prime} \left(\frac{x_{0m}\bar{x}_{mm}\bar{x}_{mn}x_{n0}}{D^{-1}_{mmn}} + \sum_{l\neq m}^{\infty\ \prime} \frac{x_{0l}\bar{x}_{lm}\bar{x}_{mn}x_{n0}}{D^{-1}_{lmn}} \right) . \qquad (7.21)
\end{aligned}
$$

Substituting Eq. 7.16 into Eq. 7.21, we obtain:

$$
\begin{aligned}
&\sum_{lmn}^{\infty\ \prime} \frac{x_{0l}\bar{x}_{lm}\bar{x}_{mn}x_{n0}}{D^{-1}_{lmn}} = \\
&\sum_{n}^{\infty\ \prime}\sum_{m}^{\infty\ \prime} \left(\frac{x_{0m}\bar{x}_{mm}\bar{x}_{mn}x_{n0}}{D^{-1}_{mmn}} + \sum_{l\neq m}^{\infty\ \prime} \frac{x_{0l}\bar{x}_{lm}\bar{x}_{mn}x_{n0}}{D^{-1}_{lmn}} \right) = \\
&\sum_{n}^{\infty\ \prime}\sum_{m}^{\infty\ \prime} \left(\frac{x_{om}\Delta x_{m0}\bar{x}_{mn}x_{ng}}{D^{-1}_{mmn}} + \sum_{l\neq m}^{\infty\ \prime} \frac{x_{0l}x_{lm}\bar{x}_{mn}x_{ng}}{D^{-1}_{lmn}} \right) = \\
&\sum_{n}^{\infty\ \prime} \left(\frac{x_{0n}\Delta x_{n0}\bar{x}_{nn}x_{n0}}{D^{-1}_{nnn}} + \sum_{m\neq n}^{\infty\ \prime} \frac{x_{0m}\Delta x_{m0}\bar{x}_{mn}x_{n0}}{D^{-1}_{mmn}} + \right. \\
&\left. \sum_{l\neq m}^{\infty\ \prime} \frac{x_{0l}x_{ln}\bar{x}_{nn}x_{ng}}{D^{-1}_{lnn}} + \sum_{l\neq m}^{\infty\ \prime}\sum_{m\neq n}^{\infty\ \prime} \frac{x_{0l}x_{lm}\bar{x}_{mn}x_{ng}}{D^{-1}_{lmn}} \right) , \qquad (7.22)
\end{aligned}
$$

where we have explicitly displayed terms with the same index.

In conclusion:

$$\sum_{lmn}^{\infty\ '} \frac{x_{0l}\bar{x}_{lm}\bar{x}_{mn}x_{n0}}{D^{-1}_{lmn}} =$$
$$\sum_{n}^{\infty\ '} \frac{x_{0n}\Delta x_{n0}\Delta x_{n0}x_{n0}}{D^{-1}_{nnn}} + \sum_{n}^{\infty\ '}\sum_{m\neq n}^{\infty\ '} \frac{x_{0m}\Delta x_{m0}x_{mn}x_{n0}}{D^{-1}_{mmn}} +$$
$$\sum_{n}^{\infty\ '}\sum_{l\neq m}^{\infty\ '} \frac{x_{0l}x_{ln}\Delta x_{n0}x_{n0}}{D^{-1}_{lnn}} + \sum_{n}^{\infty\ '}\sum_{l\neq m}^{\infty\ '}\sum_{m\neq l}^{\infty\ '} \frac{x_{0l}x_{lm}x_{mn}x_{n0}}{D^{-1}_{lmn}}. \qquad (7.23)$$

Now we will consider one by one the contributions of each term in Eq. 7.23.

7.2.1 First contribution to Eq. 7.23

The first contribution is given by:

$$\sum_{n}^{\infty\ '} \frac{x_{0n}\Delta x_{n0}x_{n0}\Delta x_{n0}}{D^{-1}_{nnn}}. \qquad (7.24)$$

This term is evaluated by rewriting Eq. 7.16 as:

$$x_{0n}\Delta x_{n0} = -\sum_{m\neq n}^{\infty\ '} \left(\frac{E_{mn}+E_{m0}}{E_{n0}}\right) x_{0m}x_{mn}, \qquad (7.25)$$

$$x_{n0}\Delta x_{n0} = -\sum_{l\neq n}^{\infty\ '} \left(\frac{E_{ln}+E_{l0}}{E_{n0}}\right) x_{nl}x_{l0}. \qquad (7.26)$$

Substituting Eqs. 7.25 and 7.26 into Eq. 7.24 yields:

$$\sum_{n}^{\infty\ '} \frac{x_{0n}\Delta x_{n0}x_{n0}\Delta x_{n0}}{D^{-1}_{nnn}} =$$
$$\sum_{n}^{\infty\ '}\sum_{m\neq l}^{\infty\ '}\sum_{l\neq n}^{\infty\ '} \frac{\left(\frac{E_{mn}+E_{m0}}{E_{n0}}\right)\left(\frac{E_{ln}+E_{l0}}{E_{n0}}\right)}{D^{-1}_{nnn}} x_{0m}x_{mn}x_{nl}x_{l0}. \qquad (7.27)$$

7.2.2 Second contribution to Eq. 7.23

The second term is evaluated using Eq. 7.16:

$$\sum_{n}^{\infty\,\prime}\sum_{m\neq n}^{\infty\,\prime}\frac{x_{0m}\Delta x_{m0}x_{mn}x_{n0}}{D_{mmn}^{-1}}=-\sum_{n}^{\infty\,\prime}\sum_{m\neq n}^{\infty\,\prime}\sum_{l\neq m}^{\infty\,\prime}\frac{\left(\frac{E_{lm}+E_{l0}}{E_{m0}}\right)}{D_{mmn}^{-1}}x_{0l}x_{lm}x_{mn}x_{n0}. \tag{7.28}$$

7.2.3 Third contribution to Eq. 7.23

Similarly, the third term can be evaluated:

$$\sum_{n}^{\infty\,\prime}\sum_{l\neq m}^{\infty\,\prime}\frac{x_{0l}x_{ln}x_{n0}\Delta x_{n0}}{D_{lnn}^{-1}}=-\sum_{n}^{\infty\,\prime}\sum_{l\neq n}^{\infty\,\prime}\sum_{m\neq n}^{\infty\,\prime}\frac{\left(\frac{E_{mn}+E_{m0}}{E_{n0}}\right)}{D_{lnn}^{-1}}x_{0l}x_{ln}x_{nm}x_{m0}. \tag{7.29}$$

After switching the dummy variables $l \leftrightarrow m$ Eq. 7.29 becomes:

$$\sum_{n}^{\infty\,\prime}\sum_{l\neq m}^{\infty\,\prime}\frac{x_{0l}x_{ln}x_{n0}\Delta x_{n0}}{D_{lnn}^{-1}}=-\sum_{n}^{\infty\,\prime}\sum_{m\neq n}^{\infty\,\prime}\sum_{l\neq n}^{\infty\,\prime}\frac{\left(\frac{E_{ln}+E_{l0}}{E_{n0}}\right)}{D_{mnn}^{-1}}x_{0m}x_{mn}x_{nl}x_{l0}. \tag{7.30}$$

7.2.4 The dipole-free expression for the diagonal term of the second hyperpolarizability

By collecting all the terms (Eqs. 7.27, 7.28 and 7.30) the general compact sum-over-states dipole free expression for the diagonal term of the second hyperpolarizability is given by:

$$\begin{aligned}&\frac{\gamma_{xxxx}(-\omega_\sigma;\omega_1,\omega_2,\omega_3)}{e^4}= \\ &\sum_{n}^{\infty\,\prime}\sum_{m\neq n}^{\infty\,\prime}\sum_{l\neq n}^{\infty\,\prime}\left\{\frac{\left(\frac{E_{mn}+E_{m0}}{E_{n0}}\right)\left(\frac{E_{ln}+E_{l0}}{E_{n0}}\right)}{D_{nnn}^{-1}}-\frac{\left(\frac{E_{ln}+E_{l0}}{E_{n0}}\right)}{D_{mnn}^{-1}}\right\}x_{0m}x_{mn}x_{nl}x_{l0}+ \\ &\sum_{n}^{\infty\,\prime}\sum_{m\neq n}^{\infty\,\prime}\sum_{l\neq m}^{\infty\,\prime}\left\{\frac{1}{D_{lmn}^{-1}}-\frac{\left(\frac{E_{lm}+E_{l0}}{E_{m0}}\right)}{D_{mmn}^{-1}}\right\}x_{0l}x_{lm}x_{mn}x_{n0}-\sum_{nm}^{\infty\,\prime}\frac{x_{0m}x_{m0}x_{0n}x_{n0}}{D_{mn}^{-1}}.\end{aligned} \tag{7.31}$$

Since it is more desirable to work with energy differences with respect to

the ground state, E_{n0}, than with energy differences respect to each other, E_{nm}, it is convenient to rewrite the dipole-free diagonal component of the second hyperpolarizability as:

$$\frac{\gamma_{xxxx}(-\omega_\sigma;\omega_1,\omega_2,\omega_3)}{e^4} = \tag{7.32}$$
$$\sum_n^{\infty\,\prime}\sum_{m\neq n}^{\infty\,\prime}\sum_{l\neq n}^{\infty\,\prime}\left\{\frac{\left(\frac{2E_{m0}-E_{n0}}{E_{n0}}\right)\left(\frac{2E_{l0}-E_{n0}}{E_{n0}}\right)}{D_{nnn}^{-1}}-\frac{\left(\frac{2E_{l0}-E_{n0}}{E_{n0}}\right)}{D_{mnn}^{-1}}\right\}x_{0m}x_{mn}x_{nl}x_{l0}+$$
$$\sum_n^{\infty\,\prime}\sum_{m\neq n}^{\infty\,\prime}\sum_{l\neq m}^{\infty\,\prime}\left\{\frac{1}{D_{lmn}^{-1}}-\frac{\left(\frac{2E_{l0}-E_{m0}}{E_{m0}}\right)}{D_{mmn}^{-1}}\right\}x_{0l}x_{lm}x_{mn}x_{n0}-\sum_m^{\infty\,\prime}\sum_n^{\infty\,\prime}\frac{x_{0m}x_{m0}x_{0n}x_{n0}}{D_{mn}^{-1}}.$$

Bibliography

[1] M. G. Kuzyk, Phys. Rev. A **72**, 53819 (2005).

Chapter 8

Off-resonance limits of the first hyperpolarizability: the quantum gap

In chapter 7 the dipole-free expressions for the first and second hyperpolarizability were introduced. Here we will illustrate how the sum rules are applied to obtain the maximum allowed value of the diagonal component of the first hyperpolarizability in the off-resonance regime, β_{xxx}, under some general assumptions.

The existence of the quantum limits was first determined by M. G. Kuzyk.[1, 2, 3, 4, 5]. Soon after the existence of the fundamental limits was established, a survey of the largest second-order molecular susceptibilities showed that there is a universal gap between the best experimental values and the fundamental limits.[1, 2, 3, 4, 5]

The nature of this universal gap was investigated - in collaboration with Kakoli Tripathy and Mark G. Kuzyk from the Department of Physics in Washington State University; Benjamin J. Coe from the Department of Chemistry in University of Manchester; Koen Clays from the Department of Chemistry in University of Leuven and Anne Myers Kelley from the School of Natural Sciences in University of California -. The theoretical results, linear spectroscopy,

Raman spectroscopy and experimentally measured values of the first hyperpolarizability were integrated and compared and the effects of energy spacing and oscillator strength upon the molecules were determined.[6, 7] Here we present the results and later we will explore different hypothesis that could explain the existence of the gap: dilution effects due to the vibrational states are shown to be negligible in Chapter 10 and a theoretical physical system with first hyperpolarizability above the gap is presented in Chapter 9.

The conclusions of this first study are presented here.

8.1 The off-resonance dipole-free first hyperpolarizability

In chapter 7.17 the dipole-free expression for the diagonal term of the first hyperpolarizability was derived (Eq. 7.17):

$$\begin{aligned}&\beta_{xxx}(\omega_\sigma;\omega_1+\omega_2)= \\ &-e^3{\sum_n}'{\sum_{m\neq n}}'\frac{x_{0n}x_{nm}x_{m0}}{D_{nm}^{-1}(\omega_1,\omega_2)}\left(1-\frac{D_{nm}^{-1}(\omega_1,\omega_2)}{D_{nn}^{-1}(\omega_1,\omega_2)}\left\{2\frac{E_{m0}}{E_{n0}}-1\right\}\right).\end{aligned} \tag{8.1}$$

In the off-resonance regime, the dispersion terms $D_{nm}(\omega_1,\omega_2)$ are simplified to:

$$D_{nm}=\frac{3}{E_{n0}E_{m0}} \tag{8.2}$$

since, by assumption, the off-resonance regime is defined through:

$$\hbar\Omega_{n0} \approx E_{n0}, \tag{8.3}$$

$$E_{n0} \gg \hbar\omega_1, \tag{8.4}$$

and

$$E_{n0} \gg \hbar\omega_2. \tag{8.5}$$

Therefore, in the off-resonance regime, the frequency independent diagonal term of the first hyperpolarizability is written as:

$$\beta_{xxx} = -e^3{\sum_n}'{\sum_{m\neq n}}'\frac{x_{0n}x_{nm}x_{m0}}{D_{nm}^{-1}}\left(1-\frac{D_{nm}^{-1}}{D_{nn}^{-1}}\left\{2\frac{E_{m0}}{E_{n0}}-1\right\}\right)$$

$$
\begin{aligned}
&= -3e^3 {\sum_n}' {\sum_{m\neq n}}' \frac{x_{0n}x_{nm}x_{m0}}{E_{n0}E_{m0}} \left(1 - \frac{E_{n0}E_{m0}}{E_{n0}} \left\{ 2\frac{E_{m0}}{E_{n0}} - 1 \right\} \right) \\
&= -3e^3 {\sum_n}' {\sum_{m\neq n}}' x_{0n}x_{nm}x_{m0} \left(1 - \frac{E_{m0}(2E_{m0} - E_{n0})}{E_{n0}^2}\right). \qquad (8.6)
\end{aligned}
$$

Eq. 8.6 can be expressed in a more compact manner if the transition dipole moments x_{mn} are real. This is equivalent to assume that the unperturbed hamiltonian of the system is conservative and non degenerate[1], which applies quite generally to many quantum mechanical systems, such as organic chromophores. Using the reality of the transition dipole moments ($x_{0n}x_{nm}x_{m0} = x_{0m}x_{mn}x_{n0}$), Eq. 8.6 can be rearranged to:

$$
\frac{\beta_{xxx}}{3e^3} = {\sum_n}' {\sum_{m>n}}' x_{0n}x_{nm}x_{m0} \times \mathbf{D}_{mn}^{(\mathrm{off})}, \qquad (8.7)
$$

where we have defined the strictly positive energy factors $\mathbf{D}_{mn}^{(\mathrm{off})}$ through:

$$
\mathbf{D}_{mn}^{(\mathrm{off})} = \frac{(E_{m0} - E_{n0})^2(2E_{m0}^2 + 3E_{m0}E_{n0} + 2E_{n0}^2)}{E_{m0}^3 E_{n0}^3} \qquad (8.8)
$$

It should be noticed that Eq. 8.7 takes already into account all the relationships derived from the generalized Thomas-Kuhn sum rule (Eq. 6.14) when $k \neq l$:

$$
\sum_n (2E_{n0} - E_{k0} - E_{l0}) x_{kn}x_{nl} = 0. \qquad (8.9)
$$

The remaining sum rules ($k = l$) provide further relationships between the energies and the transition dipole moments:

$$
\sum_n (E_{n0} - E_{k0}) |x_{nk}|^2 = \frac{\hbar^2 N}{2m}. \qquad (8.10)
$$

Therefore, the quest for a quantum mechanical system that optimizes the second order nonlinear response is directly related to the mathematical problem of optimizing the first hyperpolarizability (Eq. 8.7)as a function of $\{E_{nk}\}$ and $\{x_{nk}\}$ with a set of constraints provided by Eq. 8.10.

[1] See appendix A.

8.2 The three level ansatz

In principles the sums in Eqs. 8.7, 8.9 and 8.10 should be carried over all the available bound states of the system. However, not necessarily all states contribute to the nonlinear response. By inspection of Eq. 8.7, it is clear that two states $|n\rangle$ and $|m\rangle$, contribute to β_{xxx} only if the following conditions are satisfied simultaneously:

$$\begin{aligned} \langle n|x|0\rangle &\neq 0, && (8.11)\\ \langle m|x|0\rangle &\neq 0, && (8.12)\\ &\text{and} && (8.13)\\ \langle m|x|n\rangle &\neq 0. \end{aligned}$$

Now we consider a quantum system where only a finite number of states, N_S, contribute to the response with an off-resonance first hyperpolarizability that can be written as:

$$\frac{\beta_{xxx}}{3e^3} = \sum_{n}^{N_S\,'} \sum_{m>n}^{N_S\,'} x_{0n}x_{nm}x_{m0} \times \mathbf{D}_{mn}^{(\text{off})}. \tag{8.14}$$

As in Eq. 8.14 m must be greater than n at all times, when $n = N_S$ there is no contribution to the sum. Hence, is convenient to explicitly carry on the sum over n only to the $N_S - 1$ term as follows:

$$\frac{\beta_{xxx}}{3e^3} = \sum_{n}^{N_S-1\,'} \sum_{m>n}^{N_S\,'} x_{0n}x_{nm}x_{m0} \times \mathbf{D}_{mn}^{(\text{off})}. \tag{8.15}$$

Since we want to optimize the magnitude of β_{xxx} we can write:

$$|\beta_{xxx}^{(N_s)}| \leq 3e^3 \sum_{n}^{N_s-1\,'} \sum_{m>n}^{N_s\,'} |x_{0n}||x_{nm}||x_{m0}| \times \mathbf{D}_{mn}^{(\text{off})}, \tag{8.16}$$

where we have used the fact that $\mathbf{D}_{mn}^{(\text{off})}$ are strictly positive quantities.

Now, if we inspect Eq. 8.16, we can deduce that the minimum number of contributed states that are required to generate a nonzero first hyperpolarizability is three: ground state $|0\rangle$, first excited state, $|1\rangle$ and second excited state, $|2\rangle$.

Therefore, we will adopt the **three level ansatz**, by assuming that *at most two excited states contribute to the molecular susceptibilities when the molecule optimizes the nonlinear response.*[8]

8.3 The quantum limits

The fundamental limit of the diagonal components of the first hyperpolarizability in the off-resonance regime can be evaluated using the method first derived by M. G. Kuzyk.[8] From Eq. 8.16 taking $N_s = 2$ (which means that only a total of three states contribute to the response) the diagonal component of the first hyperpolarizability reduces to:

$$|\beta_{xxx}^{(N_s=2)}| \equiv |\beta_{xxx}^{(3L)}| \leq 3e^3 {\sum_{n}^{1}}' {\sum_{m>n}^{2}}' |x_{0n}||x_{nm}||x_{m0}| \times \mathbf{D}_{mn}^{(\text{off})} =$$

$$3e^3 {\sum_{m>1}^{2}}' |x_{01}||x_{1m}||x_{m0}| \times \mathbf{D}_{m1}^{(\text{off})} = 3e^3 |x_{01}||x_{12}||x_{20}| \times \mathbf{D}_{21}^{(\text{off})}. \quad (8.17)$$

Notice that we use the superscript $(3L)$ as a reminder on how the nonlinear response is dominated by three states.

Now we are going to make use of the conditions that are imposed by some of the remaining sum rules. First, we take $k = 0$ in Eq. 8.10 to get:

$$\begin{aligned} E_{20}|x_{20}|^2 &= \frac{\hbar^2 N}{2m} - E_{10}|x_{10}|^2 - \sum_{i=3}^{N_s} E_{i0}|x_{i0}|^2 \\ E_{20}|x_{20}|^2 &\leq \frac{\hbar^2 N}{2m} - E_{10}|x_{10}|^2 = E_{10}\left(\frac{\hbar^2 N}{2mE_{10}} - |x_{10}|^2\right), \end{aligned} \quad (8.18)$$

or:

$$|x_{20}| \leq \sqrt{\frac{E_{10}}{E_{20}}\,(x_{max}^2 - |x_{10}|^2)}, \quad (8.19)$$

where we have used the fact that the transition dipole moment to the first excited state has a maximum imposed by the sum-rules (Eq. 8.10 with $k = 0$):

$$\mu_{max}^2 = e^2 x_{max}^2 = e^2 \frac{\hbar^2 N}{2mE_{10}}. \quad (8.20)$$

Similarly, by taking $k = 1$ in Eq. 8.10 we obtain:

$$|x_{21}| \leq \sqrt{\frac{E_{10}}{(E_{20} - E_{10})} (x_{max}^2 + |x_{10}|^2)}. \tag{8.21}$$

Therefore, we use Eqs. 8.19 and 8.21 to strictly set the inequality from Eq. 8.17:

$$|\beta_{xxx}^{(3L)}| \leq 3e^2|x_{10}| \sqrt{\frac{E_{10}^2}{E_{20}(E_{20} - E_{10})} (x_{max}^4 - |x_{10}|^4)} \times \mathbf{D}_{21}^{(\text{off})}, \tag{8.22}$$

with

$$\mathbf{D}_{21}^{(\text{off})} = \frac{(E_{20} - E_{10})^2(2E_{20}^2 + 3E_{20}E_{10} + 2E_{10}^2)}{E_{20}^3 E_{10}^3}. \tag{8.23}$$

At this point we should introduce the following dimensionless quantities:

$$E \equiv \frac{E_{10}}{E_{20}}, \tag{8.24}$$

and

$$X \equiv \frac{|x_{01}|}{|x_{max}|} = \frac{|x_{01}|}{\sqrt{\frac{\hbar^2 N}{2mE_{10}}}}. \tag{8.25}$$

Notice that by definition, X and E are positive:

$$0 \leq X \leq 1, \tag{8.26}$$

$$0 \leq E \leq 1. \tag{8.27}$$

We can now rewrite Eq. 8.22 in terms of the dimensionless quantities X and E:

$$\beta_{xxx} \equiv |\beta_{xxx}^{(3L)}| \leq \beta_0 f(E) G(X), \tag{8.28}$$

where we have defined the dimensionless functions $f(E)$ and $G(X)$ through:

$$f(E) \equiv \frac{1}{2}(1 - E)^{3/2}(2 + 3E + 2E^2), \tag{8.29}$$

$$G(X) \equiv \sqrt[4]{3} X \sqrt{\frac{3}{2}(1 - X^4)}, \tag{8.30}$$

and β_0 has the same dimensions as the first hyperpolarizability and given by:

$$\beta_0 = 3\sqrt{\frac{2}{3}} \frac{1}{\sqrt[4]{3}} \frac{e^3|x_{max}|^3}{E_{10}^2} = \sqrt[4]{3} \left(\frac{e\hbar}{\sqrt{m}}\right)^2 \left[\frac{N^{3/2}}{E_{10}^{7/2}}\right]. \tag{8.31}$$

Now, assuming that the parameters E and X are independent, β_{xxx} is optimized when $f(E)$ and $G(X)$ are optimized independently. From Eqs. 8.29 and 8.30 we can find the maximum values:

$$f_{max} = f(0) = 1, \tag{8.32}$$

and

$$G_{max} = G(3^{-1/4}) = 1. \tag{8.33}$$

Therefore, the equality is reached in Eq. 8.28 (and hence the maximum value of β_{xxx}) when $X \to 3^{-1/4}$ and $E \to 0$, with:

$$\beta_{xxx}^{max} = \lim_{E \to 0} \left(\lim_{X \to 3^{-1/4}} \{\beta_{xxx}(E, X)\} \right) = \beta_0. \tag{8.34}$$

8.4 Consistency of the equations and level truncation

To calculate the quantum limits we used the three level ansatz and truncated the infinite sum in the expression for the first hyperpolarizability to three contributing states.

This, however, does not mean that the sum-rules have been truncated to three levels. As it can be seen by examining Eqs. 8.19 and 8.21, the contribution of the other states is taken into account by using inequalitities. Thus, mathematically, the maximum value of the first hyperpolarizability (Eq. 8.17) is achieved when only three-states are contributing to the response.

In this sense, the quantum limits are very likely the maximum values that can be achieved. Since evidence supports the quantum limits results, the three-level ansatz must hold for most organic chromophores.

The extension of the quantum limits to analyze the molecular performance works better with quantum mechanical systems where three states dominate the response. This does not mean that other states can not be present, but the information gathered through the analysis is based on the behavior of the dominant part of the first hyperpolarizability. When the values of functions like $f(E)$ or $G(X)$ are far from being optimized, it is not possible to determine if there are only two excited states contributing in a very inefficient manner, or if the response has been diluted through the existence of more than two domi-

nant states. Therefore, when the molecules are far away from optimization, the three-level model is used as a proxy that gives some insight of physical processes behind the response.

The conditions under which the "three level ansatz" holds have been investigated. The consistency of the generalized Thomas-Kuhn sum rules truncated to three levels was first studied in my Master's dissertation,[9] in 2004. In this study it was found that truncating the sum-rules to only three-levels could generate sets of inconsistent equations, and experimental evidence was used to rule out inconsistent equations. This type of approach was not very satisfactory since indeed assumed that the sum rules were truncated to only three levels, and was questioned by B. Kirtman and B. Champagne first,[10] and then discussed by M. G. Kuzyk.[11] Later (in 2006), M. G. Kuzyk used the dipole-free expression for the first hyperpolarizability to show that the truncation of the first hyperpolarizability to three contributing levels does not mean that the sum-rules have also been truncated.[8]

Yet, since the "three level ansatz" plays an very important role in the calculation of the quantum limits, the effects of level truncation in both the first hyperpolarizability and the Thomas-Kuhn sum rules must be evaluated in order to derive the mathematical conditions under which the "three level ansatz" is obeyed.

However, it is important to keep in mind that by adopting the "three level ansatz" we are not claiming that real molecules have only three quantum states. For example in , B. Champagne and B. Kirtman studied how the traditional sum-over-states expression and the dipole free expression for the first hyperpolarizability differ when the infinite sums are truncated.[12] In this study, it was found that the expressions might differ when not enough significant excited states are included in the sums. This result, however, does not necessarily contradict the "three-level ansatz". In order to obtain an accurate expression for the first hyperpolizability that is expressed as a sum over states, we need to include all the excited levels that contribute significantly to the sum. What the "three level ansatz" implies is that molecules where only three significant states contribute to the response can have better first hyperpolarizabilities than molecules where more than three states contribute significantly to the nonlinear response.

8.5 Molecular performance and the quantum gap

The existence of the quantum limit provides a very useful (and practical) way of evaluating the non linear performance of a molecule.

First, we notice the scaling of the limit with the number of electrons:

$$\beta_{xxx}^{max} \propto N^{3/2}. \tag{8.35}$$

This means that if two molecules are optimized, the one with the maximum number of electrons contributing to the response will have a higher first hyperpolarizability. With organic chromophores, where the response is generated by the delocalized π-electrons, the number of contributing electrons is evaluated by geometrically weighting the number of electrons in *each independent conjugated* path of the molecule,[13]

$$N_{eff} = (\sum_i N_i^{3/2})^{2/3}, \tag{8.36}$$

where N_i is the number of electrons in the i^{th} conjugated part of the molecule. This method for counting electrons is most appropriate for excitations that are typical in conjugated molecules and was proposed by H. Kuhn in 1949 in his theoretical study of the light absorption of organic dyes.[14] For other systems or other types of excitations, an appropriate method for counting electrons would need to be used.

If we want to compare the performance of two different molecules, rather than comparing the values of the first hyperpolarizabilities, we should compare $\frac{\beta_{xxx}}{N^{3/2}}$, which gets rid of the electron dependence and truly informs us about the influence of the structural properties of the molecule in the nonlinear response.

We also notice that if our original assumption that at most two excited states contribute to the response when the molecules are optimized is not obeyed, (that is, if the *three level ansatz* where not true), we might expect to find that at least some real molecules have values of $\frac{\beta_{xxx}}{N^{3/2}}$ above the quantum limit. This would indicate that for those molecules, the energy arrangement and the spread of the oscillator strength through more states results in better first hyperpolarizabilities that can not be realized when only three states contribute to the response.

The first comparison between experimental first hyperpolarizabilities and

the quantum limits was performed by M. G. Kuzyk, where he studied the performance of organic molecules based on EFISH measurements.[1, 3] From a large survey of the best molecules known at the time of the study, it was found that all molecules fall below than the quantum limit by a factor of $10^{-3/2}$. This result is presented in Fig. 8.1 The upper solid curve represents the electron-normalized "dressed" fundamental limit $\frac{\beta^*_{xxx}}{N^{3/2}}$ as a function of wavelength of maximum absorbance, λ_{max} (recall that $E_{10} \sim \frac{1}{\lambda_{max}}$). The grey dots represent the experimentally measured values of the molecules considered in this study.[1, 3, 6, 7]

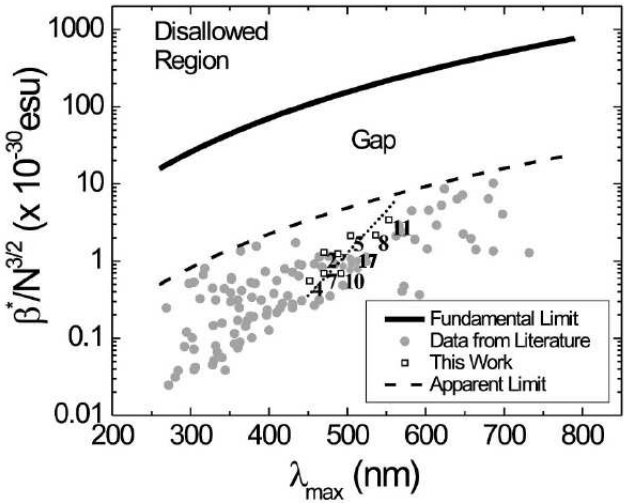

Fig. 8.1: Electron-normalized "dressed" first hyperpolarizability, as a function of wavelength of maximum absorbance of the first excited state for the experimentally measured values of the molecules using EFISH (points),[2] electron-normalized "dressed" fundamental limit (upper solid curve), the apparent limit (dashed curve),[5] and the electron-normalized first hyperpolarizabilities of the molecules studied in this chapter (squares). The dotted line shows the trend of our data.

As previously mentioned, the molecules fall bellow the fundamental limit by at least a factor of $10^{-3/2}$. This defines the *"apparent limit"* (dotted line). The area between the "apparent limit" and the quantum limit is refereed to as "the quantum gap". The "apparent limit" parallels the fundamental limit, suggesting, perhaps, the existence of further constraints that lower the response. With the aim of investigating the nature of the "quantum gap" determining whether or not the "apparent limit" was unreachable, we studied a series of molecules that approach the gap. The structure of the molecules is shown in Fig. 8.2.

The quantum limits theory was used to study the nature of the nonlinear

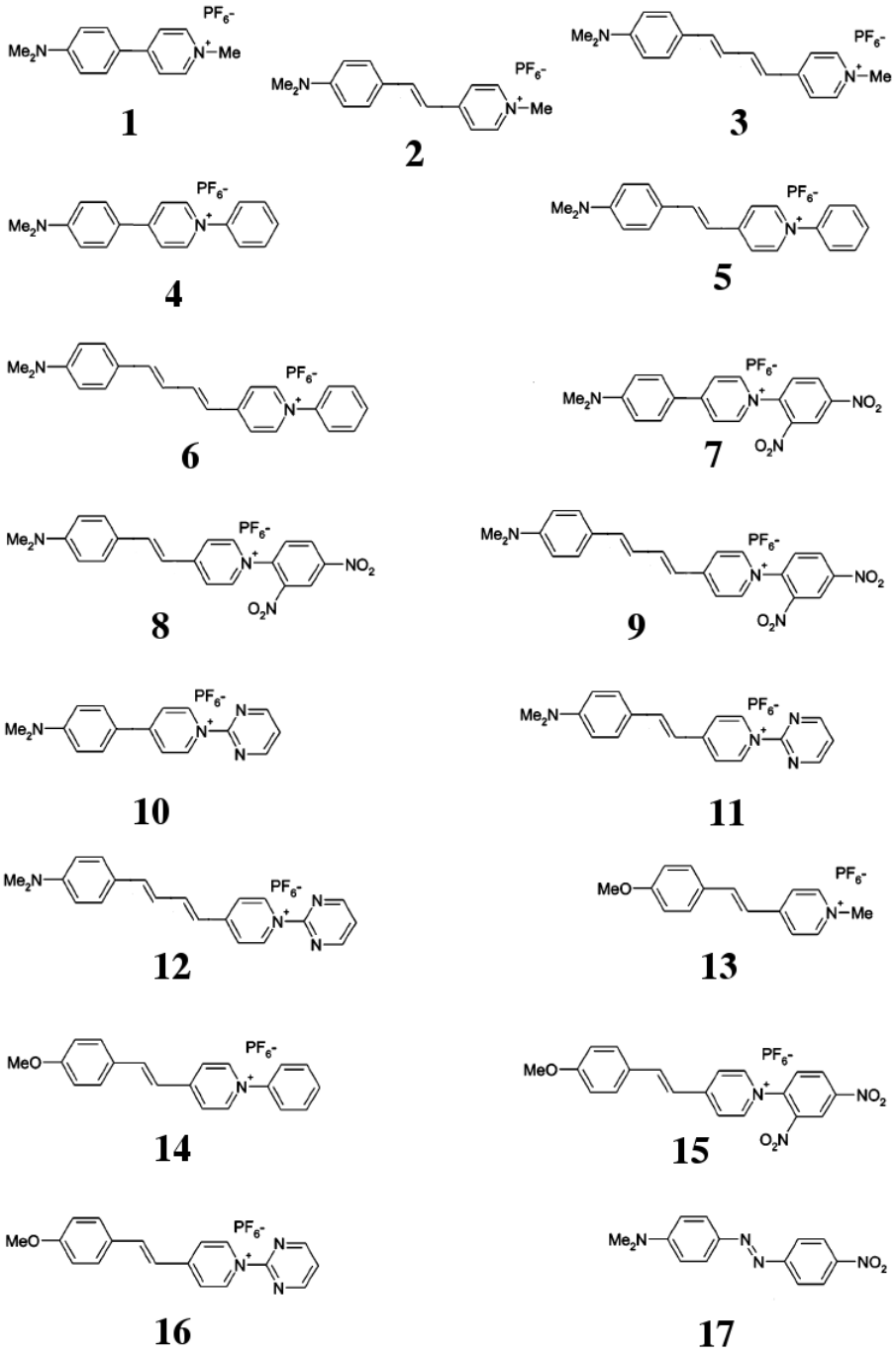

Fig. 8.2: Molecular structure of the molecules studied in this chapter.

response in the following manner:

- The first excited energy, E_{10}, and the transition dipole moment between ground and first excited state $|x_{10}|$ can be obtained from linear absorption spectroscopy.
- The quantum limit value $\beta_{xxx}^{max} = \beta_0$ is calculated from the value of the first excited energy E_{10} and the number of effective electrons N_{eff}.
- The experimental values of β_{xxx} for each molecule is obtained through HRS measurements.
- The dimensionless parameter X is obtained also through Eq. 8.25 once $|x_{10}|$, E_{10} and N are known.
- The value of the function $G(X)$ is found by substituting X into Eq. 8.30.
- Finally, by using Eq. 8.28 the energy function $f(E)$ is found and then the value of E is obtained by substituting into Eq. 8.29

8.6 Analysis of the linear absorption

The linear absorption spectrum of each sample was measured by passing a broad spectrum source of light through a solution containing the molecule in a cuvette with a path length of 1 cm. The transmitted spectrum was measured with an Ocean Optics spectrometer and the absorbance is found by comparing the transmitted light through the sample to a cuvette without a solution.

The oscillator strength is related to the area under the absorption spectrum through:[6, 7]

$$\frac{1}{N_d L}\int_0^\infty A(E_p)dE_p = \left(\frac{4\pi^2 \log(e)}{3\hbar c}\right)\sum_{n=1}^{\infty} E_{n0}\left|\mu_{n0}^*\right|^2, \tag{8.37}$$

where N_d is the number density of chromophores in solution (in units of $\frac{\text{molecules}}{cm^3}$), L is the path length (in cm), $A(E_p)$ is the absorbance as a function of the photon energy, E_p, and $\mu_{n0}^* = ex_{n0}^*$ is the "dressed" transition dipole moment and c is the speed of light. $A(E_p)$ is defined as:

$$A(E_p) = \log\frac{I(E_p)}{I_0(E_p)}, \tag{8.38}$$

where $I(E)$ is the transmitted intensity while $I_0(E_p)$ is the incident intensity.The "dressed" transition dipole moment is related to the vacuum dipole through the local field factors, as introduced in Chapter 5 (Section 5.5):

$$x^*_{n0} = \left(\frac{\epsilon + 2}{3}\right) x_{n0} \tag{8.39}$$

If we use units of eV for the values of E_p, the area under the first peak in a absorption spectrum is then related to the "dressed" transition dipole moment between the ground state and the first excited state (in units of debye) through:

$$|\mu^*_{10}|^2 = \frac{0.55 \times 10^{19}}{N_d L E_{10}} \int_0^\infty A(E_p) dE_p. \tag{8.40}$$

When the peaks are not always well separated the true area due to only one state must be estimated. A fit of the peak to a full Gaussian does not fit the data well due to the asymmetry introduced by the tail of other states. The area of an individual peak was calculated by doing a multiple peak fit to the data and taking the sum of their areas.

From the linear absorption measurements, E_{10} and $|\mu_{10}|$ where determined, and then the parameter X can be evaluated. The results of this analysis (on the molecules shown in Fig. 8.2) are listed in Table 8.1. The asterisks in the first column denote the molecules for which hyperpolarizability measurements were taken using either HRS or electrochromism. The uncertainty was determined from the standard deviation of several measurements. The normalized transition dipole moment X is calculated by dividing the measured transition moment by the calculated maximum transition dipole moment (Eq. 8.25). $G(X)$ is evaluated from X using Eq. 8.30.

Figure 8.3 shows a plot of the values from Table 8.1. The dashed curve is the theoretical curve given by Eq. 8.30 and the points represent the experimental data. The inset shows the normalized transition moment of each molecule plotted as a function of its wavelength of maximum absorption. For this set of molecules, $G(X)$ lies between the values of 0.4 and 0.6, which is consistent with our calculations that demand $G(X) \leq 1$ for all molecular systems.

Molecule	N_{eff}	E_{10}(eV)	μ_{10}(D)	μ_{10}^{max}(D)	X	$G(X)$
1∗	12	2.93	5.95(±0.17)	18.9	0.315	0.505
2∗	14	2.61	9.32(±0.07)	21.7	0.429	0.680
3∗	16	2.55	8.457(±0.007)	23.5	0.360	0.575
4∗	18	2.76	6.65(±0.04)	23.9	0.278	0.447
5∗	20	2.45	10.974(±0.014)	26.7	0.411	0.653
6∗	22	2.54	9.02(±0.10)	28.6	0.315	0.506
7∗	22	2.64	9.33(±0.09)	27.0	0.345	0.553
8∗	24	2.3	9.74(±0.04)	30.2	0.323	0.517
10∗	18	2.45	9.52(±0.09)	24.9	0.382	0.609
11∗	20	2.24	10.42(±0.20)	28.0	0.372	0.594
14∗	20	3.06	8.00(±0.04)	23.9	0.335	0.536
15	24	2.95	9.13(±0.07)	26.7	0.342	0.547
16	20	2.89	7.884(±0.014)	24.6	0.321	0.514
17	16	2.53	8.613(±0.014)	23.5	0.367	0.586

Table 8.1: Summary of linear absorption measurements and calculated quantities. The asterisks in the first column denote the molecules for which hyperpolarizability measurements were taken using either HRS or electrochromism.

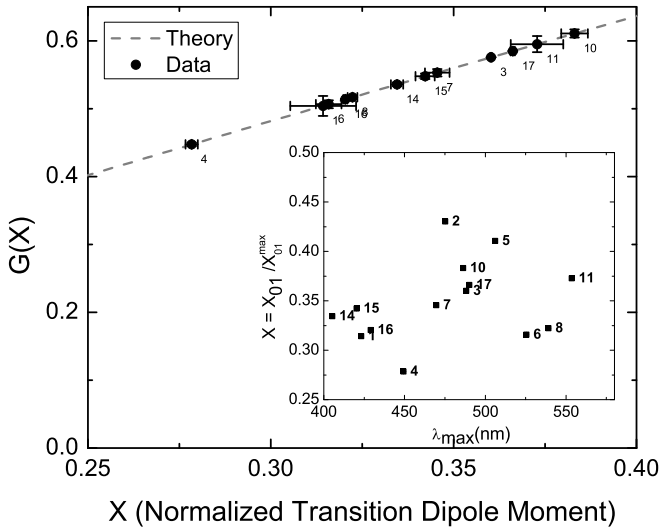

Fig. 8.3: $G(X)$ as a function of the normalized transition dipole moment (the theoretical curve is dashed, while points show measured values).

Molecule	β_{exp} $\left(\times 10^{-30}\ cm^5 \cdot esu^{-1}\right)$	β^{max} $\left(\times 10^{-30}\ cm^5 \cdot esu^{-1}\right)$	β_{exp}/β^{max}	$f(E)$
2	68(±11)	2162	0.031(±0.005)	0.046(±0.008)
3	164(±16)	2906	0.056(±0.006)	0.098(±0.010)
4	23(±4)	2593	0.089(±0.015)	0.019(±0.004)
5	112(±11)	4608	0.024(±0.002)	0.037(±0.004)
6	311(±30)	6061	0.051(±0.005)	0.101(±0.011)
7	29(±5)	4094	0.0071(±0.0012)	0.013(±0.002)
8	114(±10)	7557	0.015(±0.001)	0.029(±0.003)
10	29(±5)	3421	0.008(±0.002)	0.014(±0.003)
11	180(±13)	6306	0.029(±0.002)	0.048(±0.004)
17	47(±6)	2906	0.016(±0.002)	0.028(±0.004)

Table 8.2: Summary of nonlinear measurements and calculated quantities. Note that the experimental value of the hyperpolarizability is converted to the vacuum value with a Lorentz local field model.

8.7 Characterization of the energy function $f(E)$ from the Hyper-Rayleigh scattering measurements

The vacuum values for the first hyperpolarizability obtained through Hyper-Rayleigh scattering characterizations, β_{exp} are listed in Table 8.2. The values of β_{xxx} are obtained by extrapolation of the experimental results using the two-level model.[15]

The value of β_{xxx}^{max} is obtained once N and E_{10} are known (Eqs. 8.34 and 8.31). From Eq. 8.34 we can isolate $f(E)$ as:

$$f(E) = \frac{1}{G(X)} \frac{\beta_{exp}}{\beta_{xxx}^{max}}. \tag{8.41}$$

The values of are listed in Table 8.2.

Figure 8.4 plots the values of $f(E)$ as a function of $G(X)$. The values of β_{exp} listed in Table 8.2 were obtained from Hyper-Rayleigh scattering measurements (points) with the exception of two points that were determined through Stark spectroscopy (open circles).[2] The values of $f(E)$ determined from Stark spectroscopy measurements appear to be systematically higher than the values

determined with Hyper-Rayleigh scattering measurements. HRS is a more direct measure of the first hyperpolarizability than Stark spectroscopy. Coe and coworkers measured the hyperpolarizabilities of molecules 4 and 10 using HRS and compared the results from Stark spectroscopy.[16] It was found that Stark spectroscopy overestimated the first hyperpolarizability by a factor of three. Once these values are corrected they are consistent with the rest of the data measured through HRS. The open squares in Fig. 8.4 indicates how the Stark spectroscopy data was adjusted by a factor of three. The dashed line shows $f(E) = 10^{-3/2}$, which is the numerical value of the "apparent" limit.

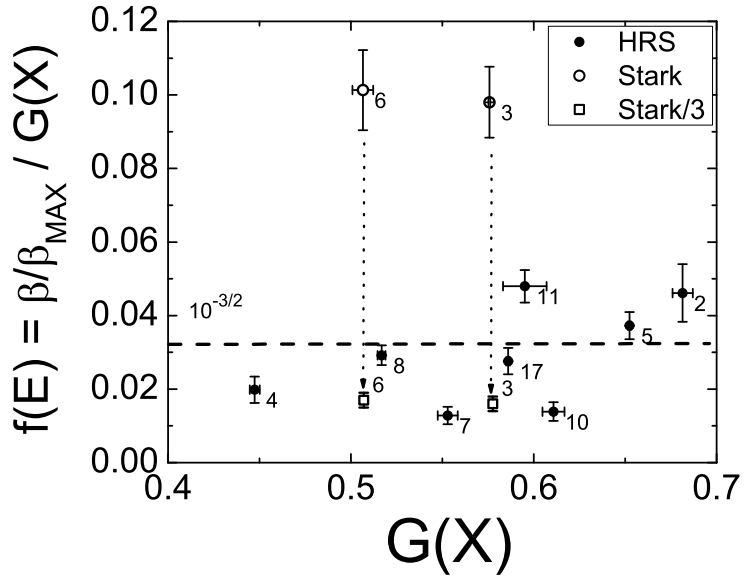

Fig. 8.4: $f(E)$ as a function of $G(X)$.

If we compare the Fig. 8.3 with 8.4 we can deduce that most of the variation on the electron-normalized first hyperpolarizability $\frac{\beta_{xxx}}{N^{3/2}}$ are due to variations in the energy spacing distribution. While the values of $G(X)$ range only from 0.4 to 0.6, we can see that $f(E)$ is never greater than 0.05. Therefore, if the performance of nonlinear molecules has to be improved, one should focus on improving the energy distribution, since there is still a lot of room for improvement, while the values of $G(X)$ are already on the order of unity. If we were able to change the energy spacing distribution of molecules so $f(E) \approx 1$, their values of β_{xxx} would increase by a factor of ≈ 20.

At this time we considered three possible scenarios that might explain why the energy distribution of organic molecules is far away from optimization:

1. The energy distribution is far from optimization due to the effects of vibrational contributions. While the optimized response was calculated considering only the motion of the electronic cloud, the existence of spacing between dominant vibronic states (associated with the nuclear motion) result in a dramatic decrease of the first hyperpolarizability.

2. Real molecules might have more than three contributing states, and therefore are far away from optimization.

3. There may be some other fundamental quantum constraints that have not yet been taken into account and result in a decrease of the fundamental limit by a factor of $10^{3/2}$.

In Chapter 9 we will introduce the "clipped harmonic oscillator", a quantum mechanical system with a vacuum first hyperpolarizability that is well above the "apparent" limit but falls below the fundamental limit. Thus, we can rule out the idea that another fundamental constraint prevents quantum systems from being in the gap.

In Chapter 10, the dilution effects of vibrational states in the first hyperpolarizability are considered. The study shows that the vibrational states are not responsible for the failure of real molecules to reach the gap.

Bibliography

[1] M. G. Kuzyk, Phys. Rev. Lett. **85**, 1218, (2000).

[2] M. G. Kuzyk, Opt. Lett. **25**, 1183, (2000).

[3] M. G. Kuzyk, Phys. Rev. Lett. **90**, 39902, (2003).

[4] M. G. Kuzyk, Opt. Lett. **28**, 135, (2003).

[5] M. G. Kuzyk, IEEE J. Select. Topics Quantum Electron. **7**, 774, (2001).

[6] K. Tripathy, J. Pérez-Moreno, M. G. Kuzyk, B. Coe, K. Clays and A. M. Kelley, J. Chem. Phys. **121**, 7932 (2004).

[7] K. Tripathy, J. Pérez-Moreno, M. G. Kuzyk, B. Coe, K. Clays and A. M. Kelley, J. Chem. Phys. **125**, 79905 (2006).

[8] M. G. Kuzyk, J. Chem. Phys. **125**, 154108 (2006).

[9] J. Pérez-Moreno, "Quantum limits of the nonlinear optical response", *M.S. Thesis* , Washington State University, Department of Physics. August 2004.

[10] B. Champagne and B. Kirtman, Phys. Rev. Lett. **95**, 109401 (2005).

[11] Phys. Rev. Lett. **95**, 109402 (2005)

[12] B. Champagne and B. Kirtman, J. Chem. Phys. **125**, 24101 (2006).

[13] M. G. Kuzyk, J. Chem. Phys. **119**, 8327 (2003).

[14] H. Kuhn, J. Chem. Phys. **17**, 1198 (1949).

[15] J. L. Oudar and D. S. Chemla, J. Chem. Phys. **66** 2664 (1977).

[16] B. J. Coe, J. A. Harris, K. Clays, A. Persoons, K. Wostyn, and B. S. Brunschwig, Chem. Commun. (Cambridge) **2001**, 1548.

Chapter 9

The clipped harmonic oscillator: a non-symmetric harmonic oscillator

The "apparent" limit was introduced in Chapter 8. One hypothesis that could explain the existence of the "apparent" gap, is that there are more fundamental constraints that prevent quantum systems to reach into the gap. Here we will introduce the "clipped harmonic oscillator", a quantum mechanical system with a vacuum first hyperpolarizability that is well above the "apparent" limit and falls below the fundamental limit.[1, 2, 3]

The following calculations were presented originally in my Master's dissertation.[4] A rather tedious description of the problem is used with the aim of clarifying the results. To calculate the first hyperpolarizability we need to compute the transition dipole moments x_{mn} for each combination of connected states. In the ordinary harmonic oscillator only adjacent levels are connected so only the "off-diagonal" elements of the form $x_{n,n+1}$ are non zero. The wavefunctions of the clipped harmonic oscillator can be determined analytically by taken the harmonic oscillator results and determining the normalization factor for the clipped harmonic oscillator. The transition dipole moments can be determined from these wavefunctions using recursion relationships.

Once the convergence of the sum over states expression for the first hyperpolarizability is confirmed we explored on how the response departed from the dominant three-states contributions.

9.1 The quantum harmonic oscillator

Since the clipped harmonic oscillator is related to the ordinary one, we consider first the quantum harmonic oscillator, as described by *Griffiths.*[5] Apart from the theoretical significance of the model (since most trapping potentials can be approximated to the lowest order by a harmonic oscillator potential), parabolic quantum wells have been fabricated by the appropriate growth of $GaAs - Al_xGa_{1-x}As$ heterostructures.[6, 7, 8]

The potential of the one-dimensional infinite quantum well is given by:

$$V(x) = \frac{m\omega^2 x^2}{2}, \tag{9.1}$$

where ω is the natural frequency of the oscillator.

The eigenenergies are given by:

$$E_n = \hbar\omega(n + 1/2), \tag{9.2}$$

with $n = 0, 1, 2, 3...$ and the transition moments are:

$$x_{n'n} = \sqrt{\frac{\hbar}{2m\omega}} \left(\sqrt{n}\delta_{n',n-1} + \sqrt{n+1}\delta_{n',n+1}\right). \tag{9.3}$$

Unfortunately, the potential of the harmonic oscillator is invariant under the transformation $x \rightarrow -x$ (the harmonic oscillator is centrosymmetric with respect to the origin, $x = 0$) so the off-resonance second order molecular susceptibility vanishes. It would be convenient to find a quantum system that behaves similarly to the harmonic oscillator but that is noncentrosymmetric, with the hope that β_{xxx} falls inside the gap between measured organic molecules and the limit provided by the three-level model [3]. The clipped harmonic oscillator is asymmetric, yet has the large transition moments and large energy spacing of the harmonic oscillator. As such, we chose this system as an exactly solvable one that has an infinite number of levels to test our hypothesis that the apparent gap is not a fundamental one.

9.2 The clipped harmonic oscillator

The clipped harmonic oscillator is described by the following potential (see Fig. 9.1.):

$$V(x) = \begin{cases} \infty & \text{for } x < 0 \\ \frac{m\omega^2 x^2}{2} & \text{for } x \geq 0. \end{cases} \tag{9.4}$$

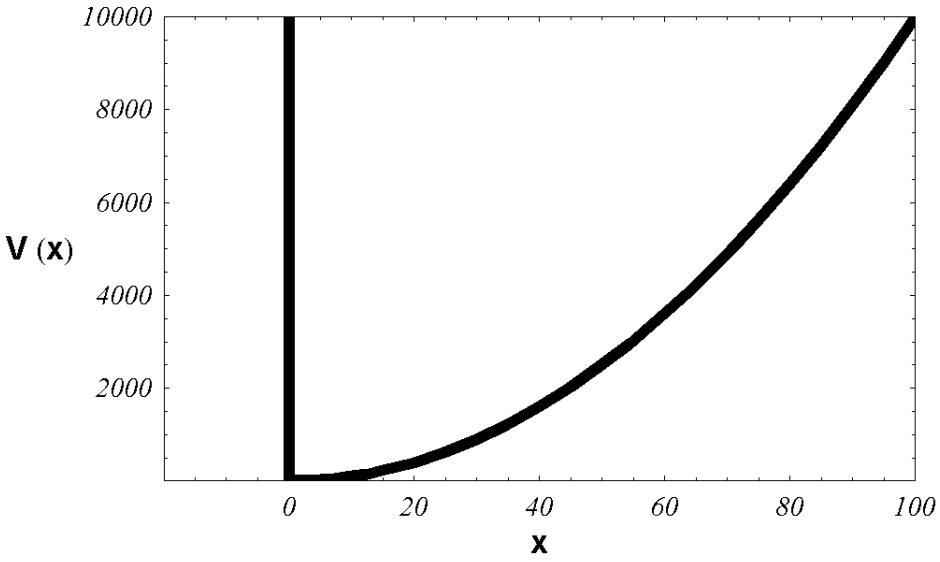

Fig. 9.1: $V(x)$ for the clipped harmonic oscillator in units given by $\hbar = m\omega$.

Due to the fact that the potential goes to infinity, the wavefunction, $\psi(x)$, must vanish for values of $x < 0$, while for the right side $x \geq 0$ it must obey the time-independent Schrödinger equation:

$$-\frac{\hbar^2}{2m}\frac{\partial^2\psi}{\partial x^2} + \frac{m\omega^2 x^2}{2}\psi = E\psi. \tag{9.5}$$

Since for $x \geq 0$ the potential is the same as the one for the regular harmonic oscillator, the wavefunctions will have the form:

$$\psi_n(\xi) \propto \begin{cases} 0 & \text{for } \xi < 0 \\ H_n(\xi)e^{-\xi^2/2} & \text{for } \xi \geq 0, \end{cases} \tag{9.6}$$

where we have introduced the dimensionless parameter:

$$\xi = \sqrt{\frac{m\omega}{\hbar}}x, \tag{9.7}$$

H_n is the nth order Hermite Polynomial and the eigenenergies are given by:

$$E = (n + \frac{1}{2})\hbar\omega, \tag{9.8}$$

where n is any positive integer including 0.

Since

$$H_n(0) = \begin{cases} 0 & \text{for } n \text{ odd} \\ \frac{(-1)^{n/2}n!}{(n/2)!} & \text{for } n \text{ even,} \end{cases} \tag{9.9}$$

continuity of the wavefunctions at $\xi = 0$ demands that we must disregard even values of n.

After normalizing, the wavefunctions are:

$$\psi_n^{CHO}(\xi) = \begin{cases} 0 & \xi < 0 \\ (2^{(n-1)}n!)^{-1/2} \left(\frac{m\omega}{\pi\hbar}\right)^{1/4} e^{-\xi^2/2} H_n(\xi). & \xi \geq 0, \end{cases} \tag{9.10}$$

where n is odd, so the ground level corresponds to $n = 1$, the first excited level to $n = 3$, the second excited level to $n = 5$ and so on. Fig. 9.2 shows plots of the first 9 wavefunctions.

By using Eq. (9.7) we can calculate the transition moments as:

$$x_{mn} = \int_0^\infty \psi_n^{CHO}(x)\ x\ \psi_m^{CHO}(x)\ dx = \frac{\hbar}{m\omega}\int_0^\infty \psi_n^{CHO}(\xi)\ \xi\ \psi_m^{CHO}(\xi)\ d\xi. \tag{9.11}$$

Substituting Eq. (9.10) into Eq. (9.11) we get:

$$x_{mn} = \left(\frac{\hbar}{\pi m\omega}\right)^{1/2} (2^{(n-1)}n!)^{-1/2}(2^{(m-1)}m!)^{-1/2}\int_0^\infty H_m(\xi)\xi H_n(\xi)d\xi. \tag{9.12}$$

We will write x_{mn} in terms of the dimensionless function g_{mn}, defined as:

$$x_{mn} = \sqrt{\frac{\hbar}{\pi m\omega}}g_{mn}, \tag{9.13}$$

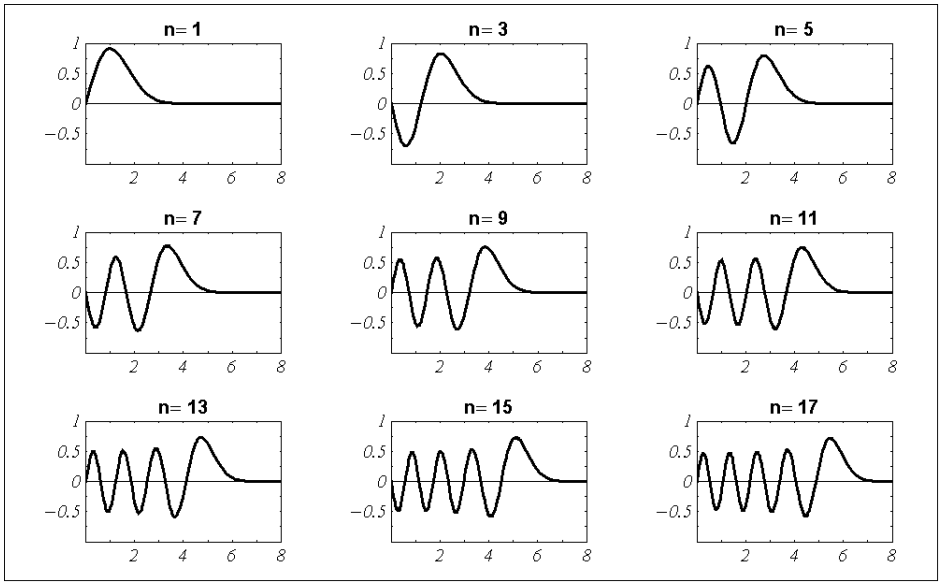

Fig. 9.2: The first 9 solutions for the Clipped Harmonic Oscillator wavefunctions, $\psi_n^{CHO}(\xi)$.

so

$$g_{mn} = (2^{(n-1)}n!)^{-1/2}(2^{(m-1)}m!)^{-1/2}\int_0^\infty H_m(\xi)\xi H_n(\xi)d\xi. \tag{9.14}$$

Unlike the harmonic oscillator, where $x_{nm} = 0$ unless $m = n-1$ or $m = n+1$,in the clipped harmonic oscillator all matrix elements of x are non vanishing. The values of g_{mn} for the first 4-levels of the clipped harmonic oscillator are listed in Table 9.1, while Fig. 9.3 plots the values of g_{mn} for the different combinations of the first 11-levels of the clipped harmonic oscillator. The details of the calculation are given in Appendix (B).

An important difference between the harmonic oscillator and the clipped harmonic oscillator is that while in the harmonic oscillator $x_{nn} = 0$, in the clipped harmonic oscillator $x_{nn} \neq 0$. Fig. 9.4 shows the values of x_{nn} for the first 51-levels.

For computational convenience, we can represent g_{mn} as a continuous function, which we call g_{xy}. As illustrated in Fig. 9.5, the continuous and discrete functions agree at integer values. Fig. 9.6 shows the behavior of g_{xx} for a wide range of values of x.

Table 9.1: Values of g_{mn} for the first 4-levels of the clipped harmonic oscillator

$\mathbf{g_{mn}}$	$\mathbf{n=1}$	$\mathbf{n=3}$	$\mathbf{n=5}$	$\mathbf{n=7}$
$\mathbf{m=1}$	2	$\sqrt{\frac{2}{3}}$	$-\frac{1}{\sqrt{30}}$	$\frac{1}{2\sqrt{35}}$
$\mathbf{m=3}$	$\sqrt{\frac{2}{3}}$	3	$\frac{\sqrt{5}}{2}$	$-\frac{1}{2}\sqrt{\frac{7}{30}}$
$\mathbf{m=5}$	$-\frac{1}{\sqrt{30}}$	$\frac{\sqrt{5}}{2}$	$\frac{15}{4}$	$\frac{5}{4}\sqrt{\frac{7}{6}}$
$\mathbf{m=7}$	$\frac{1}{2\sqrt{35}}$	$-\frac{1}{2}\sqrt{\frac{7}{30}}$	$\frac{5}{4}\sqrt{\frac{7}{6}}$	$\frac{35}{8}$

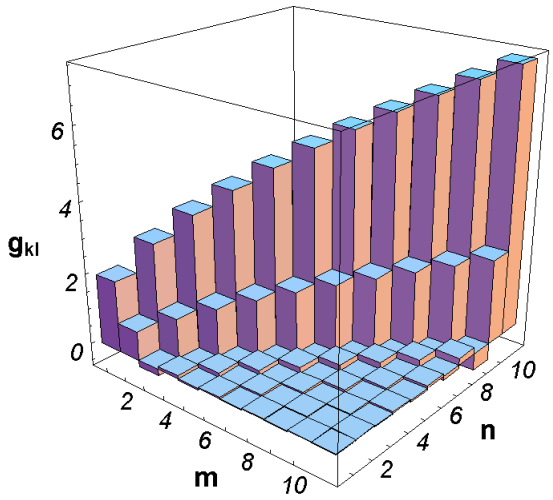

Fig. 9.3: Values of g_{kl} for the first 11 levels of the clipped harmonic oscillator. Since k and l must be odd integers, we have introduced m and n such $k = 2m+1$ and $l = 2n + 1$; so m and n run from 0 to 10. Note that some of the values are negative. The highest values correspond to the diagonal elements of g_{kl}.

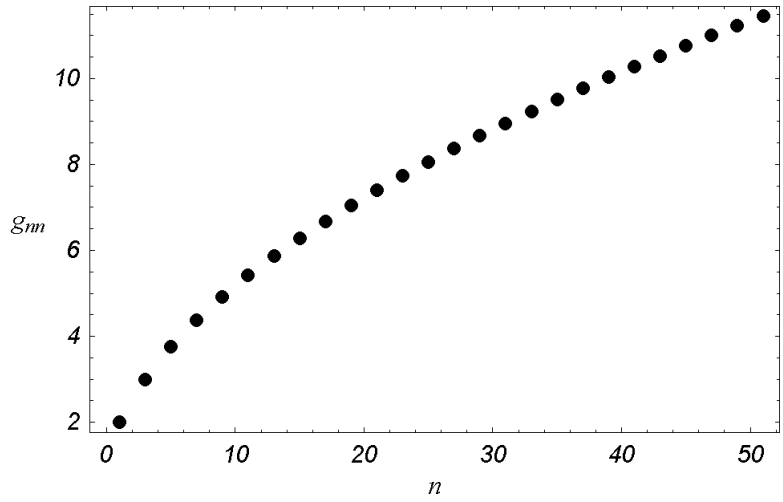

Fig. 9.4: Values of g_{nn} as a function of n for odd n.

9.3 Evaluating the first hyperpolarizability

The off-resonance diagonal term of the second-order molecular susceptibility for the clipped harmonic oscillator can be evaluated as follows. First we write the expression for the largest diagonal component of the first hyperpolarizability:

$$\beta_{xxx} = 3(-e)^3 {\sum_{m,n}}' \frac{x_{gm}\bar{x}_{mn}x_{ng}}{E_{mg}E_{ng}} \equiv -3e^3 S, \tag{9.15}$$

where we have defined the sum:

$$S = {\sum_{m,n}}' \frac{x_{gm}\bar{x}_{mn}x_{ng}}{E_{mg}E_{ng}}, \tag{9.16}$$

with n, m odd.

Equivalently we can evaluate:

$$S = \sum_{m=1,n=1}^{\infty} \frac{x_{1(2m+1)}\bar{x}_{(2m+1)(2n+1)}x_{(2n+1)1}}{E_{(2m+1)1}E_{(2n+1)g}}, \tag{9.17}$$

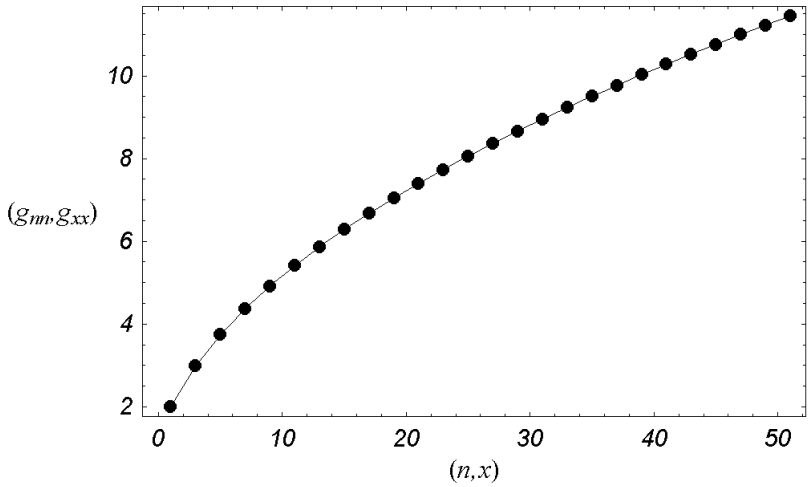

Fig. 9.5: The values of g_{nn} for discrete values of n are plotted using dots, while the values of g_{xx} for the continuous variable x are plotted using a continuous line. We see that the continuous representation of g_{xx} is well behaved and $g_{nn} = g_{xx}$ for integer values of x.

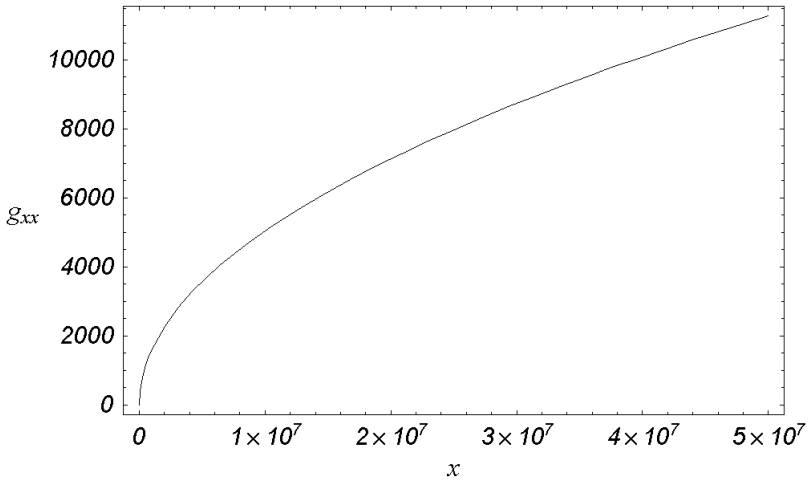

Fig. 9.6: Values of the generalized g_{xx} for the continuous variable x for a wide range of x. Note that g_{xx} is a slowly increasing function.

with n, m varying over all integers.

Using the fact that for the clipped harmonic oscillator $E_{(2m+1)} - E_1 = 2m\hbar\omega$, we can rewrite Eq: 9.16 as:

$$\begin{aligned} S &= \left(\frac{\hbar}{\pi m\omega}\right)^{3/2} \frac{1}{4(\hbar\omega)^2} \sum_{m,n}^{\infty} \frac{g_{1(2m+1)}\bar{g}_{(2m+1)(2n+1)}g_{(2n+1)1)}}{mn} \\ &\equiv \left(\frac{\hbar}{\pi m\omega}\right)^{3/2} \frac{1}{4(\hbar\omega)^2} \cdot s, \end{aligned} \tag{9.18}$$

where we have defined the dimensionless quantity:

$$s = \sum_{m,n}^{\infty} \frac{g_{1(2m+1)}\bar{g}_{(2m+1)(2n+1)}g_{(2n+1)1}}{mn}. \tag{9.19}$$

Defining the partial sum, $s(k, l)$:

$$s(k,l) = \sum_{m,n}^{k,l} \frac{g_{1(2m+1)}\bar{g}_{(2m+1)(2n+1)}g_{(2n+1)1}}{mn}, \tag{9.20}$$

we have reduced the problem to the evaluation of the quantity:

$$\lim_{m,n\to\infty} s(n,m). \tag{9.21}$$

Even though Eq. (9.21) is an infinite sum, it converges quickly to $s = 0.49$. We show the behavior of the partial sum $s(n, n)$ as a function of n in Fig. 9.7. In Fig. 9.8 we expand Fig. 9.7 to show that the sum has stabilized around the value 0.50.

Now using that

$$E_{31} = 2\hbar\omega, \tag{9.22}$$

we can write

$$|\beta_{CHO}| = 0.75(\hbar e)^3 \left(\frac{1}{m}\right)^{3/2} \frac{1}{E_{31}^{7/2}}, \tag{9.23}$$

where E_{31} is the energy difference between the first excited state, $n = 3$ and the ground state, $n = 1$.

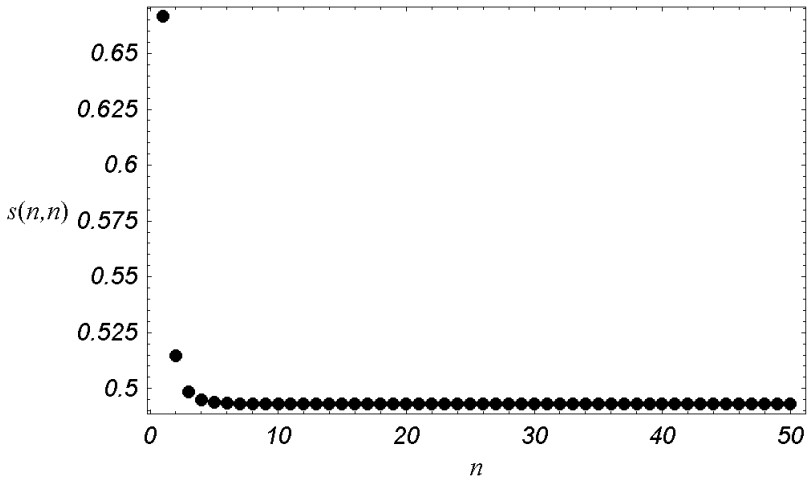

Fig. 9.7: Values of the partial sum $s(n, n)$. The sum converges fast towards the limiting value $s = 0.49$.

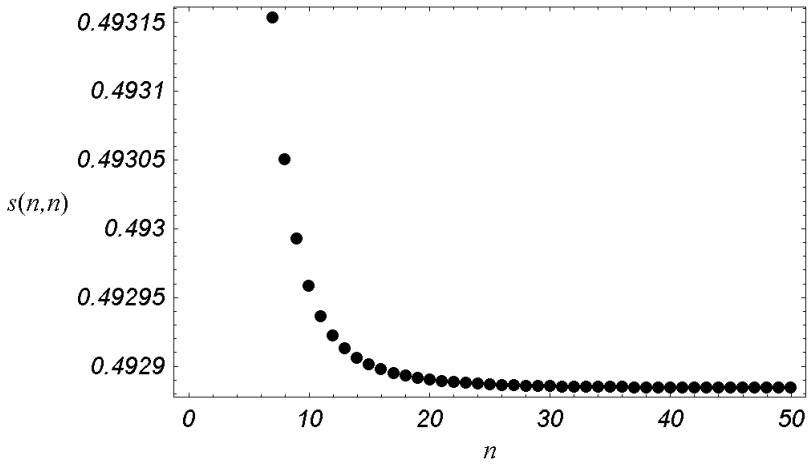

Fig. 9.8: A close up of the values of the partial sum $s(n, n)$ around the value $s = 0.49$. After the term $n = 25$ there are not changes before the 7 decimal place.

Comparing Eq. 9.23 with the maximum value of β_{xxx} obtained using the three-level model ansatz (Eq. 8.34) that although the clipped harmonic oscillator manages to breach the apparent limit, it is still lower than the quantum limit, β_{xxx}^{max}:

$$\left| \frac{\beta_{CHO}}{\beta_{xxx}^{max}} \right| \leq \frac{2}{3} \tag{9.24}$$

Thus, we have found a quantum mechanical system with an off-resonance diagonal second order molecular susceptibility which is higher than the "apparent" limit. This shows that the apparent gap is not of a fundamental nature, so the question of what prevents organic values from having values of β_{xxx} that falls into the gap is still unanswered.

In the next chapter we will analyze if the effects of vibrational contributions in organic systems could be responsible for the failure to reach above the gap.

Bibliography

[1] M. G. Kuzyk, Optics Letters **25** No. 16, 1183 (2000).

[2] M. G. Kuzyk, Phys. Rev. Lett. **85** No. 6, 1218 (2000).

[3] K. Tripathy, J. Pérez-Moreno, M. G. Kuzyk, B. Coe, K. Clays and A. M. Kelley, J. Chem. Phys. **121**, 7932 (2004).

[4] J. Pérez-Moreno, "Quantum limits of the nonlinear optical response", Washington State University, Department of Physics. August 2004.

[5] D. J. Griffiths, *Introduction to Quantum Mechanics.*, Prentice Hall, (1994).

[6] R. C. Miller, A. C. Gossard, D. A. Kleinman and O. Muntenau, Phys. Rev. B **29**, No. 6, 3740 (1984).

[7] E. L. Ivchenko and G. E. Pikus. *Superlattices and Other Heterostructures. Second Edition.* Springer Series in Solid-State Sciences 110, (1997).

[8] W. W. Bewley, C. L. Felix, J. J. Plombon and M. S. Sherwin, Phys. Rev. B **48**, No. 4, 2376 (1993).

Chapter 10

Dilution effects from the vibrational states in the off-resonance regime: First hyperpolarizability

The quantum limits for the first hyperpolarizability in the off-resonance regime were calculated by assuming that the response is purely electronic. In this chapter we relax this assumption and incorporate the nuclear motion into our calculations.

All the calculations in this chapter are performed within the framework of the Born-Oppenheimer approximation, which assumes that the Hamiltonian of the molecule is characterized by the nuclear and electronic motion and the two can be treated separately.[1] As a consequence, the stationary molecular wavefunction Ψ, can be factorized into nuclear (ψ^n) and electronic (ψ^e). The Born-Oppenheimer approximation is known to work well for most molecular systems, which is justified by the fact that electron motions occurs on a much faster scale than the nuclear motion (since the nuclei are much more massive than the electrons[1]). This means that the changes in the electronic structure of the molecule will happen while the nuclei are almost stationary. The slower changes of the nuclei positions are followed by an "instantaneous" response of the electronic cloud to the new configuration of the nuclear coordinates.

[1] Typical electron velocities are on the order of $10^6 ms^{-1}$ while nuclear velocities are of the order of $10^3 ms^{-1}$.[2]

Within the Born-Oppenheimer approximation the purely electronic states are considered first. In the second step, the vibrational effects are included by associating an infinite manifold of vibrational levels to each electronic state. The new states - combination of electronic and vibrational states - are called *vibronic* states. The vibronic states are labeled as $|n\rangle|m^n\rangle$, where the index n refers to the nth electronic state. Each nth electronic state has a manifold of associated vibrational states indexed by m^n (the n superscript reminds us the electronic level associated with the vibrational manifold). An schematic representation of the two steps - from purely electronic to vibronic states - is shown in Fig. 10.1.

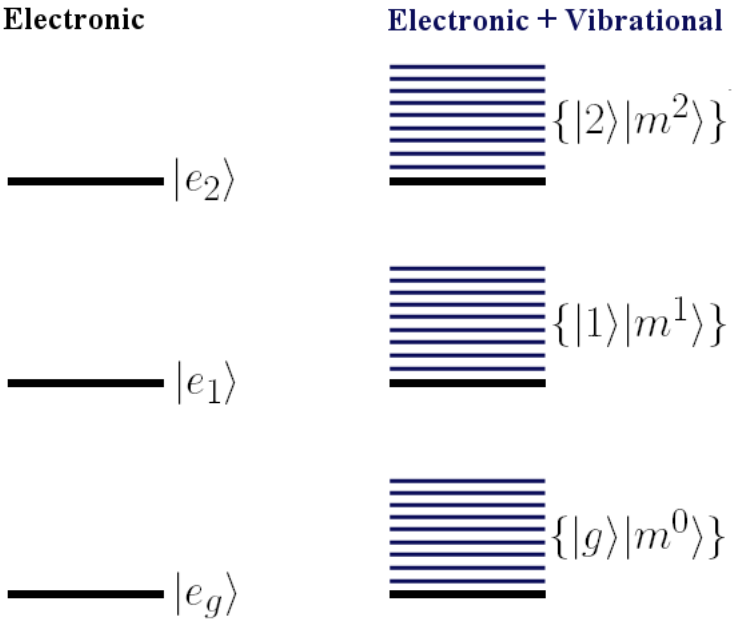

Fig. 10.1: Schematic representation of the two steps involved in the Born-Oppenheimer approximation. In the first step (left), only the electronic levels are considered - in the figure we show an electronic three-level model. In the second step (right), vibrational levels are added, so every electronic level now has associated a vibrational manifold.

In chapter 8 we calculated the off-resonance quantum limits of the first hyperpolarizability using only electronic states. For clarity, we now rewrite the expression for the first hyperpolarizability obtained from perturbation theory in terms of purely electronic states (for clarity, we will use the non-dipole free

expression):[3]

$$\beta_{xxx}^{off} \propto \frac{|x_{01}|^2 \bar{x}_{11}}{E_{10}^2} + 2\frac{x_{01}x_{12}x_{20}}{E_{10}E_{20}} + \frac{|x_{02}|^2 \bar{x}_{22}}{E_{20}^2}. \tag{10.1}$$

By using Eq. 10.1, we are carrying on with the assumptions we made in Chapter 4, when the general expression was derived. Namely, we are using the "electric dipole approximation" and assuming that the changes in the ground state state function of the molecule occur at a much slower rate than the changes in the state functions of the excited states. We evaluate the transition moments using the theoretical expressions derived by Manneback for the case of harmonic motion of the nuclei.[4] The energy of a vibronic state $|n\rangle|m^n\rangle$ is given by:

$$E_{n,m} = E_n^e + E_{m^n}^v, \tag{10.2}$$

with

$$E_{m^n}^v = \hbar\omega_n(m^n + \frac{1}{2}), \tag{10.3}$$

where E_n is the energy corresponding to the purely electronic state $|n\rangle$, while $E_{m^n}^v$ is energy contribution from the vibrational state $|m^n\rangle$, and ω_n is the characteristic frequency of a nuclear vibration in the electronic excited state.

The intensities of the vibrational spectrum in the electronic bands of the molecule are obtained using the recursion relationships:[4]

$$|\langle m^k|0^0\rangle|^2 = \frac{S_k^{m^k} \exp -S_k}{m^k!}, \tag{10.4}$$

$$\langle 0^k|0^0\rangle = \exp(-S_k/2), \tag{10.5}$$

$$\langle (n'+1)^k|n^0\rangle = \sqrt{\frac{n}{n'+1}}\langle (n')^k|(n-1)^0\rangle - \sqrt{\frac{S_1}{n'+1}}\langle (n')^k|n^0\rangle, \tag{10.6}$$

$$\langle (n')^k|(n+1)^0\rangle = \sqrt{\frac{n'}{n+1}}\langle (n'-1)^k|n^0\rangle - \sqrt{\frac{S_1}{n+1}}\langle (n')^k|n^0\rangle, \tag{10.7}$$

where S_k is a parameter that characterizes the transition for the specific transition to the kth electronic state. For most molecules, S_k falls between 0 and 1.[5, 6, 7, 8]

For clarity, we will explicitly denote the electronic part of the vibronic states. Thus, $|e_g\rangle|0^0\rangle$ is the vibronic state of the *electronic ground state* and the *vibrational ground state*, and therefore, the absolute ground state of the molecule. The state corresponding to a generic vibrational state m in the electronic ground state is denoted by $|e_g\rangle|m^0\rangle$. The ground vibrational state of the first excited

electronic state is denoted $|e_1\rangle|0^1\rangle$, and so on.

10.1 Calculations within the Frank-Condon approximation

The Frank-Condon approximation assumes that during the electronic transition, the nuclei remains essentially unchanged at the ground state equilibrium configuration. The structure of the new electronic excited state will usually differ from the ground state and the nuclear configuration will relax into a new structure determined by the electronic structure of the excited state. The probability of a transition from one vibrational energy level to another increases the more the two vibrational wave functions overlap. The overlap between the two vibrational wave functions is more pronounced if there is minimum change in the nuclear coordinates. This also implies that no vibrational transitions between the same electronic state are allowed, since the vibrational states within the same electronic level are orthogonal. The position operator x only acts on the electronic wavefunction, which means that between any two vibronic states we would have:

$$\langle e_n|\langle m^n|x|e_n\rangle|m'^n\rangle = x_{e_n e_n}\langle m^n|m'^n\rangle = x_{e_n e_n}\delta_{m^n m'^n}. \tag{10.8}$$

10.1.1 Dipolar term to the first excited electronic state

First we look at the vibrational contributions to the first term in the expansion of the first hyperpolarizability (Eq. 10.1):

$$\frac{|x_{01}|^2\bar{x}_{11}}{E_{10}^2}. \tag{10.9}$$

Each electronic state has now a manifold of vibrational states. When these vibrational states are taken into account, Eq. 10.9 becomes:

$$\frac{|x_{01}|^2\bar{x}_{11}}{E_{10}^2} \rightarrow \sum_{m^1 n^1} \frac{\langle e_g|\langle 0^0|x|e_1\rangle|n^1\rangle\langle e_1|\langle n^1|\bar{x}|e_1\rangle|m^1\rangle\langle e_1|\langle m^1|x|e_g\rangle|0^0\rangle}{E_{n^1 0}E_{m^1 0}} =$$

$$\sum_{m^1 n^1} \frac{|x_{e_1 g}|^2\bar{x}_{e_1 e_1}\langle 0^0|n^1\rangle\langle n^1|m^1\rangle\langle m^1|0^0\rangle}{E_{n^1 0}E_{m^1 0}} =$$

$$\sum_{m^1 n^1} \frac{|x_{e_1 g}|^2\bar{x}_{e_1 e_1}\langle 0^0|n^1\rangle\delta_{n^1 m^1}\langle m^1|0^0\rangle}{E_{n^1 0}E_{m^1 0}} =$$

$$|x_{e_1g}|^2\bar{x}_{e_1e_1}\sum_{n^1}\frac{|\langle 0^0|n^1\rangle|^2}{E^2_{n^10}} =$$

$$|x_{e_1g}|^2\bar{x}_{e_1e_1}\sum_{n^1}\frac{\exp(-S_1)\frac{S_1^{n^1}}{n^1!}}{(E^e_{e_1g}+\hbar\omega_1 n^1)^2} =$$

$$\frac{|x_{e_1g}|^2\bar{x}_{e_1e_1}}{(E^e_{e_1g})^2}\sum_{n^1}\frac{\exp(-S_1)\frac{S_1^{n^1}}{n^1!}}{(1+\frac{\hbar\omega_1 n^1}{E^e_{e_1g}})^2}. \tag{10.10}$$

Since the series converges quickly (due to the $n^1!$ denominator), we can use a Taylor expansion, by noticing that $\hbar\omega_1/E_{e_1g} \ll 1$:

$$\frac{|x_{01}|^2\bar{x}_{11}}{E^2_{10}} \to \frac{|x_{e_1g}|^2\bar{x}_{e_1e_1}}{(E^e_{e_1g})^2}\left\{\exp(-S_1)\sum_{n^1}\frac{S^{n^1}}{n^1!}\left(1-2\frac{\hbar\omega_1}{E_{e_1g}}n^1\right)\right\} =$$

$$\frac{|x_{e_1g}|^2\bar{x}_{e_1e_1}}{(E^e_{e_1g})^2}\left\{1-2\frac{\hbar\omega_1}{E_{e_1g}}S_1\right\}. \tag{10.11}$$

Since $\hbar\omega_1/E_{e_1g} \ll 1$ and $S_1 < 1$, we can conclude that in this regime, the vibrational contributions are negligible.

10.1.2 Octupolar term

Now we look at the vibrational contributions to the second term in the expansion of the first hyperpolarizability (Eq. 10.1):

$$\frac{x_{01}x_{12}x_{20}}{E_{10}E_{20}}. \tag{10.12}$$

In this case, there is a transition from the ground state ($|e_g\rangle|0^0\rangle$) to one of the vibronic states of the first excited electronic level ($|e_1\rangle|n^1\rangle$), then another transition to one of the vibronic states of the second excited electronic level ($|e_2\rangle|m^2\rangle$), and finally back to the ground state.

Including the vibrational contributions, Eq. 10.12 becomes:

$$\frac{x_{01}x_{12}x_{20}}{E_{10}E_{20}} \to \sum_{n_1,m_2}\frac{\langle e_g|\langle 0^0|x|e_1\rangle|n^1\rangle\langle e_1|\langle n^1|x|e_2\rangle|m^2\rangle\langle e_2|\langle m^2|x|e_g\rangle|0^0\rangle}{E_{n^10}E_{m^20}} =$$

$$\sum_{n^1,m^2} \frac{x_{ge_1}\langle 0^0|n^1\rangle x_{e_1e_2}\langle n^1|m^2\rangle x_{e_2g}\langle m^2|0^0\rangle}{E_{n^10}E_{m^20}} =$$
$$\frac{x_{ge_1}x_{e_1e_2}x_{e_2g}}{E_{e_1g}E_{e_2g}} \sum_{n^1,m^2} \frac{\langle 0^0|n^1\rangle\langle n^1|m^2\rangle\langle m^2|0^0\rangle}{\left(1+\frac{\hbar\omega_1}{E_{e_1g}}n^1\right)\left(1+\frac{\hbar\omega_2}{E_{e_2g}}m^2\right)}. \tag{10.13}$$

Now we perform a Taylor expansion of the the denominators:

$$\begin{aligned}
&\frac{x_{01}x_{12}x_{20}}{E_{10}E_{20}} \rightarrow \\
&\frac{x_{ge_1}x_{e_1e_2}x_{e_2g}}{E_{e_1g}E_{e_2g}} \sum_{n^1,m^2} \langle 0^0|n^1\rangle\langle n^1|m^2\rangle\langle m^2|0^0\rangle \left(1-\frac{\hbar\omega_1}{E_{e_1g}}n^1\right)\left(1-\frac{\hbar\omega_2}{E_{e_2g}}m^2\right) = \\
&\frac{x_{ge_1}x_{e_1e_2}x_{e_2g}}{E_{e_1g}E_{e_2g}} \sum_{n^1,m^2} \langle 0^0|n^1\rangle\langle n^1|m^2\rangle\langle m^2|0^0\rangle \left(1-\frac{\hbar\omega_1}{E_{e_1g}}n^1-\frac{\hbar\omega_2}{E_{e_2g}}m^2\right),
\end{aligned} \tag{10.14}$$

where we have ignored higher orders in $\hbar\omega_i/E_{e_ig}$ $(i=1,2)$.

We can split the sum into three contributions:

$$\begin{aligned}
&\sum_{n^1,m^2} \langle 0^0|n^1\rangle\langle n^1|m^2\rangle\langle m^2|0^0\rangle \left(1-\frac{\hbar\omega_1}{E_{e_1g}}n^1-\frac{\hbar\omega_2}{E_{e_2g}}m^2\right) = \\
&\sum_{n^1,m^2} \langle 0^0|n^1\rangle\langle n^1|m^2\rangle\langle m^2|0^0\rangle - \\
&\sum_{n^1,m^2} \langle 0^0|n^1\rangle\langle n^1|m^2\rangle\langle m^2|0^0\rangle \frac{\hbar\omega_1}{E_{e_1g}}n^1 - \\
&\sum_{n^1,m^2} \langle 0^0|n^1\rangle\langle n^1|m^2\rangle\langle m^2|0^0\rangle \frac{\hbar\omega_2}{E_{e_2g}}m^2.
\end{aligned} \tag{10.15}$$

If we use the completeness of the vibrational states:

$$\sum_{n^1} |n^1\rangle\langle n^1| = \sum_{m^2} |n^2\rangle\langle n^2| = 1, \tag{10.16}$$

we can calculate each term of the sum:

$$\sum_{n^1,m^2} \langle 0^0|n^1\rangle\langle n^1|m^2\rangle\langle m^2|0^0\rangle = \sum_{m^2} \langle 0^0|m^2\rangle\langle m^2|0^0\rangle = \langle 0^0|0^0\rangle = 1, \tag{10.17}$$

$$\sum_{n^1}\langle 0^0|n^1\rangle\langle n^1|0^0\rangle\frac{\hbar\omega_1}{E_{e_1g}}n^1 = \sum_{n^1}|\langle 0^0|n^1\rangle|^2\frac{\hbar\omega_1}{E_{e_1g}}n^1 =$$

$$\frac{\hbar\omega_1}{E_{e_1g}}\sum_{n^1}\frac{\exp(-S_1)S_1^{n^1}n^1}{n^1!} = \frac{\hbar\omega_1}{E_{e_1g}}S_1, \tag{10.18}$$

and

$$\sum_{m^2}|\langle 0^0|m^2\rangle|^2\frac{\hbar\omega_2}{E_{e_2g}}m^2 = \frac{\hbar\omega_2}{E_{e_2g}}S_2. \tag{10.19}$$

Therefore, within the Franck-Condon approximation, the inclusion of vibrational states in the octopolar term results in:

$$\frac{x_{01}x_{12}x_{20}}{E_{10}E_{20}} \rightarrow \frac{x_{ge_1}x_{e_1e_2}x_{e_2g}}{E_{e_1g}E_{e_2g}}\left(1-\frac{\hbar\omega_1}{E_{e_1g}}S_1-\frac{\hbar\omega_2}{E_{e_2g}}S_2\right). \tag{10.20}$$

Again, the effects of dilution on this term are negligible.

10.1.3 Dipolar term to the second excited electronic state

Finally we look at the vibrational contributions to the third term in the expansion of the first hyperpolarizability (Eq. 10.1):

$$\frac{|x_{02}|^2\bar{x}_{22}}{E_{20}^2}. \tag{10.21}$$

Using the results from the dipolar term to the first excited electronic state, we can quickly evaluate the vibrational contribution:

$$\frac{|x_{02}|^2\bar{x}_{22}}{E_{20}^2} \rightarrow \frac{|x_{e_2g}|^2\bar{x}_{e_1e_1}}{(E_{e_2g})^2}\left(1-2\frac{\hbar\omega_2}{E_{e_2g}}S_2\right). \tag{10.22}$$

As before, the effects of vibrational states are negligible.

10.2 Dilution effects within the Born-Oppenheimer approximation

As we have seen, within the Franck-Condon approximation, the vibrational contributions are negligible. In the Franck-Condon approximation the harmonic

motion of the nuclei is assumed to remain unchanged at the ground state equilibrium configuration during the electronic transition. Here we are going to relax our assumptions allowing for changes in the nuclear coordinates. However, within the Born-Oppenheimer approximation, the changes of the nuclei positions are much slower than the changes in the electronic structure. Therefore, we can calculate the wave functions using fixed nuclear coordinates. We then assume that the nuclei oscillate harmonically around the equilibrium position, and calculate the changes of the wave functions due to the change of the nuclear coordinates.

Since in organic molecules, double or triple bonds contribute with two electrons to the electronic excitations - giving an average of one electron per nuclei - we will consider a carbon atom of mass M and coordinate R (defined as the displacement of the nucleus from the equilibrium position R_0), that is oscillating in one of the normal modes of the molecule.

To reflect the changes in the wave functions we expand the position operator x around the equilibrium position R_0 using a Taylor expansion:

$$x = x(R_0) + \left(\frac{\partial x}{\partial R}\right)_{R=0} R, \tag{10.23}$$

where we keep only the first order term in the expansion because by assumption R is small.

We notice that in this approach, transitions between different vibrational levels from the same electronic state are allowed, and the calculations become more involved (and potentially more messy) than within the Franck-Condon approximation. Therefore, we will present only the detailed calculation for the first term in the in the expansion of the first hyperpolarizability (Eq. 10.1).

10.2.1 Dipolar term to the first excited electronic state

We consider the vibrational contributions to the second term in the expansion of the first hyperpolarizability (Eq. 10.1):

$$\frac{|x_{01}|^2 \bar{x}_{11}}{E_{10}^2}. \tag{10.24}$$

As transitions between vibrational states from the same electronic state are allowed, there are three different ways that can result in the same electronic transitions:

1. There is a transition from the ground state, $|e_g\rangle|0^0\rangle$, to a vibrational state in the first excited electronic level, $|e_1\rangle|n^1\rangle$, then to another vibrational state in the same electronic level, $|e_1\rangle|m^1\rangle$ and finally back to the ground state.

2. There is a transition from the ground state, $|e_g\rangle|0^0\rangle$, to another vibrational state still in the electronic ground state $|g\rangle|n^0\rangle$, then to a vibronic state in the first excited electronic level, $|g\rangle|m^1\rangle$ and then back to the ground state.

3. There is a transition from the ground state, $|e_g\rangle|0^0\rangle$, to a vibrational state in the first excited electronic level, $|e_1\rangle|n^1\rangle$, then to another vibrational state in the ground electronic level, $|e_1\rangle|m^1\rangle$ and finally back to the ground state.

We will now consider each possible scenario and estimate the contribution from vibrational contributions to the nonlinear response in each case.

Dipolar term to the first excited electronic state: first contribution

The first contribution is due to a transition from the ground state, $|e_g\rangle|0^0\rangle$, to a vibrational state in the first excited electronic level, $|e_1\rangle|n^1\rangle$, then to another vibrational state in the same electronic level, $|e_1\rangle|m^1\rangle$ and finally back to the ground state.

When we bracket the position operator between the different states we get:

$$\begin{aligned}
&\langle 0^g|\langle e_g|\left(x+\left[\frac{\partial x}{\partial R}\right]_{R=R_0}R\right)|e_1\rangle|n^1\rangle = \\
&x_{ge_1}\langle 0^g|n^1\rangle+\frac{\partial x_{ge_1}}{\partial R}\langle 0^g|R|n^1\rangle, \\
&\langle n^1|\langle e_1|\left(x+\left[\frac{\partial x}{\partial R}\right]_{R=R_0}R\right)|e_1\rangle|m^1\rangle = \\
&\bar{x}_{e_1e_1}\langle m^1|0^g\rangle+\frac{\partial \bar{x}_{e_1e_1}}{\partial R}\langle m^1|R|0^g\rangle,
\end{aligned} \tag{10.25}$$

$$\langle m^1|\langle e_1|\left(x+\left[\frac{\partial x}{\partial R}\right]_{R=R_0}R\right)|g\rangle|0^g\rangle =$$
$$x_{e_1g}\langle m^1|0^g\rangle+\frac{\partial x_{e_1g}}{\partial R}\langle m^1|R|0^g\rangle, \tag{10.26}$$

where we have used the shorthand notation:

$$\frac{\partial x_{ge_1}}{\partial R}\equiv\langle g|\left[\frac{\partial x}{\partial R}\right]_{R=R_0}|e_1\rangle. \tag{10.27}$$

The contribution of this term is given by:

$$\sum_{n^1m^1}\frac{\left(x_{ge_1}\langle 0^g|n^1\rangle+\frac{\partial x_{ge_1}}{\partial R}\langle 0^g|R|n^1\rangle\right)}{[E_{e_1g}+\hbar\omega_1 n^1][E_{e_1g}+\hbar\omega_1 m^1]}\times$$
$$\left(\bar{x}_{e_1e_1}\langle m^1|0^g\rangle+\frac{\partial\bar{x}_{e_1e_1}}{\partial R}\langle m^1|R|0^g\rangle\right)\left(x_{e_1g}\langle m^1|0^g\rangle+\frac{\partial x_{e_1g}}{\partial R}\langle m^1|R|0^g\rangle\right). \tag{10.28}$$

Keeping only first order on R, Eq. 10.28 becomes:

$$\sum_{n^1m^1}\frac{x_{ge_1}\langle 0^g|n^1\rangle\Delta x_{e_1g}\delta_{n^1m^1}x_{e_1g}\langle m^1|0^0\rangle}{[E_{e_1g}+\hbar\omega_1 n^1][E_{e_1g}+\hbar\omega_1 m^1]}+$$
$$\sum_{n^1m^1}\frac{\frac{\partial x_{ge_1}}{\partial R}\langle 0^g|R|n^1\rangle\Delta x_{e_1g}\delta_{n^1m^1}x_{e_1g}\langle m^1|0^g\rangle}{[E_{e_1g}+\hbar\omega_1 n^1][E_{e_1g}+\hbar\omega_1 m^1]}+$$
$$\sum_{n^1m^1}\frac{x_{ge_1}\langle 0^g|n^1\rangle\frac{\partial\Delta x_{e_1g}}{\partial R}\langle n^1|R|m^1\rangle x_{e_1g}\langle m^1|0^g\rangle}{[E_{e_1g}+\hbar\omega_1 n^1][E_{e_1g}+\hbar\omega_1 m^1]}+$$
$$\sum_{n^1m^1}\frac{x_{ge_1}\langle 0^g|n^1\rangle\Delta x_{e_1g}\delta_{n^1m^1}\frac{\partial x_{e_1g}}{\partial R}\langle m^1|R|0^g\rangle}{[E_{e_1g}+\hbar\omega_1 n^1][E_{e_1g}+\hbar\omega_1 m^1]}=$$
$$|x_{ge_1}|^2\Delta x_{e_1g}\sum_{n^1}\frac{|\langle n^1|0^g\rangle|^2}{(E_{e_1g}+\hbar\omega_1 n^1)^2}+$$
$$x_{e_1g}\Delta x_{e_1g}\frac{\partial x_{ge_1}}{\partial R}\sum_{n^1}\frac{\langle 0^g|R|n^1\rangle\langle n^1|0^g\rangle}{(E_{e_1g}+\hbar\omega_1 n^1)^2}+$$
$$|x_{ge_1}|^2\frac{\partial\Delta x_{e_1g}}{\delta R}\sum_{n^1m^1}\frac{\langle 0^g|n^1\rangle\langle m^1|0^g\rangle}{(E_{e_1g}+\hbar\omega_1 n^1)(E_{e_1g}+\hbar\omega_1 m^1)}+$$
$$x_{ge_1}\Delta x_{e_1g}\frac{\partial x_{ge_1}}{\partial R}\sum_{n^1}\frac{\langle n^1|R|0^g\rangle\langle 0^g|n^1\rangle}{(E_{e_1g}+\hbar\omega_1 n^1)^2}=$$

$$\sum_{n^1,m^1} \frac{x_{0n^1}\bar{x}_{n^1m^1}x_{m^10}}{E_{n^10}E_{m^10}} =$$
$$\frac{\Delta x_{e_1g}|x_{e_1g}|^2}{E_{e_1g}^2}\sum_{n^1}\frac{|\langle 0^g|n^1\rangle|^2}{E^2(n^1)} +$$
$$\frac{2\Delta x_{e_1g}x_{e_1g}}{E_{e_1g}^2}\frac{\partial x_{e_1g}}{\partial R}\sum_{n^1}\frac{\langle 0^g|R|n^1\rangle\langle n^1|0^g\rangle}{E^2(n^1)} +$$
$$\frac{|x_{e_1g}|^2}{E_{e_1g}^2}\frac{\partial(\Delta x_{e_1g})}{\partial R}\sum_{n^1,m^1}\frac{\langle 0^g|n^1\rangle\langle n^1|R|m^1\rangle\langle m^1|0^g\rangle}{E(n^1)E(m^1)}, \tag{10.29}$$

where we have used the reality of the harmonic oscillator wave functions ($\langle n^1|R|0^g\rangle = \langle 0^g|R|n^1\rangle$) and we have defined:

$$E(n^1) = 1 + \frac{\hbar\omega_1}{E_{e_1g}}n^1. \tag{10.30}$$

Now we can perform the sums using Taylor expansions:

$$\frac{\Delta x_{e_1g}|x_{e_1g}|^2}{E_{e_1g}^2}\sum_{n^1}\frac{|\langle 0^g|n^1\rangle|^2}{E^2(n^1)} \approx$$
$$\frac{\Delta x_{e_1g}|x_{e_1g}|^2}{E_{e_1g}^2}\left(1 - 2\frac{\hbar\omega_1 S_1}{E_{e_1g}}\right). \tag{10.31}$$
$$\sum_{n^1}\frac{\langle 0^g|R|n^1\rangle\langle n^1|0^g\rangle}{E^2(n^1)} = -\sqrt{\frac{\hbar}{2M\omega_1}}\frac{\langle 1^1|0^g\rangle}{(1+\frac{\hbar\omega_1}{E_{e_1g}})^2} =$$
$$-\sqrt{\frac{\hbar}{2M\omega_1}}\frac{S_1^{1/2}\exp(-S_1/2)}{(1+\frac{\hbar\omega_1}{E_{e_1g}})^2}, \tag{10.32}$$

and

$$\sum_{n^1,m^1}\frac{\langle 0^g|n^1\rangle\langle n^1|R|m^1\rangle\langle m^1|0^g\rangle}{E(n_1)E(n_2)} =$$
$$\sum_{n_1}\sum_{m_1}\frac{\langle 0^g|n^1\rangle\sqrt{\frac{\hbar}{2M\omega_1}}[\sqrt{m^1+1}\delta_{n^1,m^1+1} + \sqrt{m^1}\delta_{n^1,m^1-1}]\langle m^1|0^g\rangle}{E(n_1)E(n_2)} =$$
$$\sqrt{\frac{\hbar}{2M\omega_1}}\left(\sum_{n^1=1}\frac{\langle 0^g|n^1\rangle\sqrt{n^1}\langle n^1-1|0^g\rangle}{E(n^1)E(n^1-1)} +\right.$$
$$\left. + \sum_{n^1=0}\frac{\langle 0^g|n^1\rangle\sqrt{n^1+1}\langle n^1+1|0^g\rangle}{E(n^1)E(n^1+1)}\right) =$$

$$
\begin{aligned}
&2\sqrt{\frac{\hbar}{2M\omega_1}}\sum_{n^1=1}\frac{\langle 0^g|n^1\rangle\sqrt{n^1}\langle n^1-1|0^g\rangle}{E(n^1)E(n^1-1)}=\\
&2\sqrt{\frac{\hbar}{2M\omega_1}}\sum_{n^1=1}\frac{(-1)^{2n^1-1}S_1^{n^1/2+(n^1-1)/2}\sqrt{n^1}\exp\left(-S_1\right)}{\sqrt{n^1!}\sqrt{(n^1-1)!}E(n^1)E(n^1-1)}=\\
&-2\sqrt{\frac{\hbar}{2M\omega_1}}S_1^{-1/2}\sum_{n^1=1}\frac{S_1^{n^1}\exp\left(-S_1\right)}{(n^1-1)!E(n^1)E(n^1-1)}=\\
&-2\sqrt{\frac{\hbar}{2M\omega_1}}S_1^{1/2}\sum_{n^1=0}\frac{S_1^{n^1}\exp\left(-S_1\right)}{n^1!E(n^1+1)E(n^1}=\\
&-2\sqrt{\frac{\hbar}{2M\omega_1}}\sum_{n^1=0}\frac{\sqrt{S_1}S_1^{n^1}\exp\left(-S_1\right)}{n^1!\left(1+\frac{\hbar\omega_1}{E_{e_1g}}(n^1+1)\right)\left(1+\frac{\hbar\omega_1}{E_{e_1g}}n^1\right)}\approx\\
&-2\sqrt{\frac{\hbar}{2M\omega_1}}\exp\left(-S_1\right)\sum_{n^1=0}\frac{\sqrt{S_1}S_1^{n^1}}{n^1!}\left(1-\frac{\hbar\omega_1}{E_{e_1g}}(n^1+1)\right)\left(1-\frac{\hbar\omega_1}{E_{e_1g}}n^1\right)\approx\\
&-2\sqrt{\frac{\hbar}{2M\omega_1}}\exp\left(-S_1\right)\sum_{n^1=0}\frac{\sqrt{S_1}S_1^{n^1}}{n^1!}\left(1-\frac{\hbar\omega_1}{E_{e_1g}}(2n^1+1)\right)=\\
&-2\sqrt{\frac{\hbar}{2M\omega_1}}\exp\left(-S_1\right)\sqrt{S_1}\left(\sum_{n^1=0}\frac{S_1^{n^1}}{n^1!}(1-\frac{\hbar\omega_1}{E_{e_1g}})-2\sum_{n^1=0}\frac{n^1S_1^{n^1}}{n^1!}\frac{\hbar\omega_1}{E_{e_1g}}\right)=\\
&-2\sqrt{\frac{\hbar}{2M\omega_1}}\left(\sqrt{S_1}(1-\frac{\hbar\omega_1}{E_{e_1g}})-2\exp\left(-S_1\right)\sqrt{S_1}\frac{\hbar\omega_1}{E_{e_1g}}\sum_{n^1=0}\frac{n^1S_1^{n^1}}{n^1!}\right)=\\
&-2\sqrt{\frac{\hbar}{2M\omega_1}}\left(\sqrt{S_1}(1-\frac{\hbar\omega_1}{E_{e_1g}})-2\sqrt{S_1}S_1\frac{\hbar\omega_1}{E_{e_1g}}\right)=\\
&=-2\sqrt{\frac{\hbar^2}{2M\hbar\omega_1}}\sqrt{S_1}\left(1-\frac{\hbar\omega_1}{E_{e_1g}}(1+2S_1)\right).
\end{aligned}
\tag{10.33}
$$

Therefore, the contribution from this term[2]is given by:

$$
\begin{aligned}
&\sum_{n^1,m^1}\frac{x_{0n^1}\bar{x}_{n^1m^1}x_{m^10}}{E_{n^1}E_{m^1}}=\frac{\Delta x_{e_1g}|x_{e_1g}|^2}{E_{e_1g}^2}(1-2\frac{\hbar\omega_1}{E_{e_1g}}S_1)\\
&-2\frac{x_{e1g}\Delta x_{e1g}}{E_{e_1g}^2}\frac{\partial x_{ge_1}}{\partial R}\sqrt{\frac{\hbar^2}{2M\hbar\omega_1}}\left(\frac{\sqrt{S_1}\exp\left(-S_1/2\right)}{(1+\frac{\hbar\omega_1}{E_{e_1g}})^2}\right)
\end{aligned}
$$

[2]The term where there is a transition from the ground state, $|g\rangle|0^0\rangle$, to a vibronic state in the first excited electronic level, $|e_1\rangle|n^1\rangle$, then to another vibrational state in the same electronic level, $|e_1\rangle|m^1\rangle$ and finally back to the ground state.

$$-\frac{2|x_{e_1g}|^2}{E_{e_1g}^2}\frac{\partial(\Delta x_{e_1g})}{\partial R}\sqrt{\frac{\hbar^2}{2M\hbar\omega_1}}\left(\sqrt{S_1}\left(1-\frac{\hbar\omega_1}{E_{e_1g}}(1+2S_1)\right)\right). \tag{10.34}$$

There are three contributions in the above expression (Eq. 10.34). The first one is identical to the result we obtained using the Frank-Condon approximation:

$$\frac{\Delta x_{e_1g}|x_{e_1g}|^2}{E_{e_1g}^2}(1-2\frac{\hbar\omega_1}{E_{e_1g}}S_1). \tag{10.35}$$

If we take $\frac{\hbar\omega_1}{E_{e_1}g} < 0.1$ and $S < 1$, two conditions that are well obeyed for the type of molecules analyzed in this study,[5, 6, 7, 8] we conclude that the effects of vibrational contributions of this term are less that 20% of the electronic contribution .

The second contribution can be evaluated by realizing that:

$$\left(\frac{\sqrt{S_1}\exp(-S_1/2)}{(1+\frac{\hbar\omega_1}{E_{e_1g}})^2}\right)\approx\sqrt{S_1}(1-\frac{S_1}{2})(1-2\frac{\hbar\omega_1}{E_{e_1g}})\leq 1. \tag{10.36}$$

Also, for one electron, $x_{e_1g}^{max}=\sqrt{\frac{\hbar^2}{2m}}$ so we can write:

$$\sqrt{\frac{\hbar^2}{2M\hbar\omega_1}}=\sqrt{\frac{m}{M}\frac{E_{e_1g}}{\hbar\omega_1}}x_{e_1g}^{max}. \tag{10.37}$$

Therefore:

$$\begin{aligned}&\left|2\frac{x_{e1g}\Delta x_{e1g}}{E_{e_1g}^2}\frac{\partial x_{ge_1}}{\partial R}\sqrt{\frac{\hbar^2}{2M\hbar\omega_1}}\left(\frac{\sqrt{S_1}\exp(-S_1/2)}{(1+\frac{\hbar\omega_1}{E_{e_1g}})^2}\right)\right|\\&\leq 2\frac{\Delta x_{e_1g}x_{e_1g}x_{e_1g}^{max}}{E_{e_1g}^2}\left(\frac{\partial x_{e_1g}}{\partial R}\right)\sqrt{\frac{m}{M}\frac{E_{e_1g}}{\hbar\omega_1}}.\end{aligned} \tag{10.38}$$

To estimate the magnitude of the contribution given by Eq. 10.38 we notice that the factor:

$$\frac{\Delta x_{e_1g}x_{e_1g}x_{e_1g}^{max}}{E_{e_1g}^2} \tag{10.39}$$

is of the same order as the purely electronic contribution:

$$\frac{\Delta x_{e_1g}|x_{e_1g}|^2}{E_{e_1g}^2}, \tag{10.40}$$

while for a carbon nucleus and a π-electron, for typical vibronic states:[5, 6, 7, 8]

$$\sqrt{\frac{m}{M}\frac{E_{e_1g}}{\hbar\omega_1}} \leq 0.03. \tag{10.41}$$

Finally, as the π-electron is highly delocalized we expect a small change of the electron cloud position as function of the nuclear coordinate R. Taking a rather conservative estimation we assume:

$$\left(\frac{\partial x_{e_1g}}{\partial R}\right) \approx 1, \tag{10.42}$$

to obtain the dilution effect due to the full second term is only about 5% of the electronic response.

Finally, and following the same reasoning the last contribution in Eq. 10.34 evaluates to:

$$\begin{aligned}
&\left|\frac{2|x_{e_1g}|^2}{E_{e_1g}^2}\frac{\partial(\Delta x_{e_1g})}{\partial R}\sqrt{\frac{\hbar^2}{2M\hbar\omega_1}}\left(\sqrt{S_1}\left(1-\frac{\hbar\omega_1}{E_{e_1g}}(1+2S_1)\right)\right)\right| \\
&\leq \frac{2|x_{e_1g}|^2 x_{e_1g}^{max}}{E_{e_1g}^2}\frac{\partial(\Delta x_{e_1g})}{\partial R}\sqrt{\frac{m}{M}\frac{E_{e_1g}}{\hbar\omega_1}}\left(\sqrt{S_1}\left(1-\frac{\hbar\omega_1}{E_{e_1g}}(1+2S_1)\right)\right),
\end{aligned} \tag{10.43}$$

and since $S < 1$, the contribution of this term is less than 5% of the electronic response.

Dipolar term to the first excited electronic state: second contribution

The second contribution is due to a transition from the ground state, $|e_g\rangle|0^0\rangle$, to a vibrational state in the first excited electronic level, $|e_1\rangle|n^1\rangle$, then to a vibronic state in the ground electronic level, $|g\rangle|m^1\rangle$ (with $m \neq 0$) and then back to the ground state.

Following the same steps as in the calculation for the first contribution of

this dipolar term is given by:

$$\frac{|x_{ge_1}|^2 x_{e_1g}^{max}}{E_{e_1g}^2} \frac{\partial \bar{x}_{gg}}{\partial R} \sqrt{\frac{m}{M} \frac{E_{e_1g}}{\hbar\omega_0} S_1}. \tag{10.44}$$

which is less than 5% of the electronic response.

Dipolar term to the first excited electronic state: third contribution

The third contribution is due to transition from the ground state, $|g\rangle|0^0\rangle$, to another vibrational state still in the electronic ground state $|g\rangle|n^0\rangle$, then to a vibronic state in the first excited electronic level, $|g\rangle|m^1\rangle$ and then back to the ground state. The contribution from this term is evaluated to:

$$\frac{|x_{ge_1}|^2 x_{e_1g}^{max}}{E_{e_1g}^2} \frac{\partial \bar{x}_{gg}}{\partial R} \sqrt{\frac{m}{M} \frac{E_{e_1g}}{\hbar\omega_0} S_1}, \tag{10.45}$$

which is also less than 5% of the electronic response.

10.2.2 Dilution effects within the Born-Oppenheimer approximation: conclusion

In the same manner as the vibrational contributions to the dipolar term to the first excited state have been evaluated, the contributions to the octupolar term and to the second excited state can be obtained. In all the cases it is found that when the contributions of the infinite vibrational states are compared to each electronic state, it does not cause significant dilution effects (probably less than 10% for most of the molecules).[9] Therefore, we conclude that the gap cannot in principle be the consequence of dilution effect due to the presence of vibronic states.

Bibliography

[1] Kopecky, Jan, "Organic Photochemistry: A Visual Approach" *John Willey & Sons*, 1992.

[2] `http://en.wikipedia.org/wiki/Born-Oppenheimer_Approximation` (April 12, 2006).

[3] Orr, B. J., and Ward, J. F., *Mol. Phys.* **20**, 513 (1971).

[4] C. Manneback, Physica, **17**, 1001 (1951).

[5] A. M. Moran, C. Delbecque, and A. M. Kelley, J. Phys. Chem. A 105, 10208 (2001).

[6] A. M. Moran, G. P. Bartholomew, G. C. Bazan, and A. M. Kelley, J. Phys. Chem. A 106, 4928 (2002).

[7] A. M. Moran, M. Blanchard-Desce, and A. M. Kelley, Chem. Phys. Lett. 358, 320 (2002).

[8] A. M. Moran, D. S. Egolf, M. Blanchard-Desce, and A. M. Kelley, J. Chem. Phys. 116, 2542 (2002).

[9] K. P. Tripathy, J. Pérez Moreno, M. G. Kuzyk, B. J. Coe, K. Clays and A.M. Kelley, J. Chem. Phys. **2004** 121, 7932.

Chapter 11

Results: Using the quantum limits to characterize molecular nonlinear response: The amylose inclusions

The use of the Thomas-Kuhn sum rules has allowed us to obtain the limiting values of the first and second hyperpolarizability. As we are going to see, the quantum limits can be used to help us to understand some of the underlying principles behind the nonlinear response. The combination of linear and nonlinear measurements and the quantum limits framework allows one to frame the results in way that leads to a better picture of the nature of nonlinear enhancement. The work presented in this chapter has been published in the Journal of Chemical Physics,[1] and it is the result of an international collaboration between different institutions:

- Javier Pérez-Moreno, Inge Asselbergs and Koen Clays work in the Department of Chemistry, University of Leuven.
- Yuxia Zhao and Kai Song work in the Technical Institute of Physics and Chemistry, Chinese Academy of Sciences
- Hachiro Nakanishi, Shuji Okada, Kyoko Nogi work in the Institute of Multidisciplinary Research for Advanced Materials, Tohoku University.

- Oh-Kil Kim and Jongtae Je work in the Chemistry Division, Naval Research Laboratories, Washington, DC.
- Janka Mátrai and Marc De Maeyer work in the Laboratory of biomolecular modeling in the Department of Chemistry, University of Leuven.
- Mark G. Kuzyk works in the Department of Physics and Astronomy, Washington State University.

As it was explained in Chapter 3, noncentrosymmetry is required for any second-order process to be observed. The noncentrosymmetry has to be induced at the molecular level and at the bulk level. This dipolar molecule motif is one way of achieving noncentrosymmetry at the molecular level. Asymmetric substitution on opposite sides of a conjugated bridge results in a non-centrosymmetric 1-dimensional structure. At one end, an electron-rich group can act as an electron donor for this charge transfer. An electron-poor group can be substituted at the other end, which then acts as an electron acceptor, resulting in a donor-bridge-acceptor *(D-Br-A)* type organic chromophore. It is known that these types of molecules exhibit strong charge-transfer absorption bands in the visible part of the electronic spectrum.

The dipolar molecule motif has been studied extensively from the perspective of second-order nonlinear optics, theoretically and experimentally.[6, 7, 8] The small para-nitroaniline is often called the fruit-fly of nonlinear optics,[9] and more efficient organic materials have been developed, resulting in a *sub-1-Volt* half-wave electro-optic modulation voltage.[10, 11, 12]

Until the realization of Hyper-Rayleigh scattering, only dipolar molecules could be characterized in solution (using the EFISHG technique). The search for other viable non-centrosymmetric motifs for second-order nonlinear optics, such as octupoles[14, 16] and lambda-shaped molecules,[17] but especially the extension of the charge-transfer motif to ionic species,[18, 19, 20, 21, 22, 23, 24] became possible due to the availability of the more universally applicable incoherent second-order scattering technique.[25, 26, 27, 28] It has been found that ionic species have extremely large first hyperpolarizabilities, which can arrange themselves into a thermodynamically stable bulk ionic crystal arrangement with high number density.[29, 30, 31] One early promising ionic motif is based on the parent stilbazolium chromophore, and has been optimized by extension of the conjugated bridge.[20, 32, 33, 34, 35]

Theoretically, it had been predicted that the extension of the ethenyl bridge between the (dimethylamino)phenyl ring and the pyridinium ring, over the

butadienyl, hexatrienyl, octatetraenyl, to the decapentaenyl bridge, can result in an almost linear increase of the first hyperpolarizability with the number n of carbon-carbon double bond units (from n = 1 to 5).[20] This increase was experimentally confirmed for the ethenyl, butadienyl and hexatrienyl bridge (n = 1 to 3) but failed to describe the experimentally observed decrease for the octatetraenyl and the decapentaenyl bridge. The dissagreement was explained by the presence of different conformers and isomers (not only all-*trans*) that were believed to more easily occur in the longer variants of the homologue series of stilbazolium-type chromophores.[20]

At the supramolecular level, the ordering of noncentrosymmetric chromophores in a non-centrosymmetric bulk arrangement to provide for a bulk second-order nonlinear susceptibility traditionally has been based on the presence of an electric dipole moment.[2, 3, 4] Electric-field poling of the dipolar chromophore in a polymer matrix heated above its glass transition temperature results in an effective noncentrosymmetric ordering.[36] Unfortunately, the approach does not work with ionic species, because they do not commonly crystallize in a noncentrosymmetric structure unless they are molecularly engineered, such as adding chiral substituents.

The noncentrosymmetric arrangement of stilbazolium chromophores in a thin-film is achieved when the ionic species are allowed to form a self-assembled nano-size inclusion complex with an amylose helix.[37, 38, 39] The inclusion complexes can be deposited on a substrate with noncentrosymmetric orientation, as experimentally demonstrated by the generation of coherent second-harmonic generation (SHG) signal. However, from the thickness dependence of the SHG signal, it is found that the effect is mainly a surface template effect and not a homogeneous bulk effect. Also, in a previous work, an increase of the first hyperpolarizability by a factor of two for n = 1 upon inclusion was reported,[40] but no rationale for the increased molecular response had been put forward.

A homologue series of five stilbazolium-type chromophores with increasing conjugated length was characterized in combination with four amylose helices of different molecular size. This approach intends to induce the same type of enhancement that is observed for the parent stilbazolium chromophore with the n = 1 ethenyl conjugation bridge upon inclusion in an amylose helix, applied in conjunction with the elongation strategy. The combination of these two optimization strategies is expected to enhance the first hyperpolarizability. If both strategies work independently, a factor of 5 is expected from the elongation of ethenyl to decapentaenyl, in combination with a factor of 2 for the inclusion, which would result in an order of magnitude enhancement with respect to the

early parent stilbazolium chromophore. The hypothesis was investigated using HRS measurements to characterize a series of such molecules, molecular modelling to try to understand the effects of the inclusion in amylose helices on the chromophores and the off-resonance fundamental limit analysis to determine the underlying principles behind the enhancement.

11.1 Chromophores as guest molecules

The structure of the ionic chromophores used in this study are shown in Fig 11.1. They form a consistent series of five homologues, based on the parent (dimethylamino)stilbazolium (DAST) chromophore. The systematic name of the parent molecule is 4-{2-[4-(dimethylamino)phenyl]-ethenyl}-N-octadecylpyridiniumbromide, and is represented by the number n of conjugated carbon-carbon double bonds in the conjugation path between the (dimethylamino)phenyl and pyridinium ring. Such hemicyanine stilbazolium chromophores have been extensively studied with regards to their second-order nonlinear optical properties,[41, 42, 43] especially those with long alkyl chains in combination with the charged pyridinium ring. The amphiphilic properties allow film deposition with the Langmuir-Blodgett nanostructuring technique. The arrangement of the aliphatic alkylchains on opposite ends of the chromophoric moiety, alternating Y-type deposition of oppositely embedded polar moieties, has allowed the monolayer-by-monolayer nano-engineering of non-centrosymmetric thin films for second-harmonic generation.[44, 45, 46]

The parent stilbazolium (n = 1) is represented by structure **18**, while the longer homologues of the parent stilbazolium are represented by **19**, **20**, **21** and **22**. The longer homologues **19**, **20**, **21** and **22** have as the conjugating path respectively a butadienylene (n = 2), a hexatrienylene (n = 3), an octatetraenylene (n = 4) and a decapentaenylene (n = 5) bridge instead of the short (n = 1) ethylene link. The synthesis of these compounds has been described elsewhere.[46, 47]

The linear and second-order nonlinear optical properties of these 5 chromophores had been measured previously in chloroform solution.[20] In such a hydrophobic environment, the chromophores do not dimerize. The UV-VIS absorption is characterized by a well-separated charge-transfer absorption band that exhibits a clear red-shift upon extension of the conjugation (see Table 11.1). The charge transfer is from the dimethylamino electron donor group to the pyridinium acceptor group. The first hyperpolarizability of these chromophores in chloroform initially increases with conjugation, but only up

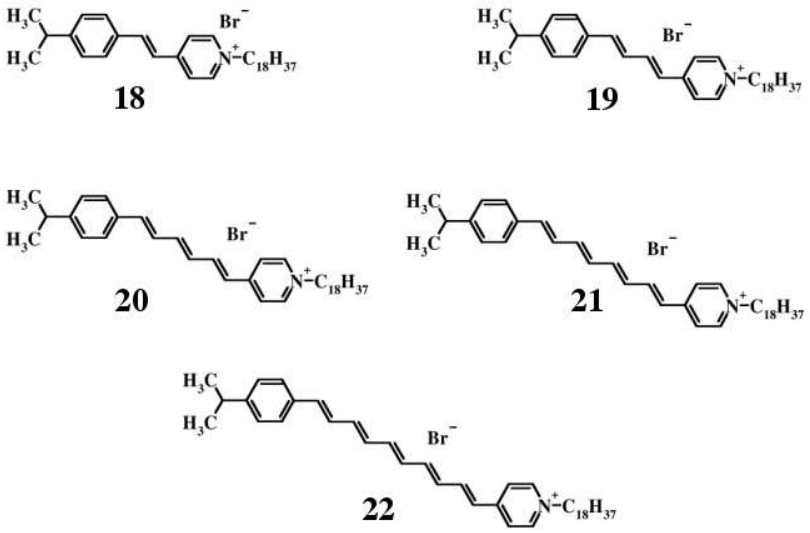

Fig. 11.1: Molecular structure of stilbazolium homologues used in this study both as free molecules in chloroform solution and complexed as guests in a supramolecular amylose host.

to n = 3 (the hexatrienylene link). The experimental finding of a decrease in hyperpolarizability upon further extension is in contradiction with the theoretical predictions, based on the optimized geometries for the isolated molecules - though it is interesting to note that at n = 3 (structure **20**), the hyperpolarizability is at the *apparent limit*. This deviation had previously been attributed to the existence of different conformers (trans or cis configuration of a single bond) or isomers (trans or cis substituted double bond).[20] The hyperpolarizabilities for the cis-isomers were calculated to be lower. It was suggested that since the chromophores show (multi-photon) fluorescence when excited at 1300 nm, they reach a real excited state and are prone to excited-state trans-to-cis isomerization.[20]

11.1.1 Analysis in terms of the fundamental limits

The quantum limits of the off-resonance first hyperpolarizability were calculated in chapter 8 using the three-level ansatz[64, 65] for the off-resonant hyperpolarizability βzzz in terms of the normalized moment X and energy E. For clarity, we will summarize the results here again.

Molecule	λ_{1300} (nm)	$\beta_{zzz,1300}$ ($\times 10^{-30} esu$)	$\beta_{zzz,0}$ ($\times 10^{-30} esu$)
18 in chloroform	496	100($\pm$6)	36($\pm$2)
19 in chloroform	524	1640($\pm$40)	481($\pm$12)
20 in chloroform	546	2045($\pm$35)	496($\pm$8)
21 in chloroform	556	780($\pm$120)	171($\pm$30)
22 in chloroform	570	1200($\pm$180)	224($\pm$40)

Table 11.1: Wavelength of maximal absorption, λ_{max}, average dynamic SHG hyperpolarizability at fundamental $1300nm$, $\beta_{zzz,1300}$, and static first hyperpolarizability, $\beta_{zzz,0}$ for the chromophores **18**, **19**, **20**, **21** and **22** in chloroform.

The diagonal component of the first hyperpolarizability is simplified using the three-level ansatz[64, 65] for the off-resonant hyperpolarizability β_{zzz}:

$$\beta_{zzz}(E, X) = \beta_{zzz}^{max} \cdot f(E) \cdot G(X), \tag{11.1}$$

where β_{zzz}^{max} is the fundamental limit of the off-resonant first hyperpolarizability in terms of the effective number of electrons N and the energy difference E_{10} between ground and first excited state;

$$\beta_{zzz}^{max} = \sqrt[4]{3} \left(\frac{e\hbar}{\sqrt{m}} \right)^3 \frac{N^{3/2}}{E_{10}^{7/2}}, \tag{11.2}$$

where

$$f(E) = (1 - E)^{3/2}(E^2 + \frac{3}{2}E + 1), \tag{11.3}$$

and

$$G(X) = \sqrt[4]{3} X \sqrt{\frac{3}{2}(1 - X^4)}, \tag{11.4}$$

with

$$X \equiv \frac{|\mu_{10}|}{|\mu_{10}^{max}|} = \frac{|\mu_{10}|}{\sqrt{\frac{(e\hbar)^2 N}{2m}}} \tag{11.5}$$

and

$$E \equiv \frac{E_{10}}{E_{20}}. \tag{11.6}$$

Both X and E can have values ranging between 0 and 1 and $f(x)$ and $G(X)$ can be optimized separately. Equations 11.3 and 11.4 yield maximum values when $f_{max} = f(0) = 1$ and $G_{max} = G(3^{-1/4}) = 1$ resulting in

Molecule (eV)	E_{10} ($\times 10^{-30} esu$)	β_{zzz}^{theory} ($\times 10^{-30} esu$)	β_{zzz}^{max} ($\times 10^{-30} esu$)	β_{zzz}^{exp} ($\times 10^{-30} esu$)
18 in chloroform	2.48	222	2600($\pm$60)	36($\pm$2)
19 in chloroform	2.34	399	3890($\pm$90)	481($\pm$12)
20 in chloroform	2.30	632	4900($\pm$120)	496($\pm$8)
21 in chloroform	2.21	855	6600($\pm$160)	171($\pm$30)
22 in chloroform	2.14	1087	8600($\pm$200)	224($\pm$40)

Table 11.2: Energy difference between ground and first excited level, E_{10}; theoretical values for the first hyperpolarizability calculated using the semiepirical method, β_{zzz}^{theory};[20] fundamental limit value, β_{zzz}^{max}; and experimental values, β_{zzz}^{exp} for the chromophores **18**, **19**, **20**, **21** and **22** in chloroform.

$\beta_{zzz} \cdot f(0) \cdot G(3^{-1/4}) = \beta_{zzz}^{max}$. That is, in the off-resonance regime, the molecule is optimized when its transition dipole moment strength is approximately three quarters of the maximum sum-rule-allowed dipole moment strength to the first excited state, and when the energy to the second excited state becomes infinitely large compared to the first excited state energy.

First, we will compare the results of the maximum values for β_{zzz} as predicted from the fundamental limits analysis (Eq. 11.2) with the theoretical values that were calculated using the semiempirical Hartree-Fock method Austin Model 1.[20] The values are summarized in Table 11.2, where, for completeness, we also list the experimental values and the difference of energy between the first excited and ground state levels - obtained from the wavelength of maximum absorption.

The values of E_{10} decrease as the conjugation length increases. This is in agreement with the simple one-dimensional particle-in-a-box model: the level spacing decreases as the size of the molecule is increased. The semiempirical theoretical calculations predict an almost linear increase with the number of carbon-carbon double bond units. This linear increase is indeed observed in the case of the first three homologues, but is in contradiction with the experimental results for the last two chromophores. The decrease of the first hyperpolarizability had been explained by configurational effects. In contrast, the calculations are performed assuming isolated molecules with fully optimized geometry, measurements are carried out in solution and the molecules could reach an excited state, which explains why the calculations do not predict the decrease. The presence of different conformers and isomers (not only all-*trans*) is more pronounced in the longer molecules.[20]

Although the maximum value of the first hyperpolarizability, β_{zzz}^{max}, and the semiempirical theoretical predictions, β_{zzz}^{theory}, differ by an order of magnitude, they turn out to be linearly related:

$$\beta_{zzz}^{theory} = \kappa \cdot \beta_{zzz}^{max}, \tag{11.7}$$

with:

$$\kappa = (0.12 \pm 0.02). \tag{11.8}$$

Fig. 11.2 shows that the fundamental limit increases linearly with respect to the number of carbon-carbon double bond units. So, the fundamental limit has the same trend as the semiempirical theoretical calculations, without the need of knowing any details about the molecular wavefunctions - only N and E_{10} are required to calculate β_{zzz}^{max} according to Eq. 11.2.

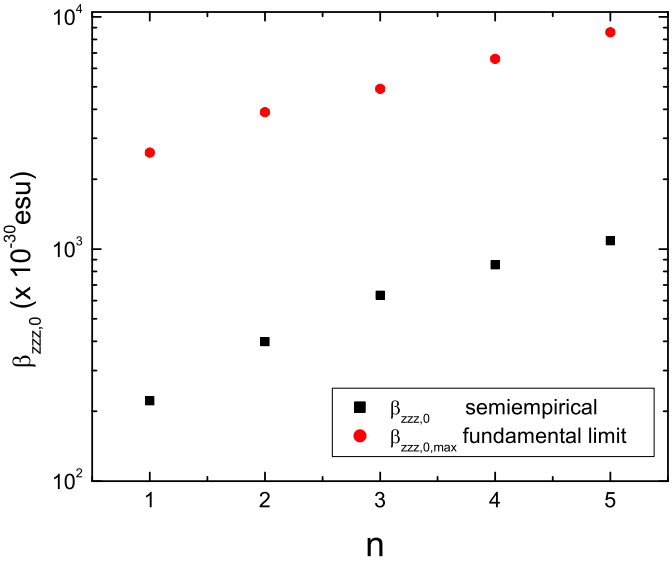

Fig. 11.2: Semiempirical theoretical hyperpolarizability, $\beta_{zzz,0}$ and fundamental limit values, $\beta_{zzz,0,max}$ as a function of bridge length.

The fundamental limits analysis can also be used together with experimental values to provide a deeper insight in the mechanisms of the non linear response. To understand why the first hyperpolarizability of a molecule in a particular environment is not optimal, we study $G(X)$ and $f(E)$. To get these functions, we first need to evaluate both X and E, as follows:[58] X can be calculated from

Molecule	X	$G(X)$	$f(E)$
18 in chloroform	0.240(±0.005)	0.386(±0.008)	0.035(±0.004)
19 in chloroform	0.288(±0.005)	0.463(±0.008)	0.27(±0.02)
20 in chloroform	0.300(±0.005)	0.482(±0.008)	0.210(±0.012)
21 in chloroform	0.307(±0.005)	0.493(±0.008)	0.053(±0.010)
22 in chloroform	0.343(±0.008)	0.549(±0.013)	0.047(±0.010)

Table 11.3: Values of X, $G(X)$ and $f(E)$ for the chromophores **18**, **19**, **20**, **21** and **22** in chloroform.

the effective number of electrons N and by retrieving the value for μ_{10} and E_{10} from the UV-VIS absorption spectrum. From the value for X, we can calculate $G(X)$. From these sets of measurements/calculations, we can determine $f(E)$ from Eqs. 11.1, 11.2 and the experimental value of β_{zzz}. From $f(E)$, we obtain E by numerical inversion. This procedure, which determines the values for X and E, allows us to analyze the nonlinear response of a molecule in terms of the normalized transition dipole moment parameter X and the energy parameter E (the excited-state energy normalized to the first excited state). It is important to note that in a system with many levels, the energy function, $f(E)$, and the normalized energy, E, must be visualized as a proxy for the energy-level spacing of the molecule. When $f(E) = 1$, the energies are arranged in a way that is optimal, while when $f(E)$ is small, the energy level spacing causes β_{zzz} to vanish.

Table 11.3 summarizes the results of the fundamental limits analysis for the chromophores in chloroform. We can observe an increase of X as a function of the number of carbon-carbon double bond units. Since X corresponds to a ratio, what this is telling us is that the actual transition dipole moment $|\mu_{10}|$ grows faster than the maximum limit $|\mu_{10}^{max}|$ as the conjugated length increases. As the value of X increases, so does $G(X)$, according to Eq. 11.4.

Before considering the energy function, let us once again use the one-dimensional particle-in-a-box model analogy. On one hand, the fundamental limit predicts that the energy function, $f(E)$, is maximized when the level spacing is increased and goes to zero as the first and second excited levels get closer. However, the level spacing is expected to decrease as the size of the molecule is increased. This means that if the structure of the molecules is similar - as it would be expected for homologues - the values of the energy function, $f(E)$ should also decrease as the length of the conjugated path increases. In fact, with the exception of molecule **18**, this trend is observed in the series of molecules. The values of $f(E)$ for molecules **18**, **21** and **22** are of the same order of magnitude as the values reported in the past for other organic molecules.[58] Molecules

19 and **20** have a better energy function than any other molecule previously studied, although none of them breach the fundamental limit. The decrease of $f(E)$ is dramatic when we go from molecules **19** and **20** to molecules **21** and **22** - and the fact that molecule **18** does not follow the predicted trend - shows that the particle-in-a-box analogy only works qualitatively. The failure of molecules **18**, **21** and **22** to achieve a good energy function indicates that the first and second excited levels are close. In the case of molecules **21** and **22** the spacing of the levels could be due to the presence of different conformers and isomers of the longer molecules.[20]

11.2 Chromophores as ligand molecules

11.2.1 Amylose as host material

In this section we describe how the chromophores described in section 11.1 are the molecular guest materials that are made into the inclusion complexes. As such, they are also called the ligand molecules for the docking experiments with the amylose host (see part 11.2.2). As a linear optical host material, a total of 4 different types of amylose have been used. The first experiment, with the short (n = 1) parent stilbazolium chromophore (structure **18**), has been performed with a low-molecular weight amylose (type *I*, $MW_{ave} = 4500$). The specific properties of this type of amylose host in conjunction with the short ethenyl linkage in the chromophore guest results in a 1:1 complex.[39, 40] For the set of inclusion experiments with the longer homologues, three types of amylose hosts have been used, characterized by a high (type *II*, $MW_{ave} = 80,000$); a medium (type *III*, $MW_{ave} = 16,000$); and a low (type *IV*, $MW_{ave} = 8,000$) molecular weight. The choice was limited by commercial availability (Aldrich and TCI). The amyloses were reagent grade and used as received. The solutions of **21** and **22** in *III* were centrifuged at 3000 rpm for 30 min prior to the measurements. The supernatant was used for the measurements. The other solutions remained clear after the complexation and were used as received from Naval Research Labs (NRL). The concentration of the chromophore in the solutions was determined by adding 9 ml DMSO to 1 ml of the water solutions. It has been shown that above a DMSO volume fraction of 0.7, negligible complexation occurs.[38] The effective chromophore concentrations were determined based on the absorption coefficients for the chromophores in 90% vol DMSO/water solutions. This procedure leads to identical results for the samples that were used as received from NRL. The UV-VIS absorption spectra were taken with a Perkin-Elmer Lambda 900 spectrophotometer.

The octupolar crystal violet in methanol was used as a reference at the fun-

damental wavelength of 800 nm, with $\beta_{zzz,800nm} = 338 \times 10^{-30}$ esu.[16, 50] The effect of the different symmetry (octupolar for the reference, dipolar for the chromophores) and the effective local fields at the optical frequencies were all taken into account in the same manner as described in Chapters 5 and 8. The chromophore concentration was kept low enough for the HRS measurements to ensure an absorbance below 0.1 at the second-harmonic wavelength. This avoids self-absorption of the HRS signal at 400 nm. The dynamic hyperpolarizability value is also a function of the measurement wavelength due to the electronic resonance, so not only is the real and imaginary part of the linear polarizability (refractive index and extinction coefficient) dependent on wavelength, but so is the hyperpolarizability β_{zzz}. For the simple case of a single charge transfer band as is typically found in these systems, the simple two-level model should be applicable to extrapolate the measured values to the static hyperpolarizability value, $\beta_{zzz,0}$.[51] Since the two-level model is known to work well when the fundamental and second harmonic wavelengths are both on the low-energy side of the excitation, we have also performed HRS measurements at 1300 nm on one chromophore-amylose (chromophore **19** in amylose *III*) combination, which was more resonantly enhanced than the other case, to compare the static hyperpolarizability values,$\beta_{zzz,0}$ derived from the two different measurements. For the HRS experiments at 1300 nm, the value of $\beta_{zzz,1300nm} = 54 \times 10^{-30}$ esu for the hyperpolarizability of the dipolar Disperse Red 1 molecule in chloroform was used as a reference.[20]

11.2.2 Molecular modelling

To gain a more in-depth understanding of the effects of nano-engineering by inclusion, theoretical docking experiments using the autodock3 program with the Autodock Tools (ADT) interface were performed.[52] The docking simulations were performed with two types of amylose (type *I*, $MW_{ave} = 4500$; and type *III*, $MW_{ave} = 16000$). These types were selected because the first experiment showing the enhancement strategy was based on type *I*, while the best enhancement results in the present study were obtained with type *III*. All 5 chromophore variants, with the number of carbon-carbon double bonds ranging from n = 1 to 5, were used as ligands in the docking algorithm.

A number of different simulations were allowed to run, with both amylose types as host. The ligands were either completely rigid, fully flexible or with only torsional flexibility for the aliphatic alkyl chain or for the chromophoric moiety. The ligands were considered both with and without bromide counteranion complexation. The ring systems in the chromophoric moiety were planar and rigid in each simulation. For the type *III* amylose, docking of a second chromophore ligand was considered in an amylose helix containing

already one ligand in the middle of the host.

Each amylose helix molecule was subjected to the docking procedure with Gasteiger-Marsili empirical atomic partial charges,[53] with explicit polar hydrogens and solvation parameters corresponding to an aqueous environment. Prior to docking, all chromophore ligand structures were optimized at the PM3 semi-empirical level, using the HyperChem 7.0 program package.[54] These structures were used as the starting structures.

To explore the tendency for *cis*-to-*trans* isomerisation, simulations were started using the initial all-trans conformation, with the Br^- complexed ligand and the type *III* amylose. A series of simulations with different starting conditions and torsional freedom were performed:

1. In the conformation of the chromophore the alkyl chain is kept rigid, resulting in n + 2 degrees of torsional freedom for the chromophores with n conjugated carbon-carbon double bonds (see Fig. 11.3 for n = 2).
2. The conformation of the ligand allows fully flexible torsions.
3. The single bonds in the aromatic part of the ligand are rigid and the alkyl chain is flexible.
4. The conformation of the ligand is fully rigid.

Fig. 11.3: The flexible (black) and rigid (red) torsions for the final molecular modelling docking simulations with initial conformation of the chromophore ligand bent and the alkyl chain rigid, resulting in n+2 degrees of torsional freedom for these chromophores with n conjugated carbon-carbon double bonds; shown here with n = 2.

In the autodock3 version, the Genetic Algorithm (GA) is combined with the phenotypic local search (LS) by using the pseudo-Solis and Wets algorithm. This combined algorithm (GALS) was used here, with the majority of the parameter settings as suggested by the manual.[55] Specifically for this study, some of the default setting parameters were changed. The maximum number of energy evaluations was set to 1,500,000. The number of grid points for the grid-box defining the docking area was set to 40 along the x- and y-axes and to 126, i.e. the maximum, along the z -axis. The latter is the longitudinal

axis of the amylose helix. For the type *II* amylose, this grid-box, covering approximately one third of the helix, was positioned in two different ways: in the center of the amylose and at the end. For the type *I* amylose, the grid box covered the complete helix and consequently, only one type of grid-box position was used. Additionally for the short stilbazolium parent chromophore, docking simulations were performed with this grid-box shifted 60 grid-points outwards along the z-axis to check the effect of coverage.

In all simulations, the initial state of the ligand, the dihedral offset and the relative dihedrals were chosen randomly. A platform-independent library was used to generate the random numbers. Initially, the number of GALS runs was set to 10 and the maximum number of energy evaluations to 270,000. This protocol performs well for all the ligands (n = 1 to 5) without bromide counteranion and docking in the middle of the host; and for the shorter ligands (n = 1 to 2) with a bromide counteranion. For the simulations with longer ligands (n $\geq$ 3) and complexed with bromide, or for the grid-box shifted towards the end of the host, the number of necessary runs was estimated using the genetic algorithm without the local search extension, which is faster than GALS. The appropriate number of runs was found to be 50, more simulations did not change the final result. Finally, a simulation protocol combining the GALS method with the number of runs equal to 50 and with the maximum number of energy evaluations set to 1,500,000 was applied.

For each docking simulation, five different energy data belonging to the conformation with the best docked energy were obtained: the Final Docked Energy (FDE), the Final Energy of Binding (FEB), the Inter Molecular Energy (IME), the Internal Energy of Ligand (IEL), and the Torsion Free Energy (TFE). The FDE is the sum of the IME and IEL, while the FEB is the sum of the IME and TFE.

11.3 Experimental Results

The inclusion experiments for chromophores **19**, **21** and **22** were initially tried in a new low-molecular weight amylose, type *IV* ($MW_{ave} = 8,000$). The low MW type *I* amylose ($MW_{ave} = 4500$) that was used for the inclusion of **18** was no longer commercially available and the type *IV* was chosen as the best replacement. However, the type *IV* amylose failed to form inclusion complexes in this study. The molecular weight is possibly not the only parameter that differs between type *I* and type *IV*. Other parameters relevant for inclusion that can be related to the molecular weight (solubility, purity of amylose in terms

of content of branched amylopectine, etc.) can also play a role. Chromophore **20** was no longer available at sufficient quantities at the time of preparing the inclusion complexes, so was not used. Therefore, chromophore **18** was embedded in amylose type *I*, and chromophores **19**, **21** and **22** were embedded in amylose type *II* and *III*, with MW_{ave} of 16,000 and 80,000, respectively.

The UV-VIS absorption spectra for the new inclusion complexes of chromophores **19**, **21** and **22** in amylose type *II* and *III* indicate that there is only a marginal difference in spectral position of the charge transfer absorption band for each of the 3 chromophores when embedded in each of the two types of amylose. The red shift for longer conjugation links, as previously observed for free chromophores in chloroform, is also observed when embedded in amylose, but less pronounced, suggesting that the helical environment is more polar relative to chloroform. By the same token, a large red-shift of λ_{max} in chloroform for each chromophore relative to DMSO is indicative of a negative solvatochromism, in that λ_{max} tends to decrease with increasing solvent polarity.[66]

Experimentally, it is determined that at this wavelength all 6 hyperpolarizability values (for 3 different chromophores in 2 types of amylose) do not show any appreciable demodulation. Therefore, we obtain an accurate (fluorescence free) and precise (low estimated statistical uncertainty) average for the dynamic hyperpolarizability at the measurement wavelength, $\beta_{average}$. From the spectral position of the charge transfer resonance, λ_{max}, and assuming the validity of the two-level model - which we address below, it is then possible to deduce a value for the static hyperpolarizability, $\beta_{zzz,0}$, also tabulated in Table 11.4.

We have also performed HRS experiments on chromophore **19** in amylose *III* at a fundamental wavelength of 1300nm, as shown in Table 11.4 - in italics - to test the validity of the extrapolation from the measured value of β to the static value of β using the simple two-level model when the second harmonic wavelength photon has higher energy than the charge transfer state. Because of the multiphoton fluorescence contribution at this longer wavelength, the hyperpolarizability value is determined by taking the AM high frequency limit. Therefore, the estimated uncertainty for $\beta_{zzz,1300}$ is larger than for $\beta_{ave} = \beta_{zzz,800}$, the hyperpolarizability value that was determined at 800 nm, where no multiphoton fluorescence contribution was observed. Because the systematic error has been removed by our fluorescence demodulation technique, the accuracy of the result at 1300 nm is still better than 20%.

A control experiment on free amylose was also performed. No HRS signal

Compound	$\lambda_{max,complex}$ (nm, in water)	$\beta_{zzz,800}$ ($\times 10^{-30} esu$)	$\beta_{zzz,0}$ ($\times 10^{-30} esu$)
19 in *II*	524	372(±)	152(±2)
21 in *II*	534	634(±5)	275(±2)
22 in *II*	545	1520(±15)	700(±10)
19 in *III*	521	403(±9)	162(±4)
19 *in III*		$\beta_{zzz,1300}$ *600*(±*100*)	*180*(±*30*)
21 in *III*	531	760(±4)	324(±2)
22 in *III*	540	2390(±30)	1070(±13)

Table 11.4: Wavelength of maximal absorption, λ_{max}, average dynamic first hyperpolarizability at 800 nm, $\beta_{zzz,800}$, and static first hyperpolarizability, $\beta_{zzz,0}$, for the chromophores **19**, **21** and **22** in amylose type *II* and *III* in water. For completeness, we include the average dynamic first hyperpolarizability of chromophore **19** in amylose *III* at a fundamental wavelength of 1300nm, $\beta_{zzz,1300}$, and the corresponding value of $\beta_{zzz,0}$ - in italics -.

could be detected and the upper limit of the value of the hyperpolarizability of an amylose helix is found to be much lower than for free chromophores or the chromophores in amylose.

It is also clear from the values in Table 11.4 that host amylose *III*, the lower molecular weight type, has the largest effect on the nonlinear response of all the guest chromophores. Both types of amylose hosts show a reduction in hyperpolarizability for **19**, yet an increase for **21** and **22**. The nature of the effect is clearly the same for the two types of amylose, but the effect of type *III* with MW_{ave} of 16,000 is most profound.

Table 11.5 shows the values for the experimentally-determined static hyperpolarizabilities in the amylose inclusion complexes for **19**, **21** and **22** in amylose type *III*, together with the same values for the free chromophores in chloroform solution. From the good agreement between the static hyperpolarizability values that have been obtained from the dynamic hyperpolarizability values at 800 and at 1300 nm for chromophore **19** in amylose *III* ($162(\pm 4)\times 10^{-30}$esu versus $180(\pm 30)\times 10^{-30}$esu, respectively) we conclude that the simple two-level model works well for these chromophores even when near resonance due to the single dominant charge transfer band. More importantly, the differences on the static hyperpolarizability obtained from these two different measurements are small enough that our analysis can yield meaningful results.

	$\lambda_{max,chloroform}$ (nm)	$\beta_{zzz,0,chloroform}$ ($\times 10^{-30} esu$)	$\lambda_{max,III}$ (nm)	$\beta_{zzz,0,III}$ ($\times 10^{-30} esu$)
18	496	36(±2)		
18′	477	100(±10)	492	200(±5)
19	524	481(±12)	521	162(±4)
20	546	496(±8)		
21	556	171(±30)	531	324(±2)
22	570	224(±40)	540	1070(±13)

Table 11.5: Wavelength of maximal absorption, $\lambda_{max,III}$, and static first hyperpolarizability, $\beta_{zzz,o,III}$, for the chromophore 18' in amyloses type *I* and for chromophores **19**, **21** and **22** in amylose type *III* in water, and wavelength of maximum absorption, $\lambda_{max,chloroform}$, and static first hyperpolarizability, $\beta_{zzz,0,chloroform}$, for the chromophores **18** to **22** in chloroform. Note that chromophore 18' has a *docosyl* group, while chromphores **18** to **22** have an octadecyl group of the pyridinium nitrogen.

We observe slight increase in the static hyperpolarizability upon complexation for **21**, a slight decrease for **19** and a significant increase for **22**. This latter increase would agree with the earlier observation for the parent stilbazolium dye **18**, which also exhibited an increase in the hyperpolarizability upon complexation. This would be, in conjunction with the earlier rationale, good evidence that indeed, the additional conformational freedom for the longer homologues in solution reduces the effective second-order nonlinear response. Upon reducing this freedom by fixing the all-*trans* conformation in a helix, the hyperpolarizability is enlarged. Quite to the contrary, however, for the shorter homologue in this study, **19**, a decrease in hyperpolarizability is observed upon complexation. Also, the quantitative analysis shows that only for **18** and **22**, this explanation would be valid, and only for some types of amylose.

11.4 Modelling Results

To build an understanding of the effect of the inclusion in amylose helices on the chromophores, and especially to try to understand the differences in behavior upon complexation between the different chromophore lengths, molecular modelling was invoked to study the conformation and orientation of the chromophore guest molecules in the amylose host.

First, the geometry-optimized isolated ligand structures all show the all-*trans* and linear conformation at their energy minimum. This is in agreement with earlier geometries obtained by the semiempirical Hartree-Fock method Austin Model 1 (AM1) by use of the MOPAC program package.[20]

Secondly, the basic assumption that the chromophore is allowed and prefers to go inside the amylose helix and is not simply complexed to the outer surface of the amylose is confirmed by the docking simulations. When the grid-box is shifted out of the amylose host, providing lower coverage of the chromophore, the interaction energy is worse than when the grid-box is positioned in the middle of the helix, when the chromophore is fully covered. This observation holds independently of the number n of carbon-carbon double bonds in the chromophore moiety, the length of the amylose host, and the degree of flexibility of the chromophore ligand: the best energy parameters were found for the ligands that are fully covered by the amylose, even if the alkyl chain has to be in a wrinkled form. In general, the length of the alkyl chain reduces from its fully extended length of 22.6 to between 17 $\overset{\circ}{A}$ and 20 $\overset{\circ}{A}$. A schematic representation of the docking of the n = 1 ligand (chromophore **18**) in the amylose type *I* with $MW_{ave} = 4500$ is shown in Figs. 11.4 and 11.5.

Both types of amylose can harbor the ligand, but for type *III* amylose, it was found that both orientations of the ligand with respect to the host (polar chromophore head pointing to the middle or aliphatic chain oriented toward the middle of the longer amylose) resulted in equivalent docking energies. While this is not relevant for the second-order nonlinear response in terms of the non-centrosymmetry of a single nonlinear chromophore in the linear amylose matrix, the longer type *III* amylose could accommodate up to at least 2 ligands with room for a third one (n = 1) in any combination of head-to-tail, head-to-head and tail-to-tail. This clearly is important, since it would allow for the centrosymmetric arrangement of two dipolar chromophores in amylose type *III* ($MW_{ave} = 16,000$). By the same token, in the even longer amylose type *II* ($MW_{ave} = 80,000$) an even larger occurrence of centrosymmetric arrangements of dipolar chromophores should be expected. However, since the hyperpolarizability values found for these two types of amylose do not differ drastically, the centrosymmetric arrangement can be ruled out on the basis of experimental evidence.

In each docking simulation with flexible ligand, the initial all-*trans* conformation is conserved, independent of amylose length or docking position. For the longer chromophore ligands, this all-*trans* conformation could be observed only in the middle of the longer amylose without bromide counterion complexation or in the terminal amylose part with Br^- complexation. On the other hand, in

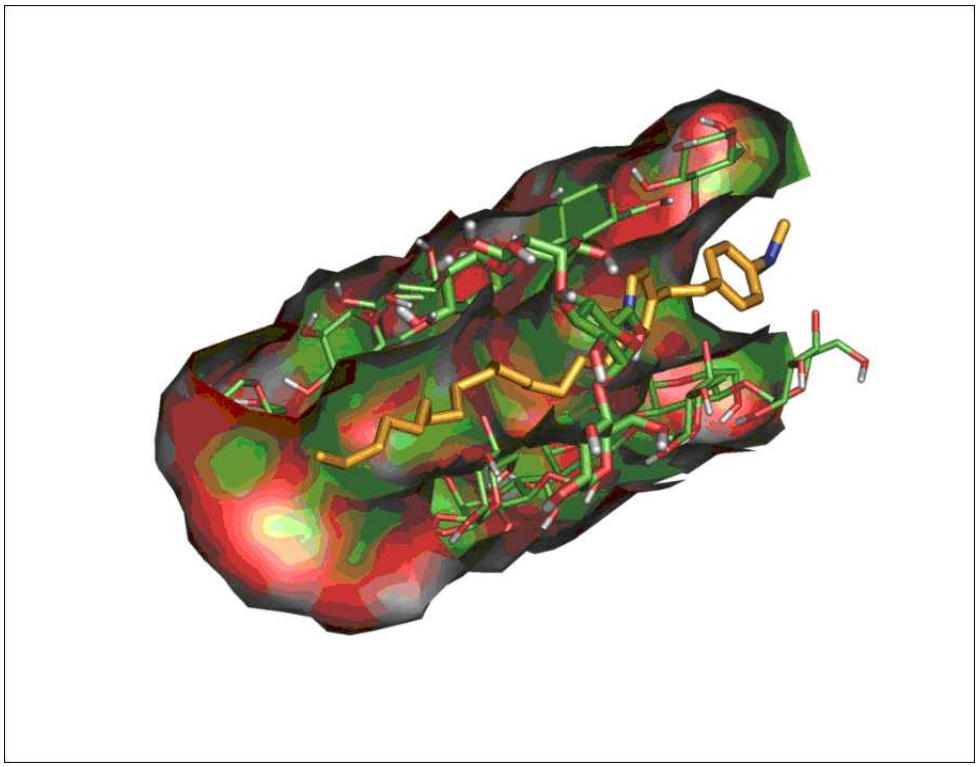

Fig. 11.4: Schematic representation of the inclusion complex between chromophore **18** guest molecule (ligand) and amylose type *I* (docking) host. Notice that for clarity we have removed part of the amylose to provide an inside view.

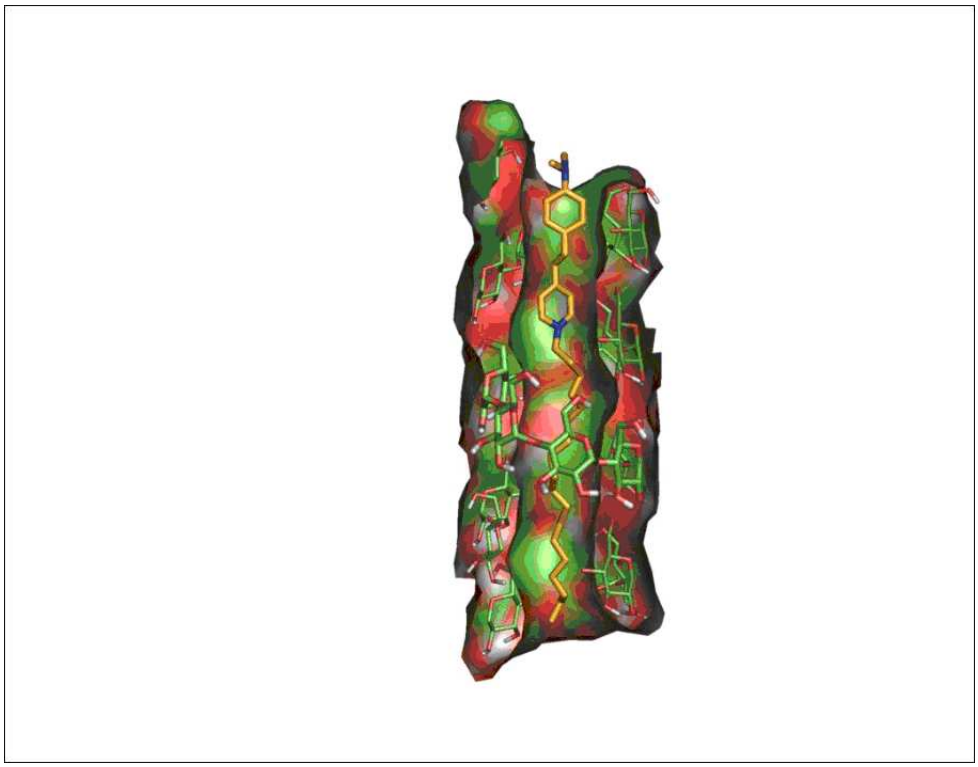

Fig. 11.5: Schematic representation of the inclusion complex between chromophore **18** guest molecule (ligand) and amylose type *I* (docking) host. Notice that for clarity, we have removed part of the amylose to provide an inside view.

the shorter amylose type, at a terminal of the longer type *III* amylose without bromide ion, or with bromide complexed structures in the middle position, up to 3 *cis* linkages could be observed along the conjugation path. This indicates that the coverage by a long amylose host might indeed have some stabilizing effect on the all-*trans* conformation.

On the other hand, the co-planarity of the two rings (arbitrarily defined as angles between the two rings smaller than 20 degrees) did not show any correlation with the number n of carbon-carbon double bonds. However, it was also found that coplanarity of the phenyl and pyridinium rings and all-trans conformation of the conjugation path are never simultaneously present in ligands other than the short parent stilbazolium **18**. From the final series of 4 simulations with the different initial conditions and different flexibilities, we found that the final conformations of the included dyes corresponding to the lowest energy were coplanar for **18** and **22** only, while the conjugating path showed a trend from *trans* for **18** and **19**, 1-*cis* for **20**, all-*trans* again for **21**, and finally 2-*cis* for **22**.

11.5 Discussion in terms of fundamental limits

The usefulness of the theory of fundamental limits, expressed in terms of the largest diagonal tensor component of the off-resonant hyperpolarizability, $\beta_{zzz,0}$, in the context of these elongated molecules with a major molecular charge-transfer along the z-axis, has been discussed previously.[33, 67]

The combined analysis of the linear (UV-VIS absorption spectral data) and nonlinear ($\beta_{zzz,0}$) optical results has been applied to the chromophores **18** - **22**, as guest molecules in the amylose host complexes. The results of this analysis are given in Table 11.6 for the dyes as guest chromophores in the amylose hosts.[1] The function $G(X)$ and $f(E)$ for the 5 chromophores free in solution and complexed in amylose type *III* are shown in Fig. 11.6. We stress that because β_{zzz} is far from the fundamental limit, the system is not representable by a three-level model. However, we have found in past analyses[58, 75] that the function $f(E)$ limits β_{zzz} for all non-encapsulated molecules. Here, we apply the same analysis to study the effect of encapsulation on $f(E)$. While the three-level model may not hold, a large $f(E)$ would be a proxy for more favorable energy level spacing and as an indicator of potentially new physics.

[1] The results for the free chromophores in chloroform were listed in Table. 11.3.

Molecule	E_{10} (eV)	X	$G(X)$	$f(E)$
18 in *I*	2.54	0.104(±0.004)	0.168(±0.006)	0.25(±0.04)
19 in *III*	2.42	0.098(±0.006)	0.158(±0.010)	0.30(±0.03)
20	*n.a.*	*n.a.*	*n.a.*	*n.a.*
21 in *III*	2.36	0.066(±0.004)	0.106(±0.006)	0.58(±0.05)
22 in *III*	2.25	0.096(±0.006)	0.155(±0.010)	0.96(±0.10)

Table 11.6: Energies and transition moments determined from UV-vis absorption spectra for the amylose inclusions. $f(E)$ is determined from a combination of linear absorbance spectrum, measurements of β and the sum rules.[58]

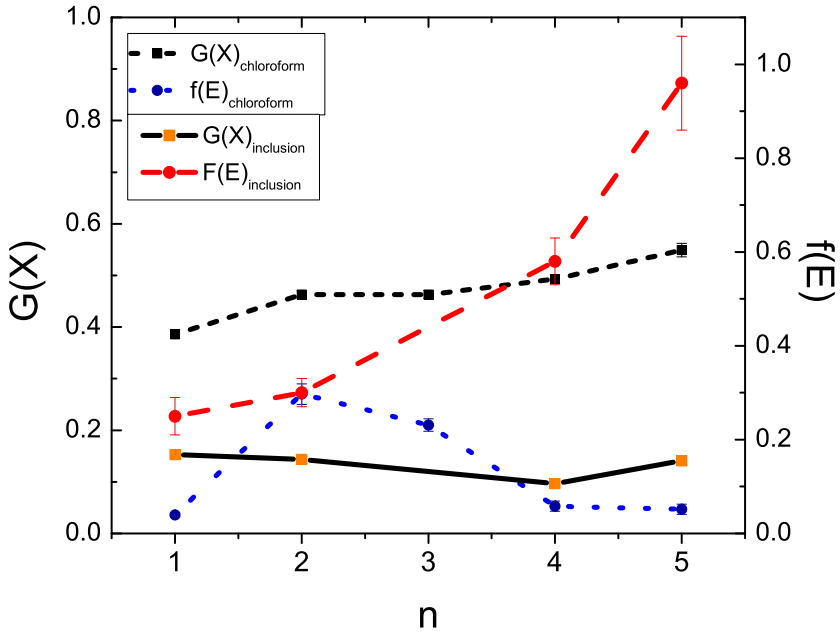

Fig. 11.6: Function $G(X)$ of transition dipole moment parameter X, and function $f(E)$ of energy for the chromophores **18** (n=1), **19** (n=2), **20** (n=3), **21** (n=4) and **22** (n=5) in solution (free chromophores) and in amylose type *III* (inclusion complexes).

For all chromophores, the function $G(X)$ of the transition dipole parameter X is near the optimal value to maximize the hyperpolarizability in solution but reduced by a factor of 3, on average, in amylose. This is a consequence of the parameter X itself being reduced by (on average) the same factor. $G(X)$ is a linear function of X for values of X smaller than 0.7. The transition probability for a molecule isolated in an amylose helix is thus reduced relative to this probability in a free chromophore.

The inclusion of the chromophores inside the amylose has a positive effect on the energy function, $f(E)$, for the chromophores that had a small $f(E)$ performance in chloroform (chromophores **18**, **21** and **22**). For chromophore **19**, which already had a relatively large value of the energy function in chloroform, the increase of $f(E)$ is minimal, and hence, the nonlinear response decreases due to the effects of reduced $G(X)$. For the other chromophores, $f(E)$ increases. This increase in most pronounced for the chromophores **21** and **22**, which show very low values of $f(E)$ in solution. As previously explained, the implication is that for **21** and **22** in solution, the energy ratio E is near unity, or that the transition energy E_{20} is very similar to E_{10}. In other words, for chromophores **21** and **22** in solution, the excited-energy levels are closely-spaced, so they draw oscillator strength from the two lowest states with energy difference E_{10}, thereby decreasing the nonlinear response. In the inclusion complex, these states are situated at much higher energy, so that they do not destructively interfere with the two lowest states.

It is clear from Tables 11.3-11.6 and Fig. 11.6, which compares $f(E)$ and $G(X)$ for the chromophores in solution with those incorporated into amylose type *III*, that the largest effect of the inclusion are seen for the energy function $f(E)$ for chromophore **21** (factor of 10 increase) and chromophore **22** (factor of 20 increase). This is significant because according to past studies the energy function $f(E)$ appears to be the dominant factor in suppressing the hyperpolarizability below the apparent limit.[58] In fact the energy function for chromophore **22** is very close to unity. To our knowledge, this is the largest energy function ever reported.

It is also interesting that while $f(E)$ increases, $G(X)$ decreases, so that the best molecules are still at the apparent limit. It would be most important if a paradigm was found that could independently vary $G(X)$ and $f(E)$; and the present work, which shows that we can significantly increase $f(E)$ by a factor that is much greater than the decrease in $G(X)$ is the first step in this direction. Modelling results show that **21** is in the all-*trans* conformation without coplanarity between the two rings, yet **22** is coplanar with the loss of the *trans* conformation in favor of 2-*cis*. This leads to the conclusion that loss

of coplanarity when chromophores are free in solution has the most detrimental effect on the energy function $f(E)$, while the restoration of the coplanarity upon complexation for **22** increases the energy function to a very sizeable value (0.95 out of a maximum of 1). This means that we need to add loss of coplanarity to our chemical picture of causes of non-optimal excited-state energy levels.

Fig. 11.7 shows graphically the relative performance of the free chromophores in chloroform solution and in the amylose complex. The electron-normalized value of the static hyperpolarizability is shown as a function of wavelength of maximum absorption, together with the apparent upper limit for hyperpolarizabilities. There is a clear correspondence between the increase in the energy function $f(E)$ and improved nonlinear response. Chromophore **22**, which shows the largest increase in $f(E)$ due to the restored coplanarity between the two rings in the stilbazolium-type chromophore motif in the amylose complex, exceeds the apparent limit within experimental uncertainty but is still well below the fundamental limit. To our best knowledge, this is the first such observation of the hyperpolarizability falling into the gap between the fundamental and apparent limit for a single molecule. A second hyperpolarizability of a cross-linked material has been found to breach the gap, but a collective excitation of several molecules is responsible.[68]

11.6 Conclusions

We have shown that the combination of increasing the conjugation path in ionic donor-acceptor charge-transfer chromophores with the inclusion of these chromophores in a supramolecular amylose helix is indeed a good bottom-up nano-engineering strategy to experimentally obtain the theoretically predicted large hyperpolarizability values. The theoretically predicted enhancement was linear in the number of conjugated double bonds. Hence, with the synthetic availability of the decapentaenyl bridge instead of the ethenyl linkage between the (dimethylamino)phenyl and the pyridinium ring, an increase of a factor of 5 should be achievable. Incorporating the molecule in an amylose inclusion had been shown to result in a doubling of the hyperpolarizability. The combination had promised an order of magnitude improvement when starting from 4-2-[4-(dimethylamino)phenyl]-ethenyl-N-octadecylpyridiniumbromide in solution. For this stilbazolium dye, a hyperpolarizability in solution of 100 ($\pm$ 10) $\times 10^{-30}$ esu had been experimentally determined. For the 4-2-[4-(dimethylamino)phenyl]-decapentaenyl-N-octadecylpyridiniumbromide system, a hyperpolarizability of 1070 ($\pm$13) $\times 10^{-30}$ esu is experimentally measured in

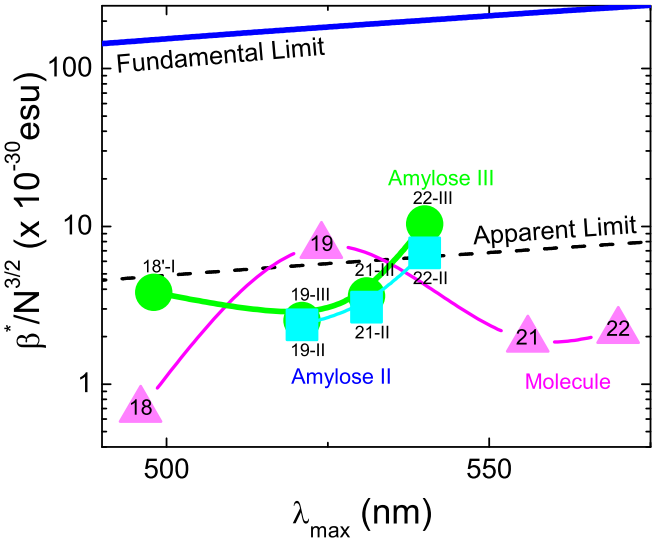

Fig. 11.7: Experimental electron-normalized values for the static hyperpolarizability, $\beta^*/N^{3/2}$, as a function of the wavelength of maximal absorption, λ_{max} for chromophores in chloroform, chromophores in amylose *II* in water and chromophores in amylose *III* in water. For comparison, 18'-I has been taken from an earlier inclusion study[40] of chromophore 18' with amylose type *I*.

amylose type *III*. This is indeed exactly an order of magnitude enhancement by increasing the length of conjugation. Therefore, we can conclude that the two enhancement strategies are independent of each other and can be applied independently to arrive at nano-engineered molecular complexes with strong second-order nonlinear optical responses.

From the combination of an accurate experimental determination of fluorescence-free hyperpolarizabilities of the chromophores in chloroform solution and in amylose inclusion complexes in water, and with the results of modelling of this docking with an extensive variation of modelling parameters, it follows that the most important structural feature for optimizing the molecular second-order nonlinear response is not so much the all-trans configuration of the long conjugated path between donor and acceptor ring moiety, but that the rings be coplanar. When this coplanarity is retained, as in chromophores **18** and **22** when embedded in an amylose helix, the theoretically predicted enhancement can be achieved. When the inclusion strategy fails to result in coplanarity, the theoretical enhancement is not observed.

From the fact that amylose type *I* ($MW_{ave} = 4500$) and amylose type *IV* ($MW_{ave} = 8000$) - with similar molecular weight - give such differing degrees of inclusion (1:1 inclusion with type *I* and no inclusion with type *IV*), while higher MW amylose results in inclusion, it has to be concluded that other parameters describing the amylose, possibly related to the MW, also come into play. This is confirmed by the finding that the nature of the inclusion effect is similar for amylose type *II* and *III*, but the extent of the effect is also different (largest for type *III*). Therefore, we have to conclude that the nature of amylose is not effectively described by its molecular weight alone. For inclusion complexes, we conclude that amylose of similar molecular weight but from alternative sources should be used and compared. Additionally, we have found experimentally that for chromophore **19** in amylose type *III*, the simple two-level model appears to correctly account for dispersion to get the static hyperpolarizability. It has long been recognized that this model, which neglects damping, should theoretically be inadequate close to resonance. Different attempts to refine the two-level model include considering vibrational substates,[69, 70, 71] or damping and the concomitant imaginary part of the hyperpolarizability.[72, 73, 74] However, none of these refinements has been shown to provide for an adequate description of the dispersion. Here, we have found good experimental agreement between the static hyperpolarizabilities derived from different measurement wavelengths in one control experiment. Thus, we can conclude that our analysis provides to good approximation the static hyperpolarizability.

By comparing the experimental data with the apparent limit of the hy-

perpolarizability as derived from sum rules, we have experimentally confirmed that closely-spaced excited-state energy levels are the main cause of suppressing the hyperpolarizability to well below the fundamental theoretical maximum and below the apparent limit. Incorporating the chromophores into an amylose complex has a pronounced positive effect on the energy level spacing, resulting in the expected strong increase in second-order nonlinear response by increasing the energy function $f(E)$. This approach has guided the use of nano-engineering to improve the best molecules, and, we have found that making the rings planar seems to have the most pronounced effect.

11.7 Perspectives

With the demonstration that the effects of making longer molecules and the inclusion strategy to enhance the second-order nonlinear optical response act independently, it is only natural to look towards the combination of these two strategies with other proven enhancement strategies. One such strategy that has already been shown to be valid independently from, yet in combination with the elongation strategy, is the N-arylation strategy in stilbazolium-type chromophores.[33] Therefore, one can indeed envision the inclusion in an amylose helix of an N-arylated stilbazolium-type chromophore with extended conjugation.

One important property that affects the second-order nonlinear optical properties of a material is symmetry. For the longer type *III* amylose, the modelling has indicated that more than one chromophore can be included in the interior of the helix, and that all relative orientations of head-to-head, tail-to-tail and head-to-tail can be obtained with only very small differences in energy. However, the centrosymmetric head-to-head and tail-to-tail nano-arrangement of the chromophores in the amylose host will have a detrimental effect on all even-order nonlinear-optical susceptibilities. Therefore, for an even more quantitative understanding of the effect of the inclusion, these symmetry considerations should be taken into account. This will most probably be reflected in the thermodynamics of the interaction versus the kinetics of the inclusion: the very small energy difference between the centrosymmetric (head-to-head or tail-to-tail) and the non-centrosymmetric (head-to-tail) inclusion will not likely result in a preponderance of the thermodynamically favored configuration. The inclusion by itself, irrespective of symmetry, induces by far the largest energy change.

Bibliography

[1] J. Pérez-Moreno et al. J. Chem. Phys. **126**, 74705 (2007).

[2] P. N. Prasad and D. J. Williams, *Introduction to Nonlinear Optical Effects in Molecules and Polymers* (Wiley: New York, 1991).

[3] D. J. Williams, *Nonlinear Optical Properties of Organic and Polymeric Materials* (ACS: Washington, D.C., 1983; Vol. 233) .

[4] D. J. Williams, Angew. Chem. Int. Ed. Engl. **23**, 690 (1984).

[5] K. D. Singer, J. E. Sohn, L. A. King, H. M. Gordon, H. E. Katz, and C. W. Dirk, J. Opt. Soc. Am. B, **6**, 1339 (1989).

[6] C. C. Teng and A. F. Garito, Phys. Rev. B,**28**, 6766 (1983).

[7] L. -T. Cheng, W. Tam, S. H. Stevenson, G. R. Meredith, G. Rikken, and S. R. Marder, J. Phys. Chem. **95**, 10631 (1991).

[8] L. -T. Cheng, W. Tam, S. R. Marder, A. E. Stiegman, G. Rikken, and C. W. Spangler, J. Phys. Chem. **95**, 10643 (1991).

[9] C. C. Teng and A. F. Garito, Phys. Rev. Lett. **50**, 350 (1983).

[10] L. R. Dalton, Synth. Met. **124**, 3 (2001).

[11] Y. Shi, C. Zhang, H. Zhang, J. H. Bechtel, L. R. Dalton, B. H. Robinson, and W. H. Steier, Science **288**, 119 (2000).

[12] G. H. Robinson, et al. Chem. Phys. **245**, 35 (1999).

[13] K. D. Singer, and A. F. Garito, J. Chem. Phys. **75**, 3572 (1981).

[14] J. Zyss, Chem. Phys. **98**, 6583 (1993).

[15] J. Zyss and I. Ledoux, Chem. Rev. **94**, 77 (1994).

[16] T. Verbiest, K. Clays, C. Samyn, J. Wolff, D. Reinhoudt, and A. Persoons, J. Am. Chem. Soc. **116**, 9320 (1994).

[17] M. Yang and B. Champagne, J. Phys. Chem. A **107**, 3942 (2003).

[18] T. Verbiest, K. Clays, A. Persoons, F. Meyers, and J.-L. Brédas, Opt. Lett. **18**, 525 (1993).

[19] T. Kodaira, A. Watanabe, I. Osamu, M. Matsuda, K. Clays, and A. Persoons, J. Chem. Soc. Faraday Trans. **93**, 3039 (1997).

[20] K. Clays, K. Wostyn, G. Olbrechts, A. Persoons, A. Watanabe, K. Nogi, X. -M. Duan, S. Okada, H. Oikawa, H. Nakanishi, H. Vogel, D. Beljonne, and J. -L. Bredas, J. Opt. Soc. Am. B **17**, 256 (2000).

[21] K. Clays, K. Wostyn, K. Binnemans, and A. Persoons, TOPS (2001).

[22] B. J. Coe, Chem. Eur. J. **5**, 2464 (1999).

[23] B. J. Coe et al. Adv. Func. Mat. **12**, 110 (2001).

[24] B. J. Coe, L. A. Jones, J. A. Harris, B. S. Brunschwig, I. Asselberghs, K. Clays, and A. Persoons, J. Am. Chem. Soc. **125**, 862 (2003).

[25] R. W. Terhune, P. D. Maker, and C. M. Savage, Phys. Rev. Lett. **14**, 681 (1965).

[26] K. Clays, and A. Persoons, Phys. Rev. Lett. **66**, 2980 (1991).

[27] K. Clays, and A. Persoons, Rev. Sci. Instrum. **63**, 3285 (1992).

[28] K. Clays, A. Persoons, and L. De Maeyer, L. *Hyper-Rayleigh Scattering in Solution; 1 ed.*, John Wiley & Sons, Inc.: New York, **85**, 455 (1994).

[29] F. Pan, G. Knopfle, C. Bosshard, S. Follonier, R. Spreiter, M. S. Wong, and P. Gunther, Appl. Phys. Lett. **69**, 13 (1996).

[30] U. Meier, M. Bösch, C. Bosshard, F. Pan, and P. Günter, J. Appl. Phys. **83**, 3486 (1998).

[31] F. Pan, K. McCallion, and M. Chiappetta, M., Appl. Phys. Lett. **74**, 492 (1999).

[32] B. J. Coe, et al. Adv. Func. Mat. **13**, 347 (2003).

[33] K. Clays and B. Coe, Chem. Mater. **15**, 642 (2003).

[34] S. R. Marder, J. W. Perry, and W. P. Schaeffer, Science **245**, 626 (1989).

[35] S. R. Marder, J. W. Perry, C. P. Yakymyshyn, Chem. Mater. **6**, 1137 (1994).

[36] K. D. Singer, M. G. Kuzyk, and J. E. Sohn, J. Opt. Soc. Am. B **4**, 968 (1987).

[37] O.-K. Kim, L. -S. Choi, H. -Y. Zhang, X -H. He, and Y. -A. Shih, Thin Solid Films **329**, 172 (1998).

[38] O. -K. Kim and L. -S. Choi, Langmuir **10**, 2842 (1994).

[39] O. -K. Kim, L. S. Choi, H. -Y. Zhang, X. -H. He, and Y. -H. Shih, J. Am. Chem. Soc. **118**, 12220 (1996).

[40] K. Clays, G. Olbrechts, T. Munters, A. Persoons, O. -K. Kim, and L. -S. Choi, Chem. Phys. Lett. **293**, 337 (1998).

[41] I. R. Girling, N. A. Cade, P. V. Kolinsky, R. J. Jones, I. R. Peterson, M. M. Ahmad, D. B. Neal, M. C. Petty, G. G. Roberts, and W. J. Feast, J. Opt. Soc. Am. B **4**, 950 (1987).

[42] G. Marowsky, L. F. Chi, D. M"obius, R. Steinhoff, Y. R. Shen, D. Drosch, and B. Rieger, Chem. Phys. Lett. **147**, 420 (1988).

[43] V. Alain, M. Blanchard-Desce, I. Ledoux-Rac, I., and J. Zyss, J. Chem. Commun. 353 (2000).

[44] J. S. Schildkraut, T. L. Penner, and C. S. Willand, Optics Letters **13**, 134 (1998).

[45] D. Lupo, W. Prass, U. Scheunemann, A. Laschewsky, H. Rignsdorf, and I. Ledoux, J. Op. Soc. Am. B **5**, 300 (1998).

[46] K. Nogi, *Master Thesis*, Tohoku University, Sendai, Japan (in Japanese) 1999.

[47] K. Nogi, Anwar, K. Tsuji, Y. -M. Duan, S. Okada, H. Oikawa, H. Matsuda, H. Nakanishi, Nonlinear Opt. 24, 35 (2000).

[48] O. F. J. Noordman and N. F. van Hulst, Chem. Phys. Lett. **253** 145 (1996).

[49] G. Olbrechts, R. Strobbe, K. Clays, and A. Persoons, Rev. Sci. Instrum. **69**, 2233 (1998).

[50] K. Clays and A. Persoons, Rev. Sci. Instrum. **65**, 2190 (1994).

[51] J. L. Oudar and D. S. Chemla, J. Chem. Phys. **66**, 2664 (1977).

[52] G. M. Morris, D. S. Goodsell, R. S. Halliday, R. Huey, W. E. Hart, R. K. Belew, and A. J. Olson, J. Computational Chemistry, **19**, 1639 (1998).

[53] J. Gasteiger and M. Marsili, Tetrahedron Lett. 3181 (1978).

[54] M. Froimowitz, Biotechniques, **14**, 1010 (1993).

[55] `http://www.scripps.edu/mb/olson/ doc/autodock/ad305/Using_AutoDock_305.html`

[56] M. G. Kuzyk, Circuits and Devices **19**, 8 (2003).

[57] M. G. Kuzyk, Optics and Photonics News **14**, 12 (December issue) 26 (2003).

[58] K. Tripathy, J. Pérez-Moreno, M. G. Kuzyk, B. J. Coe, K. Clays, and A. M. Kelley, J. Chem. Phys., **121**, 7932 (2004).

[59] M. G. Kuzyk, Phys. Rev. Lett. **85**, 1218 (2000).

[60] M. G. Kuzyk, Opt. Lett. **25**, 1183 (2000).

[61] M. G. Kuzyk, IEEE J. Select. Topics Quantum Electron. **7**, 774 (2001).

[62] M. G. Kuzyk, Phys. Rev. Lett. **90**,039902 (2003).

[63] M. G. Kuzyk, Opt. Lett. **28**, 135 (2003).

[64] M. G. Kuzyk, Phys. Rev. A **72**, 053819 (2005).

[65] M. G. Kuzyk and D. S. Watkins, J. Chem. Phys. **124**, 244104 (2006).

[66] R. Reichardt, *Solvents and Solvent Effects in Organic Chemistry* (VCH, Weiheim, 1990).

[67] K. Clays, Opt. Lett. **26**, 1699 (2001).

[68] Q. Chen, L. Kuang, Z. Y. Wang, E. H. and Sargent, Nano Letters **4**, 1673 (2004).

[69] J. N. Woodford, C. H. Wang, and A. K. Y. Jen, Chem. Phys. **271**, 137 (2001).

[70] M. A. Pauley, and C. H. Wang, Rev. Sci. Instrum. **70**, 1277 (1999).

[71] C. H. Wang, J. Chem. Phys. **112**, 1917 (2000).

[72] G. Meshulam, G. Berkovic, and Z. Kotler, Opt. Lett. **26**, 30 (2001).

[73] G. Meshulam, G. Berkovic, Z. Kotler, Z. and A. Sa'ar, Rev. Sci. Instrum. **71**, 3490 (2000).

[74] G. Berkovic, G. Meshulam, and Z. J. Kotler, J. Chem. Phys. **112**, 3997 (2000).

[75] K. Tripathy, J. Pérez-Moreno, M. G. Kuzyk, B. J. Coe, K. Clays, and A. M. Kelley, J. Chem. Phys., **125**, 79905 (2006).

Chapter 12

Results: Using the quantum limits on resonance: two-photon absorption

The calculations shown in the previous chapters for the truncated three-level model were relatively "simple" since we considered the off-resonance limits of the diagonal components, where the expressions are relatively compact.

Armed with the tools provided by the analysis of the Thomas-Kuhn sum rules, in this chapter, we tackle the more complex problem of predicting the limits for the resonant two-photon cross-section on a molecule. One of the advantages of using the "Method of Averages" in the calculations for the molecular susceptibilities instead of traditional perturbation theory is that the expressions are explicitly valid for resonant regimes, as long as we assume that there is no creation of significant excited state population.

This work was started in Washington State University and was part of my Master's dissertation.[1] The work was carried over to University of Leuven were it was corrected and completed. The experimental evidence and some new theoretical calculations were developed to study the consistency of the three-level ansazt. The results were published in the Journal of Chemical Physics.[2] The rest of the chapter is taken directly from this article and although it could be

read as an independent chapter, it serves as an example on how the techniques used to characterize the first hyperpolarizability can be extended to characterize the second hyperpolarizability. Because the calculations were performed before the dipole-free expressions were introduced, we use the traditional expression for the second hyperpolarizability. However, recent calculations (in progress) confirm that the same results are obtained from the dipole-free expression.

12.1 Introduction

Two-photon absorption was first observed by *Kaiser* and *Garret* in 1961,[3] even though the possibility of simultaneous absorption of two quanta had been predicted by *Goeppert-Mayer* in 1931.[4] Two-photon absorption is the fundamental process behind most resonant applications such as three-dimensional photolithography,[5] photodynamic therapy,[6] high-density storage [7] and optical power limiters.[8] All these applications require a large resonant two-photon absorption (TPA) cross-section.

12.2 Theory

The TPA cross-section δ (in units of $cm^4 s$) is related to the imaginary part of the diagonal component of the second hyperpolarizability, γ_I, through:[9]

$$\delta(\omega) = \frac{4\pi^2 \hbar \omega^2}{n^2 c^2} \langle \gamma_I^* \rangle, \tag{12.1}$$

where $\gamma_I = Im(\gamma) \equiv Im(\gamma_{xxxx}(-\omega; \omega, \omega, -\omega))$, n is the refractive index of the bulk material, ω the frequency of the incident light, c the speed of light, and the brackets indicate the average over all-possible orientations of the molecule. For a one-dimensional molecule $\langle \gamma \rangle = \gamma/5$ and for a spherical molecule $\langle \gamma \rangle = \gamma$. The effects of the local fields are included in the dressed hyperpolarizability, γ_I^*.

Two photon absorption is inherently a resonant process because it quantifies the strength of absorption of two photons - each with energy $\hbar\omega$ - from the ground state of energy E_0 to the second excited state with energy E_2, where $E_{20} \equiv E_2 - E_0 = 2\hbar\omega$. Consequently, the exact expression for the diagonal component of the second hyperpolarizability given by the sum-over-states (SOS) expression[10] is often approximated by the explicitly resonant term in the sum,

γ_{res}:

$$\gamma \approx \gamma_{res} \equiv \frac{\mu_{01}^2 \mu_{12}^2}{(E_{10} - \hbar\omega - i\Gamma_{10})^2 (E_{20} - 2\hbar\omega - i\Gamma_{20})}, \tag{12.2}$$

where E_{n0} is the transition energy between the excited state n and the ground state, μ_{nm} is the transition dipole moment between states n and m, and Γ_{n0} is the damping factor (inverse radiative lifetime) between the state n and the ground state. When the approximation $\gamma \approx \gamma_{res}$ is made, the contributions of all the non-explicitly resonant terms to γ are ignored. For such an approximation to be valid, γ_{res} should dominate the response in the domain of interest for TPA processes.

Two different regimes can be distinguished in TPA processes: the single resonance regime and the double resonance regime. In both cases $E_{20} \approx 2\hbar\omega$; but, in the single resonance regime, the photon energy $\hbar\omega$ does not match the transition energy E_{10} (i.e. $|E_{10} - \hbar\omega| \gg \Gamma_{10}$) while in the double resonance regime $E_{10} \approx \hbar\omega$. For γ_{res} to dominate the second hyperpolarizability γ, it is necessary to work in the single-resonance regime to ensure that γ_{res} is the only "resonant" term in the sum-over-states expression.

Studies of the first and second hyperpolarizabilities in the off-resonance regime clearly show that individual terms in the sum-over-states (SOS) expression cannot be independently adjusted since the terms are related to each other through the sum rules.[11, 12] In fact, in the SOS expression for γ there are additional two-photon resonant terms similar to Eq. 12.2 that contribute to γ. Even if certain terms appear to dominate the response, all the contributions must be included since the contribution of just one term might not be representative of the full result - especially if there are cancellations between large terms. Therefore, our calculations of the maximum limit of the TPA cross-section includes all contributions to γ. We also evaluate the relevance of the different terms in the SOS expression with the aim of determining whether or not Eq. 12.2 is in general a good approximation to γ_I; an approximation that is used in determining the TPA cross-section (and μ_{12}) with TPA fluorescence measurements.

The exact sum-over-states expression for $\gamma_{xxxx}(-\omega;\omega,\omega,-\omega)$[10] can be split into two types of contributions as follows:

$$\gamma_{xxxx}(-\omega;\omega,\omega,-\omega) \equiv S_1 + S_2 + S_3 + S_4 + T_1 + T_2 + T_3 + T_4, \tag{12.3}$$

where

$$S_1 = (\hbar)^{-3} I_{123} \sum_{lmn}{}' \frac{\mu_{gl}\bar{\mu}_{lm}\bar{\mu}_{mn}\mu_{ng}}{(\Omega_{lg}-\omega)(\Omega_{mg}-2\omega)(\Omega_{ng}-\omega)}, \tag{12.4}$$

$$S_2 = (\hbar)^{-3} I_{123} \sum_{lmn}{}' \frac{\mu_{gl}\bar{\mu}_{lm}\bar{\mu}_{mn}\mu_{ng}}{(\Omega^*_{lg}-\omega)(\Omega_{mg}-2\omega)(\Omega_{ng}-\omega)}, \tag{12.5}$$

$$S_3 = (\hbar)^{-3} I_{123} \sum_{lmn}{}' \frac{\mu_{gl}\bar{\mu}_{lm}\bar{\mu}_{mn}\mu_{ng}}{(\Omega^*_{lg}+\omega)(\Omega^*_{mg}+2\omega)(\Omega_{ng}+\omega)}, \tag{12.6}$$

$$S_4 = (\hbar)^{-3} I_{123} \sum_{lmn}{}' \frac{\mu_{gl}\bar{\mu}_{lm}\bar{\mu}_{mn}\mu_{ng}}{(\Omega^*_{lg}+\omega)(\Omega^*_{mg}+2\omega)(\Omega^*_{ng}+\omega)}, \tag{12.7}$$

$$T_1 = -(\hbar)^{-3} I_{123} \sum_{mn}{}' \frac{\mu_{gm}\mu_{mg}\mu_{gn}\mu_{ng}}{(\Omega_{mg}-\omega)(\Omega_{mg}+\omega)(\Omega_{ng}-\omega)}, \tag{12.8}$$

$$T_2 = -(\hbar)^{-3} I_{123} \sum_{mn}{}' \frac{\mu_{gm}\mu_{mg}\mu_{gn}\mu_{ng}}{(\Omega_{mg}+\omega)(\Omega^*_{ng}+\omega)(\Omega_{ng}-\omega)}, \tag{12.9}$$

$$T_3 = -(\hbar)^{-3} I_{123} \sum_{mn}{}' \frac{\mu_{gm}\mu_{mg}\mu_{gn}\mu_{ng}}{(\Omega^*_{mg}+\omega)(\Omega^*_{mg}-\omega)(\Omega^*_{ng}+\omega)}, \tag{12.10}$$

$$T_4 = -(\hbar)^{-3} I_{123} \sum_{mn}{}' \frac{\mu_{gm}\mu_{mg}\mu_{gn}\mu_{ng}}{(\Omega^*_{mg}-\omega)(\Omega_{ng}-\omega)(\Omega^*_{ng}+\omega)}. \tag{12.11}$$

where I_{123} denotes the average over all distinct permutations of ω_1, ω_2 and ω_3, where $\omega_1 = \omega$, $\omega_2 = \omega$ and $\omega_3 = -\omega$. The prime in the sum indicates that the sum is over the excited states, Ω_{n0} is a complex quantity defined as:

$$\hbar\Omega_{n0} = E_{n0} - i\Gamma_{n0}, \tag{12.12}$$

and:

$$\bar{\mu}_{lm} = \begin{cases} \mu_{lm} & \text{for } l \neq m \\ \mu_{mm} - \mu_{00} & \text{for } l = m. \end{cases} \tag{12.13}$$

Note that the explicitly two-photon single-resonant terms (when $E_{20} = 2\hbar\omega$) are all contained in S_1 and S_2 (Eqs. 12.4 and 12.5). T_1 and T_2 (Eqs. 12.8 and 12.9) contain terms that will be resonant in the double-resonance regime (when $E_{10} = \hbar\omega$ and $E_{20} = 2\hbar\omega$).

Since we are using the SOS expression to optimize the second hyperpolarizablity, we need to review the assumptions utilized in its derivation.[10] It is assumed that the light emitted by a molecule is electric dipole in nature, so magnetic transitions as well as higher-order electric terms are ignored. In addition, since the SOS expression is derived from perturbation theory, the energy of interaction between the light and the molecule must be small compared with the binding energy. As such, the light can not excite the molecule into a real high-lying state. Finally, we focus on purely electronic

transitions, so vibronics are not considered. However, in Chapter 10 it has been shown that neglect of nuclear motion has only a small effect on the limits of the calculated nonlinear-optical response.

Again, we use the three-level ansatz to obtain relationships between the different parameters that determine γ. Unlike the previous chapters, the present work includes the effects of dispersion, so the widths of each state are included by using an imaginary part of the frequency, as shown in Equations 12.4 through 12.11.

The full set of self-consistent three-level Thomas-Kuhn sum rules yield relationships between transition dipole moments and energy differences as follows:

$$E_{10}\mu_{10}^2 + E_{20}\mu_{20}^2 = \frac{(\hbar e)^2 N}{2m}, \tag{12.14}$$

$$(2E_{20} - E_{10})\mu_{20}\mu_{21} + E_{10}\mu_{10}\Delta\mu_{10} = 0, \tag{12.15}$$

$$-E_{10}\mu_{10}^2 + (E_{20} - E_{10})\mu_{21}^2 = \frac{(\hbar e)^2 N}{2m}, \tag{12.16}$$

$$(2E_{10} - E_{20})\mu_{10}\mu_{21} + E_{20}\mu_{20}\Delta\mu_{20} = 0, \tag{12.17}$$

where $\Delta\mu_{mn} = \mu_{mm} - \mu_{nn}$, e is the charge of an electron, N is the number of electrons in the molecule and m is the mass of an electron.

A direct consequence of the first sum rule given by Eq. 12.14, is that the values of $|\mu_{10}|$ are constrained:[11]

$$\mu_{10}^2 \leq \frac{(\hbar e)^2 N}{2mE_{10}} \equiv |\mu_{10}^{MAX}|^2. \tag{12.18}$$

Therefore, as in the off-resonance analysis, we define the dimensionless quantity, X:

$$X = \frac{|\mu_{10}|}{|\mu_{10}^{MAX}|} \leq 1, \tag{12.19}$$

where $0 \leq X \leq 1$. We also define the dimensionless quantity E as:

$$E = \frac{E_{10}}{E_{20}}, \tag{12.20}$$

with $0 \leq E \leq 1$. We note that this explicitly assumes that $E_{10} \leq E_{20}$ and that E_{20} is the two-photon state. These criteria are obeyed for all of the molecules analyzed in this dissertation. Note that systems such as the longer polyenes have lower-energy two-photon states. As such, a separate calculation in the spirit of the one that follows would need to be developed. While we do not do

such a calculation in this paper since it is not relevant to our studies, interesting results are possible. Secondly, we note that if the first two excited states in an asymmetric molecule become degenerate, then the next excited state will need to be considered and the energy ratio redefined, i.e. $E \rightarrow E_{10}/E_{30}$.

Our objective is to express γ_I in terms of X and E and determine the fundamental limits of the TPA cross-section, $\delta(\omega)$, by finding the values of X and E that maximize δ. It is important to emphasize that the calculation of the fundamental limits makes only one assumption: the forces between the charges are described by a potential energy that depends exclusively on the coordinates of the electrons and the nuclei. The tools that we use to calculate the fundamental limits, the generalized Thomas-Kuhn sum rules, are fundamental identities derived from the Schödinger equation, and are applicable to all electronic excitations, regardless of the particular details of the molecule. However, we use the three-level ansatz to approximate the molecule as a three-level system to model the response using the sum rules.

12.2.1 Contribution of the explicitly resonant two-photon terms

We first evaluate the contributions of the terms $Im(S_1)$ and $Im(S_2)$ to γ_I, since they contain all the two-photon resonant contributions (when $E_{20} = 2\hbar\omega$). Using the three-level-truncated Thomas-Kuhn sum rules, we are able to parameterize $Im(S_1)$ and $Im(S_2)$ in terms of E_{10}, E_{20}, X, Γ_{10}, and Γ_{20}. Since these expressions are constrained by the three-level Thomas-Kuhn sum rules, they are labeled S_i^{TK3}. We assume at all times that the two-photon resonance condition is obeyed, that is $E_{20} = 2\hbar\omega$; and we vary the other parameters.

We find that both $Im(S_1^{TK3})$ and $Im(S_2^{TK3})$ vanish when $X = 0$ and reach their maximum value when $X = 1$. Also, as Γ_{10} and Γ_{20} increase as a fraction of E_{10}, the values of $Im(S_1^{TK3})$ and $Im(S_2^{TK3})$ approach zero. For our calculations we consider only one electron (N=1) and we use typical values of the parameters for organic molecules:

$$X = 0.5, \tag{12.21}$$

$$\Gamma_{10} = \Gamma_{20} = 0.1eV, \tag{12.22}$$

$$\text{and } E_{10} = 2eV. \tag{12.23}$$

Fig. 12.1 shows a plot of $Im(S_1^{TK3})$ and $Im(S_2^{TK3})$ individually as a

function of the energy ratio $E = E_{10}/E_{20}$. Also plotted is the behavior of their sum, $Im(S_1^{TK3}) + Im(S_2^{TK3})$, and $Im(\gamma_{res})$ (Eq. 12.2). Both $Im(S_1^{TK3})$ and $Im(S_2^{TK3})$ are peaked at $E = 1/2$, and fall quickly to zero as $E \to 1$ and $E \to 0$. As we later discuss, this is the general trend for all the terms that contribute to γ_I, resulting in an imaginary third-order susceptibility that peaks around $E = 1/2$. As such, to maximize the TPA cross-section, the two lowest excited state energies of a molecule must be equally spaced to allow for the double-resonance condition ($E_{20} = 2E_{10} = 2\hbar\omega$).[13]

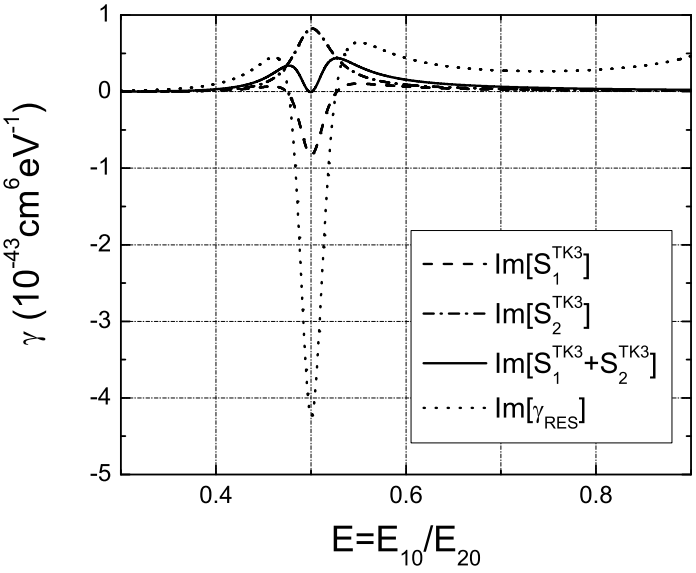

Fig. 12.1: $Im(S_1^{TK3})$, $Im(S_2^{TK3})$, $Im(S_1 + S_2)$ and $Im(\gamma_{res})$ as a function of the energy ratio, E, with $X = 0.5$, $\Gamma_{10} = \Gamma_{20} = 0.1eV$, $E_{10} = 2eV$, and $N = 1$.

While individually $Im(S_1^{TK3})$ and $Im(S_2^{TK3})$ are peaked functions at $E = 1/2$, they have opposite signs, so these two terms partially cancel. More importantly, although $Im(S_1^{TK3} + S_2^{TK3})$ contains the term $Im(\gamma_{res})$, it is obvious from the spectrum predicted by $Im(S_1^{TK3} + S_2^{TK3})$ that it is quantitatively and qualitatively different from $Im(\gamma_{res})$. Furthermore, $Im(\gamma_{res})$ diverges as $E \to 1$, while $Im(S_1^{TK3})$ and $Im(S_2^{TK3})$ approach zero. When all terms are included, the divergences from individual terms in $Im(S_1^{TK3})$ and $Im(S_2^{TK3})$ cancel in the same way as it does in the off-resonance calculations.[11, 12]

12.2.2 Full three-level calculation of γ_I

The analysis of the sum $Im(S_1^{TK3}) + Im(S_2^{TK3})$ shows that to get a substantial TPA cross-section the system must be close to the double-resonant condition (when $E_{20} = 2E_{10} = 2\hbar\omega$). In this regime, contributions of terms such as $Im(T_1^{TK3})$ and $Im(T_2^{TK3})$ can play an essential role, since they explicitly contain one-photon resonant terms ($E_{10} = \hbar\omega$). Therefore, we now study the behavior, individually, of all the terms that contribute to the second hyperpolarizability as constrained by the three-level truncated sum rules, γ_I^{TK3}. We plot each term (defined by Eqs. 12.4-12.11) as a function of E in Figs. 12.2 and 12.3. For simplicity we have used the values defined in Eqs. 12.21, 12.22 and 12.23 since these are the typical values for organic molecules that absorb light in the visible.

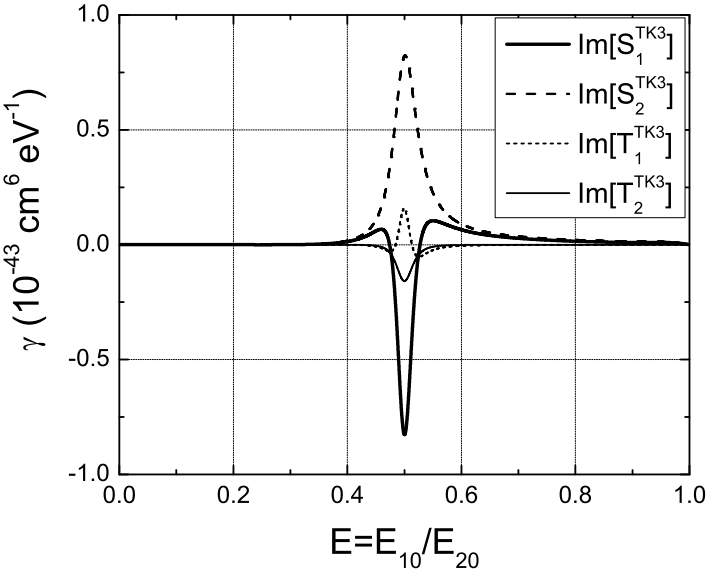

Fig. 12.2: $Im(S_1^{TK3})$, $Im(S_2^{TK3})$, $Im(T_1^{TK3})$ and $Im(T_2^{TK3})$ as a function of the energy ratio, E, with $X = 0.5$, $\Gamma_{10} = \Gamma_{20} = 0.1eV$, $E_{10} = 2eV$, and $N = 1$.

Before proceeding, we must take a small detour to deal with the fact that on double resonance, we must consider the other excited states that may contribute to the SOS expression for γ_I. This is certainly a crucial issue when modelling real molecules, which have many excited states beyond the first three. However, we must also recall that our analysis focuses on understanding the fundamental limits. Thus, our calculations are based on the ansatz that the hyperpolarizability, of any order, will be maximized for any system when all

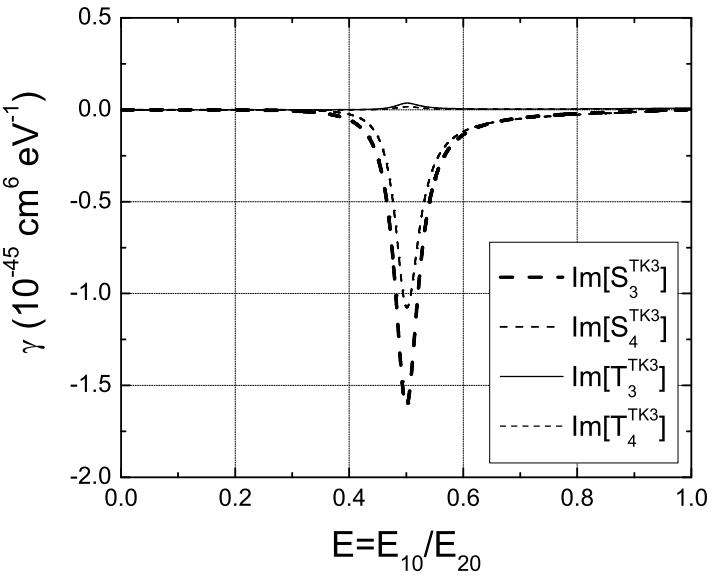

Fig. 12.3: $Im(S_3^{TK3})$, $Im(S_4^{TK3})$, $Im(T_3^{TK3})$ and $Im(T_4^{TK3})$ as a function of the energy ratio, E, with $X = 0.5$, $\Gamma_{10} = \Gamma_{20} = 0.1eV$, $E_{10} = 2eV$, and $N = 1$.

of the transitions are concentrated into three states.[14] As such, when we are dealing with *ideal molecules* that are near the fundamental limit, the problems of higher lying states contributing to γ_I is moot. The next section addresses this issue for the explicitly-resonant term.

While the contributions of $Im(S_3^{TK3})$, $Im(S_4^{TK3})$, $Im(T_3^{TK3})$ and $Im(T_4^{TK3})$ are negligible in comparison with $Im(S_1^{TK3})$ or $Im(S_2^{TK3})$, it is obvious from the plots that the contributions of $Im(T_1^{TK3})$ and $Im(T_2^{TK3})$ are comparable to the contributions of $Im(S_1^{TK3})$ and $Im(S_2^{TK3})$. This is so because T_1^{TK3} and T_2^{TK3} contain one-photon resonant contributions. Since all the terms have different signs around $E \approx 1/2$ it is impossible to estimate the value of γ_I^{TK3} by just looking at one individual term.

Fig. 12.4 shows a three-dimensional plot of γ_I^{TK3} as a function of E and X with $\Gamma_{10} = \Gamma_{20} = 0.1eV$, and $E_{10} = 2eV$. γ_I^{TK3} has been plotted for all possible values of E and X to show that indeed, γ_I^{TK3} is zero when $X = 0$ and reaches its maximum value when $X = 1$. In terms of the energy ratios, the function is sharply peaked around $E \approx 1/2$. γ_I^{TK3} also gets smaller and approaches zero as the values of Γ_{10} and Γ_{20} increase relative to E_{10}. In order

to obtain bigger values of γ_I^{TK3}, the ratio between Γ_{10} (and Γ_{20}) and E_{10} has to be minimized.

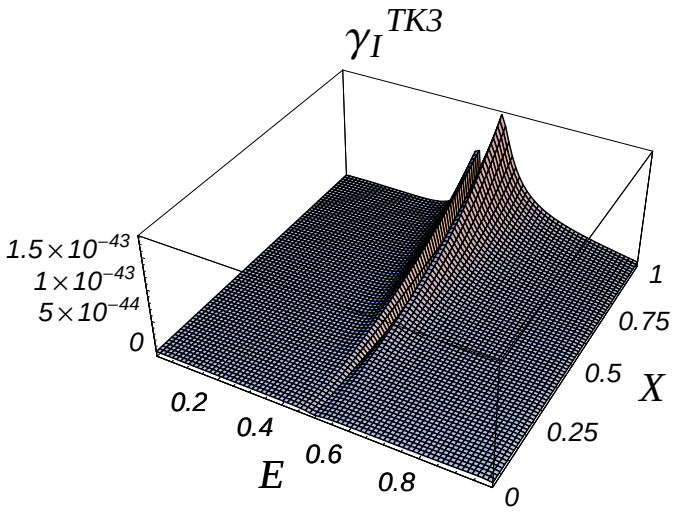

Fig. 12.4: γ_I^{TK3} as a function of E and X, with $\Gamma_{10} = \Gamma_{20} = 0.1eV$, $E_{10} = 2eV$, and $N = 1$.

In order to compare γ_I^{TK3} and $Im(\gamma_{res})$ we plot the two functions together in Fig. 12.5 along with their ratio. γ_I^{TK3} and $Im(\gamma_{res})$ are both calculated as a function of E, with $X = 0.5$, $\Gamma_{10} = \Gamma_{20} = 0.1eV$ and $E_{10} = 2.0eV$ (typical values). The typical range of E for many organic molecules is also shown. From the plot, it is obvious that the approximation that $Im(\gamma_{res})$ dominates γ_I^{TK3} is not a good one for most values of E; and, in the range of typical E, γ_I is smaller than $Im(\gamma_{res})$ by as much as a factor of 3. Clearly, there are big differences between the two at various values of E. For example, while γ_I^{TK3} remains well behaved and goes to zero at $E \to 1$, $Im(\gamma_{res})$ diverges. Furthermore, while $\gamma_I^{TK3} = 0$ at $E = 1/2$, $Im(\gamma_{res}) \approx -4 \times 10^{-43} cm^6 eV^{-1}$. We conclude that γ_I^{TK3} can not be approximated on or near double resonance by $Im(\gamma_{res})$. For the typical values of E that are found in organic molecules, the two are - on average - different by a factor of 3.

In conclusion, for a given value of E_{10}, in order to maximize γ_I^{TK3} we must maximize the value of the transition moment to the first excited state ($X = 1$), minimize the damping factors (i.e. the inverse radiative lifetime) as a fraction of E_{10} and operate near double resonance, where the imaginary part of second hyperpolarizability is a maximum (when $E_{10} \approx E_{20}/2$). The influence of the values of the inverse radiative lifetimes is evaluated in Table 12.1, where we list

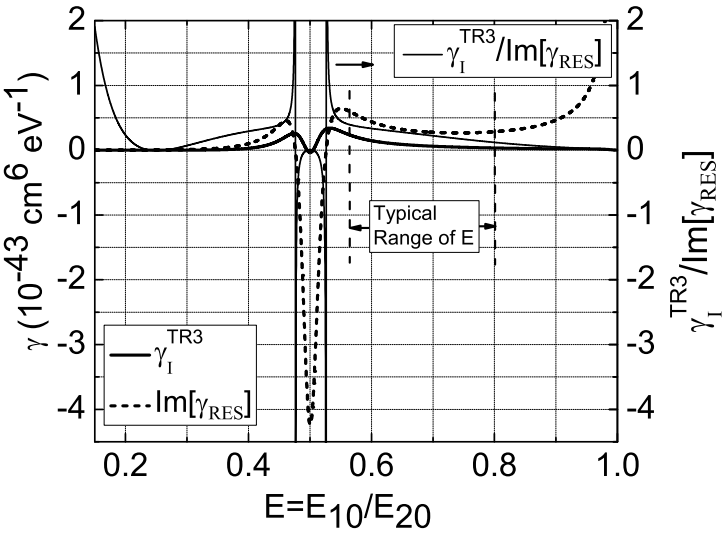

Fig. 12.5: A comparison between γ_I^{TK3} and $Im(\gamma_{res})$ as a function of E, with parameters that are typical for organic molecules: $X = 0.5$, $E_{10} = 2eV$, $\Gamma_{10} = \Gamma_{20} = 0.1eV$, and $N = 1$.

the maximum values of γ_I^{TK3} together with the value of E that maximizes γ_I^{TK3} for different ratios between the inverse radiative lifetimes and E_{10}.

12.3 Maximum value of γ_{res} for molecules with three or more energy levels

As discussed above, it could be argued that the limits obtained using a three-level model do not necessarily hold for real molecules with more than three energy levels. That is, it is in principle possible that when a molecule has more levels, the energy distributions allowed by the sum-rules result in a higher limit than the values of γ_I^{max} listed in table 12.1. This seems unlikely, since, as we will see in the next section, all the measured values of $\delta(\omega)$ are much lower than the maximum limit values allowed by the sum-rules, indicating that real molecules, with more than three available levels, do much more poorly in terms of TPA cross-sections than the idealized three-level model.

We argue that the three-level model gives the best possible value of γ_I^{max}. In other words, as the oscillator strengths are spread out over more excited

$\Gamma_{10} = \Gamma_{20}$ (eV)	γ_I^{max} $(10^{-44} cm^6 \cdot eV^{-1})$	E^{max}
0.02	387	0.49
0.04	51.9	0.51
0.06	15.6	0.52
0.08	6.65	0.53
0.10	3.42	0.53
0.12	1.98	0.54
0.14	1.25	0.55
0.16	0.829	0.56
0.18	0.576	0.57
0.20	0.414	0.58

Table 12.1: Maximum value of γ_I^{TK3} as a function of the inverse radiative lifetime. E^{max} is the value of E that maximizes γ_I^{TK3}. We have used typical values of the parameters for organic chromophores of: $X = 0.5$ and $E_{10} = 2eV$.

levels, the value of γ_I^{max} decreases. Although we were not able to prove this rigorously for the case of $\gamma_I^{TK\infty}$ using all the SOS contributing terms, it can be shown that if the values of E_{10} and E_{20} are known, the explicitly resonant term, γ_{res} is a bounded quantity for **any number of levels** available and that, indeed, the best performance of γ_{res} is achieved when only three states are available.

To prove our assertion that the explicitly resonant term is bounded, we start with the expression for the explicitly resonant term, Eq. 12.2, which, in the TPA regime $E_{20} = 2\hbar\omega$, can be written as:

$$\gamma \approx \gamma_{res} \equiv \frac{\mu_{10}^2 \mu_{12}^2}{(E_{10} - \frac{E_{20}}{2} - i\Gamma_{10})^2(-i\Gamma_{20})}. \tag{12.24}$$

Since we assume that E_{10} and E_{20} have fixed values, we optimize γ_{res} using μ_{10}^2 and μ_{12}^2 as adjustable parameters.

Now we apply the Thomas-Kuhn sum-rules to a general system with N'-

levels. The sum-rules can be written as:

$$\sum_{i}^{N'}(2E_i - E_k - E_l)\mu_{ki}\mu_{il} = \frac{e^2\hbar^2 N}{m}\delta_{kl}, \tag{12.25}$$

where δ_{kl} is the Kronecker delta. We generate a sum-rule equation by choosing one pair of values of (k, l). They can each be any integer between 0 and N'.

First we consider the choice of parameters $(k, l) = (0, 0)$, which yields,

$$E_{10}\mu_{10}^2 + E_{20}\mu_{20}^2 + E_{30}\mu_{30}^2 + \cdots + E_{N'0}\mu_{N'0}^2 = \frac{(\hbar e)^2 N}{2m}. \tag{12.26}$$

Since all the terms on the left side of the sum are positive, it is obvious that μ_{10}^2 and μ_{20}^2 will be maximized when:

$$E_{30}\mu_{30}^2 + E_{40}\mu_{40}^2 + \cdots + E_{N'}\mu_{N'0}^2 = 0, \tag{12.27}$$

that is, when only states 0, 1 and 2 are present.

Now we consider the combination $(k, l) = (1, 1)$, which generates the following sum-rule:

$$-E_{10}\mu_{10}^2 + E_{21}\mu_{10}^2 + E_{31}\mu_{31}^2 + \cdots + E_{N'1}\mu_{N'1}^2 = \frac{(\hbar e)^2 N}{2m}, \tag{12.28}$$

which can be rewritten as:

$$E_{21}\mu_{21}^2 + E_{31}\mu_{31}^2 + \cdots + E_{N'1}\mu_{N'1}^2 = \left(\frac{(\hbar e)^2 N}{2m} + E_{10}\mu_{10}^2\right). \tag{12.29}$$

All the terms on the left side sum on Eq. 12.29 are positive which implies that μ_{21}^2 will be maximum when:

$$E_{31}\mu_{31}^2 + \cdots + E_{N'1}\mu_{N'1}^2 = 0, \tag{12.30}$$

which again would imply that only the states 0, 1 and 2 contribute. Therefore, if more states contribute and the result is an enhancement of the response, it would necessarily be due to the contribution of terms exclusive of the γ_{res} term since we have proven that γ_{res} gets smaller as the number of levels increases.

To summarize, we have found that the non-explicitly-non-resonant terms can not be neglected in a strict three-level system, and that if adding more states results in an increase of the TPA response, it will be due to the contribution of

the non-explicitly-resonant terms in the SOS expression.

12.4 Applications

In this section we apply the theoretical results to evaluate the literature values of the measured TPA performance of organic molecules. We do so by comparing the measured value of the TPA cross-section of a real molecule with the maximum value of the TPA cross-section allowed by the sum-rules. The effective number of electrons contributing to a third-order response is calculated by geometrically weighting the number of electrons in each conjugated path of the molecule,[9]

$$N_{eff} = \sqrt{\sum_i N_i^2}, \tag{12.31}$$

where N_i is the number of electrons in the i^{th} conjugated part of the molecule. We note that our method for counting electrons is most appropriate for excitations that are typical in conjugated molecules. For other systems or other types of excitations, an appropriate method for identifying the correlated electrons would need to be used.

The molecules under analysis are listed in Figures 12.6, 12.7, and 12.8, together with the effective number of electrons, N_{eff}.

The TPA cross-section values of molecules **23** to **34** have been reported by Rumi and coworkers;[15] the values for molecules **35** to **41** have been reported by Albota and coworkers;[16] and the values for molecules **42** to **45** have been reported by Drobizhev and coworkers.[17] The value of E_{10} for each molecule is calculated from the wavelength of maximum linear absorption. The values of the inverse radiative lifetimes are estimated to be: $\Gamma_{10} \approx \Gamma_{20} \approx 0.1eV$.

We note that Frank-Condon considerations suggest that a more appropriate estimate for the energy of an excited state is the energy at the onset of absorption rather than the energy at the absorption peak. For a typical excited state energy of $2\,eV$ and width $100\,meV$, the onset is about $50\,meV$ from the peak, leading to a fractional error of 2.5 %. For functions that vary as the fifth power of the energy, this contributes an error of less than 15 % – the low end for the experimental uncertainty of the more accurate nonlinear-optical measurements. So, in using the peak values to obtain the energies, our calculations have an uncertainty of about 15 %; and, the positions of the energy levels can be off by

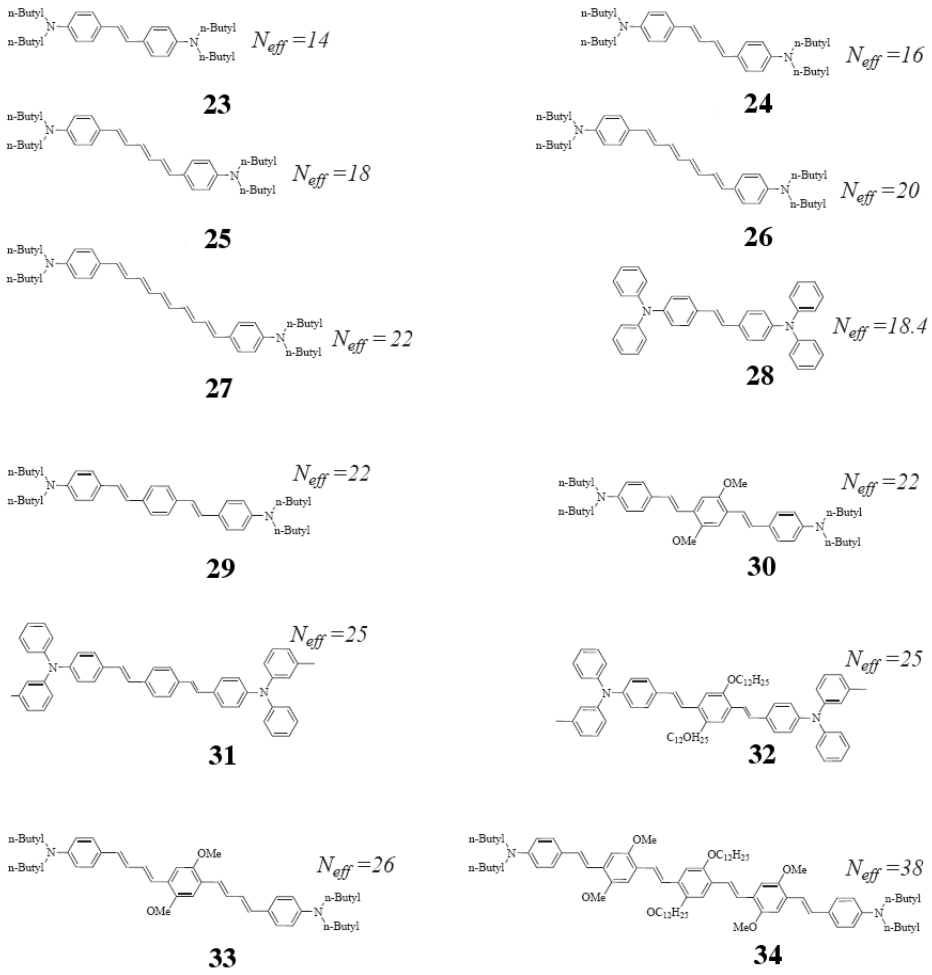

Fig. 12.6: Molecular structures for the two-photon absorption measurements reported by Rumi and coworkers.[15]

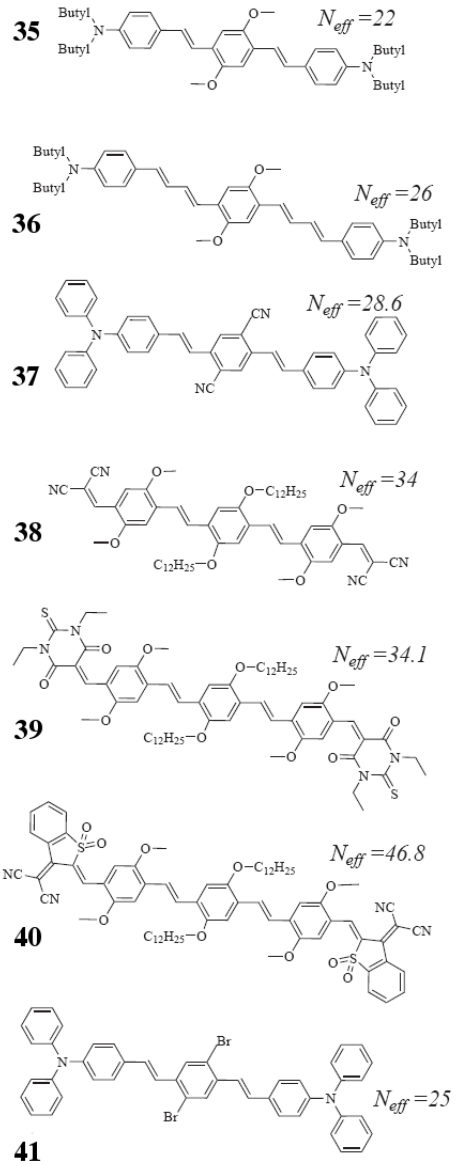

Fig. 12.7: Molecular structures for the two-photon absorption measurements reported by Albota and coworkers.[16]

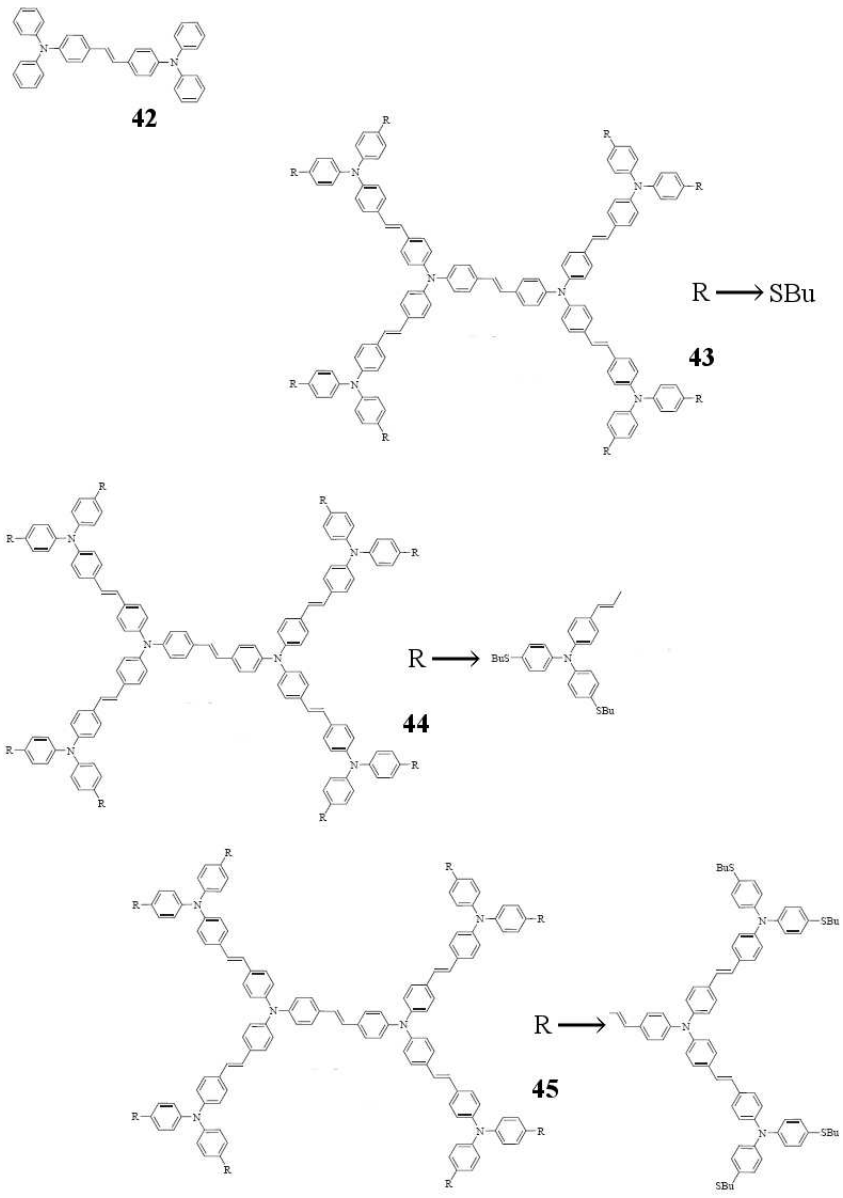

Fig. 12.8: Molecular structures for the two-photon absorption measurements reported by Dhrovizhev and coworkers. The effective number of electrons are $N_{eff} = 18.4$ for molecule **42**, $N_{eff} = 35.6$ for molecule **43**, $N_{eff} = 55.8$ for molecule **44** and $N_{eff} = 82.7$ for molecule **45**.[17]

about $50\,meV$.

12.4.1 Influence of the number of electrons

A simple consequence of the Thomas-Kuhn sum-rules is that the two-photon cross-section of a molecule depends quadratically on the effective number of electrons. With the aid of the sum-rules one can rewrite $\gamma_I^{TK\infty}$ as:

$$\gamma_I^{TK\infty} = \left(\frac{\hbar e}{\sqrt{2m}}\right)^2 \frac{N_{eff}^2}{E_{10}^5}\Phi, \tag{12.32}$$

where Φ is a dimensionless function that depends on the energy ratios, the transition dipole moment ratios and the inverse radiative lifetimes but *does not depend on* N_{eff}. This is a general result that applies to molecules with any number of levels. Eq. 12.32 together with Eq. 12.1 predict a quadratic dependence on the effective number of electrons for the TPA cross-section:

$$\delta(\omega) \propto \frac{E_{20}^2}{E_{10}^5} N_{eff}^2 \Phi. \tag{12.33}$$

Fig. 12.9 shows a plot of the TPA cross-sections of the different molecules as a function of N_{eff}^2. The data follow an approximately linear relationship, indicating that even though the performance of a molecule is dictated by many factors, it correlates with the square of the effective electrons. Note that while this scaling appears to be approximately universal for the molecules studied, it may not hold in other classes of molecules.

12.4.2 Predicting the limiting values for real molecules

Using a three-level model, from the experimental values of N_{eff}, E_{10}, Γ_{10} and Γ_{20}, we can find the maximum value of γ_I^{TK3} allowed by the sum rules, as follows. From the theoretical section, the fundamental limit of γ_I^{TK3} occurs when $X = 1$, so the problem is reduced to finding the optimal value of E_{20} that is consistent with the sum-rules. We will denote this optimal value as E_{20}^{max}.

The value of E_{20}^{max} is substituted into Eq. 12.1 to obtain the maximum value of $\delta(\omega)$, which we will denote δ_{3L}^{max}. Since in the resonant TPA regime,

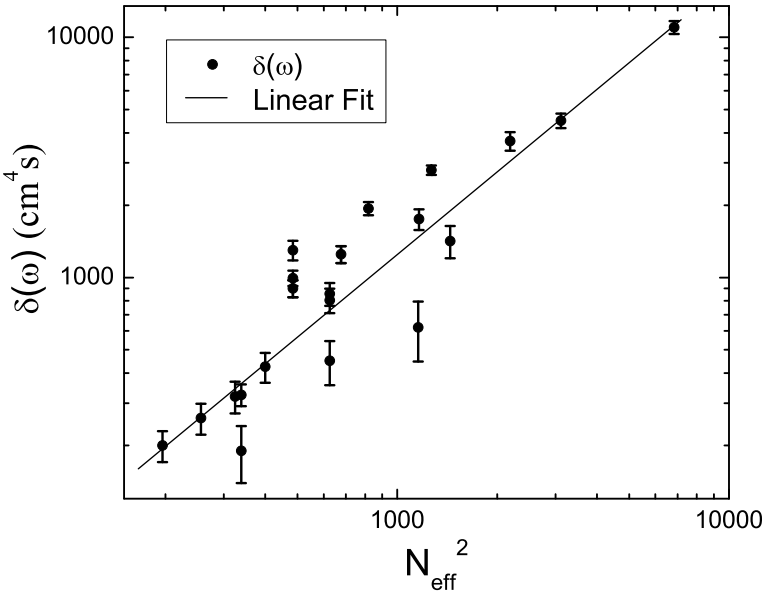

Fig. 12.9: $\delta(\omega)$ as a function of N_{eff}^2 for the collection of measured molecules. The data fits to a line with correlation coefficient of 0.90394.

$E_{20} = 2\hbar\omega$, δ_{3L}^{max} can be written as:

$$\delta_{3L}^{max} = \frac{\pi (E_{20}^{max})^2}{\hbar n^2 c^2} \langle \gamma_I^{max*} \rangle, \tag{12.34}$$

where $\langle \gamma_I^{max*} \rangle$ is the orientational average of the fundamental limit of the dressed second hyperpolarizability. In this manner, the maximum values of the TPA cross-section are calculated for the different molecules. Since most of the molecules are geometrically one-dimensional (aside from the dendrimers), an isotropic orientational average yields $\langle \gamma_I \rangle = \gamma_I/5$. The local fields are calculated using the Lorentz-Lorenz[18] model with $n = 1.4$. Fig. 12.10 shows the two photon performance (the ratio between the experimental value of $\delta(\omega)$ and δ_{3L}^{max}).

All the measured TPA cross-sections fall below the predicted limits by an average factor of $\approx 1.5 \times 10^{-3}$. This shows that real molecules are far below the maximum limit that is allowed by quantum mechanics. Perhaps, as in the case of γ_I, the low performance ratio is due to the existence of many states beyond the dominant three-levels, which results in a dilution of the oscillator strengths.

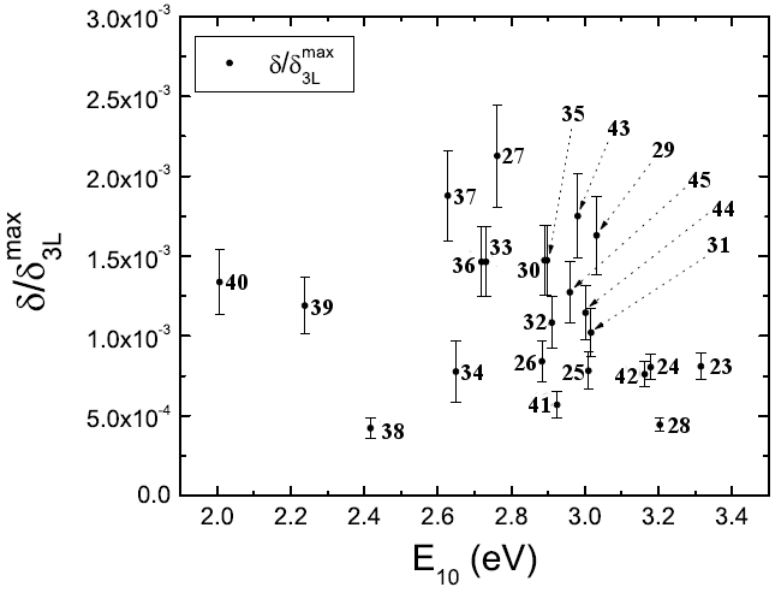

Fig. 12.10: TPA performance as a function of E_{10} for the collection of molecules studied here. The performance is evaluated by calculating the ratio between the experimental value of $\delta(\omega)$ and δ_{3L}^{max} (maximum value allowed by quantum mechanics in a three-level system).

The molecule with highest experimental TPA cross-section is **45** with $\delta(\omega) = (11000 \pm 1100) cm^4 s$ - a similar performance to the rest of the molecules, even though its experimental value of $\delta(\omega)$ is 2 orders of magnitude higher than any other molecule in the collection. This indicates molecule **45** owes its high TPA cross-section mostly to the huge number of electrons contributing to the nonlinear response, rather than to a better design strategy that increases the effectiveness of those electrons. In fact, in the collection of molecules reported by Drobizhev and coworkers, the best performance is achieved by molecule **43**. Molecule **45** would need to have a $\delta(\omega)$ value of approximately 1.4 times bigger than its experimentally-determined value in order to be as efficient as molecule **43**.

The best performance is achieved by molecule **27**. This is a somewhat odd result, because molecule **27** belongs to the group of homologues **23-27** and the performance of all the other homologues is much worse. Rumi and coworkers report that the experimental uncertainty on molecule **27** is bigger than for the rest of their reported molecules, which could explain the discrepancy. The rest of homologues **23-26** behave as expected: the values of $\delta(\omega)$ increase as the number of electrons is increased, but the TPA performance is the same within experimental uncertainty and low in comparison to the other molecules.

This may be better understood if both excited state energies are considered. First, the longer the homologue, the smaller the value of E_{10} (red shifting), which increases the molecular performance due to the $1/E_{10}^5$ dependence. However, for molecules **23** to **26**, there is also a red shifting of E_{20} in such a manner that E increases with the length of the homologue. The values of E for molecules (**23**, **24**, **25**, and **26**) are respectively (0.80, 0.82, 0.86, and 0.86). This increase of E results in a lower performance. However, although E_{10} is red shifted for molecule **27** in comparison with the homologues, E_{20} stays the same as for molecule **26**, resulting in a better-optimized energy ratio ($E = 0.81$). Therefore, for molecules **23** to **26**, the red shifting of E_{10} is accompanied by the red shifting of E_{20}, and the performance doesn't change appreciably. In contrast, for molecule **29**, the increase in $1/E_{10}^5$ is not counterbalanced by an increase in E, so the performance of the molecule is increased.

Molecule **33** which extends the conjugated path of molecule **30** shows the same performance factor as its homologue and molecule **36** which extends the conjugated path of molecule **35** shows a performance factor that is the same as its homologue, within experimental uncertainty.

Molecules **30** and **35** have the same performance factor and also approximately the same value of E_{10}. Since they differ structurally only by the type of radicals attached to the central ring, we conclude that the effects of both types of radicals are similar in both the TPA performance and the wavelength of maximum absorption. Similarly, molecules **33** and **36** have the same performance and similar values of E_{10}. Again, they only differ structurally by the type of radicals attached to the central ring; so we conclude that the effects of both types of radicals are similar.

Molecules **31**, **32**, **37** and **41** share a similar design strategy and differ by the type of groups attached to the central rings. This difference has an influence on the TPA performance. The best approach appears to be the attachment of CN radicals, which makes molecule **37** the second best molecule in the whole collection.

12.4.3 Comparison with other models

In the previous section, δ_{3L}^{max} was calculated by finding the optimal value of $E = E_{10}/E_{20}$ and taking the limit $X \to 1$. This requires "tuning" both the values of E_{20} and $|\mu_{10}|$ for the given molecule. A more realistic approach is to take the actual experimental values of E_{10} and E_{20}, calculate E, substitute these values into $\delta(\omega)$ and calculate the maximum value possible for those energy values in the limit $X \to 1$. We will denote the maximum value calculated in this way as $\delta(E)^{max}$.

Thus, for every molecule, we first compute E as the ratio between the experimental values of E_{10} and E_{20} and then we calculate the maximum TPA cross-section allowed for that energy ratio, $\delta(E)^{max}$. This can be compared with the maximum TPA cross-section possible for the same value of E_{10} (with an optimized value of E), δ_{3L}^{max}. Figure 12.11 plots the ratios of the experimentally-determined values normalized to each calculated limiting value, $\delta(\omega)/\delta_{3L}^{max}$ and $\delta(\omega)/\delta(E)^{max}$, as a function of E_{10} for each molecule.

From Fig. 12.11 it is clear that the energy ratio, E, is far from optimized for all the molecules studied. If it were possible to independently "tune" the value of E_{20} and the value of X, the TPA cross-sections could be improved by three orders of magnitude. However, if the experimental value of E_{20} stays fixed, the possible improvement for typical molecules such as the ones studies here (by tuning X) is only an order of magnitude.

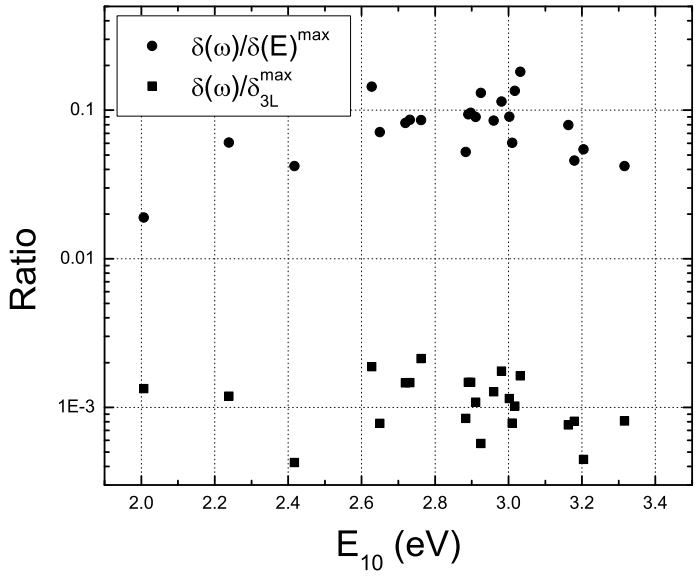

Fig. 12.11: The ratio between the experimental value of $\delta(\omega)$ and $\delta(E)^{max}$ (maximum TPA cross-section allowed for the measured molecular energy ratios). This is compared with the ratio between $\delta(\omega)$ and δ_{3L}^{max} (maximum TPA cross-section allowed for that value of E_{10}).

To determine the relevance of the non-explicitly-resonant terms, the maximum TPA cross-section allowed for a particular value of E for a molecule, $\delta(E)^{max}$, can be compared with the maximum value that would be possible if the response were determined only by the explicitly resonant contribution, γ_{res} (Eq. 12.2). We will denote this maximum value δ_{res}.

We can also calculate the maximum values predicted by Kuzyk's approximation technique of extrapolating from the off-resonance results.[9] This off-resonance extrapolation technique (ORET) assumes that γ_I^{TK3} is dominated by γ_{res}, and predicts the following:

$$\begin{aligned} \delta_{ORET}^{res} &= 63.5\left\{\frac{1}{n^2}\left(\frac{n^2+2}{3}\right)^4\right\} \\ &\times \left[\frac{\left(E_{10}-\frac{E_{20}}{2}\right)^2-\Gamma_{10}^2}{\left(\left(E_{10}-\frac{E_{20}}{2}\right)^2+\Gamma_{10}^2\right)^2}\right]\left(\frac{E_{20}}{\Gamma_{20}}\right)\left(\frac{N_{eff}^2}{E_{10}^3}\right). \end{aligned} \tag{12.35}$$

In the off-resonance case, when $\Gamma_{n0} \ll E_{10} - E_{20}/2$, Eq. 12.35 can be approximated by:

$$\begin{aligned} \delta_{ORET} &= 63.5\left\{\frac{1}{n^2}\left(\frac{n^2+2}{3}\right)^4\right\} \\ &\times \left[\frac{1}{E_{10}-\frac{E_{20}}{2}}\right]\left(\frac{E_{20}}{\Gamma_{20}}\right)\left(\frac{N_{eff}^2}{E_{10}^3}\right). \end{aligned} \tag{12.36}$$

Fig. 12.12 plots the ratio between the measured TPA cross-section, $\delta(\omega)$, and the various calculated limits: $\delta(\omega)/\delta_{res}$, $\delta(\omega)/\delta_{ORET}$, and $\delta(\omega)/\delta(E)^{max}$, and $\delta(\omega)/\delta_{ORET}^{res}$, which shows that both δ_{ORET} and δ_{res} are about an order of magnitude higher than $\delta(E)^{max}$. (Recall that $\delta(E)^{max}$ is the fundamental limit of TPA absorption using all terms in the three-level model for a fixed E that is determined from experiment.) The ORET extrapolation using the resonant expression (Eq. 12.35) appears to be of the same order of magnitude as the exact calculation while the off-resonant approximation (Eq. 12.36) deviates by about an order of magnitude. Table 12.2 shows a comparison of the ORET extrapolation and the exact results. On average, variations between the ORET extrapolation and the exact results are just over 30% – the variation being the price of ignoring the non-explicitly resonant contributions to γ_I^{TK3}.

Next, we consider extrapolating the off-resonance ORET term, given by Eq. 12.36. So, while the δ_{ORET} values are consistently larger than $\delta(E)^{max}$ for

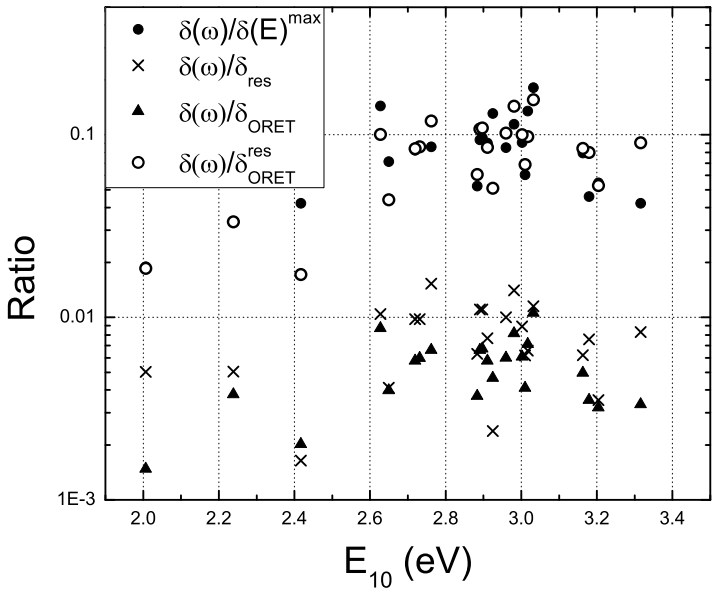

Fig. 12.12: The ratio between the experimental value of $\delta(\omega)$ and $\delta(E)^{max}$, δ_{res}, δ_{ORET} and δ^{res}_{ORET}.

Molecule	$\delta(E)^{max}$ (GM)	δ_{ORET} (GM)	% Diff.
23	4745	2213	53
24	5664	3250	43
25	5291	4663	12
26	8110	7001	14
27	15124	10936	28
28	3482	3598	3
29	5480	6395	17
30	9574	8358	13
31	5960	8232	38
32	9474	10019	6
33	14515	14523	0.06
34	19931	32272	62
35	9338	8247	12
36	15212	14894	2
37	13456	19322	44
38	14695	36080	146
39	28897	52513	82
40	195446	199497	2
41	3432	8835	157
42	4090	3862	6
43	24460	19519	20
44	49604	44996	9
45	129198	107574	39

Table 12.2: The values of $\delta(E)^{max}$ compared with the results of Eq. 12.35 for the set of molecules studied here, and the percentage difference between the exact result and the the resonant ORET formula (Eq. 12.35).

each molecule, they are approximately related logarithmically by:

$$\ln(\delta(E)^{max}) = \lambda \ln(\delta_{ORET}), \tag{12.37}$$

or

$$\delta(E)^{max} = (\delta_{ORET})^{\lambda}, \tag{12.38}$$

where $\lambda \approx 0.773$.

To illustrate the validity of Eq. 12.38, we list the values of $\delta(E)^{max}$ and $(\delta_{ORET})^{0.773}$ for the different molecules in Table 12.3. Within $\pm 20\%$, Eq. 12.38 is a good approximation for most of the molecules. The case of molecule **41**, which has the largest variance, will be discussed later in terms of the consistency of the three-model. Thus, in our collection of 23 molecules there are only 4 outside the $\pm 20\%$ range. As such, Eq. 12.38 is a good approximation of the limit, which includes the effects of the contributions of the non-explicitly-resonant terms to γ_I^{TK3}. This approximation is simpler to use and is more accurate than the resonant expression, so provides the researcher with a simple expression to evaluate molecules.

12.4.4 Consistency of the three-level model

In the previous section, $\delta(E)^{max}$ was calculated by substituting the experimental values of E_{10} and E_{20} into $\delta(\omega)$ and taking the limit $X \to 1$. Alternatively, with the experimental values of E_{10}, E_{20} and $\delta(\omega)$ we can find the value of X that, using the three-level model, would yield the same experimental value $\delta(\omega)$.

So, for a given molecule, we can calculate X^{3L}, the ratio of $|\mu_{10}|/|\mu_{10}^{max}|$ that is derived from the sum-rule-restricted sum-over-states three-level model and the experimental data. Three different scenarios might result:

1. The value of X^{3L} is physically impossible (i.e. an imaginary quantity, $X^{3L} > 1$, etc). In this case we can conclude that the three-level model does not describe the molecule.
2. The value of X^{3L} is physically allowed but inconsistent with the typical values of X for organic molecules. For instance, the three-level model could predict $X^{3L} = 10^{-4}$ which is possible but highly unlikely for real molecules. In this case we would also conclude that the three-level model is not likely to accurately approximate the molecule's TPA cross-section.

Molecule	$\delta(E)^{max}$ (GM)	$\delta_{ORET}^{0.773}$ (GM)	% Diff.
23	4745	4932	4
24	5664	5802	2
25	5291	6054	14
26	8110	8142	0.4
27	15124	12337	18
28	3482	4899	41
29	5480	7002	28
30	9574	9302	3
31	5960	8050	35
32	9474	9927	5
33	14515	12958	11
34	19931	19601	2
35	9338	9171	2
36	15212	13308	13
37	13456	13621	1
38	14695	17432	19
39	28897	23953	17
40	195446	88272	55
41	3432	7155	108
42	4090	5283	29
43	24460	19015	22
44	49604	34445	31
45	129198	69466	46

Table 12.3: The values of $\delta(E)^{max}$ and $(\delta_{ORET})^{0.773}$ (Eq. 12.38) for the set of molecules studied here, and the percentage difference between the exact result and the approximation (Eq. 12.38).

3. The value of X^{3L} is consistent with physically-allowed values of X in a range that is typical for organic molecules. In this case, although we can not conclude definitively that the three-level model accurately describes the molecule, the reasonableness of the result suggests that it may be suitable as a model for real molecules.

Table 12.4 lists the values of X^{3L} for the collection of molecules reviewed here. The predicted values are all consistent with what is normally observed for typical molecules, except for molecules **38** and **41**, which yield complex values of X. Note that these two molecules show the largest discrepancies in Table 12.2. Clearly, for these two molecules, the three level model does not do a good job of modelling the TPA cross-section. Interestingly, these two molecules have the smallest TPA performance ratio (together with molecule **28**), a result that is consistent with our assertion that molecules with more contributing excited states are less efficient per electron. The rest, however, can consistently be described by our simplified three-level model.

12.5 Conclusions

We have applied the sum rules to the SOS expression to calculate the fundamental limits of the dispersion of the two-photon absorption cross-section. These results apply at all wavelengths, so can be used both on and off resonance. Our new rigorous analysis shows that the three-level model and truncated sum rules together give a reasonable fundamental limit and is a good approximation when modelling most molecules. This conclusion partly follows from an analysis that applies the sum rules to the resonant terms with an infinite number of states, and shows that the resonant term is at its maximum in the three-level limit. This result is significant because it suggests that our ansatz that the three-level model accurately describes molecules whose nonlinear susceptibilities approach the fundamental limit is reasonable.

We have shown that the non-explicitly-resonant terms, which are often ignored, can not be neglected in real molecules even near resonance since these terms have a profound effect on resonant dispersion. As such, experiments measuring TPA cross-sections that are analyzed near resonance using only the resonant terms may yield unreliable conclusions.

We find that the simple process of extrapolating the fundamental limit of the off-resonant two-photon absorption cross-section to resonance using only

Molecule	Energy Ratio E	X^{3L}
23	0.80214	0.26118
24	0.82051	0.2633
25	0.86165	0.26714
26	0.84884	0.25194
27	0.81292	0.36609
28	0.89147	0.17847
29	0.89242	0.47829
30	0.85082	0.36386
31	0.90633	0.36377
32	0.87441	0.32751
33	0.85352	0.33781
34	0.89744	0.13118
35	0.8528	0.36753
36	0.84978	0.33168
37	0.88453	0.4101
38	0.91618	
39	0.87545	0.12717
40	0.76456	0.15067
41	0.9434	
42	0.8801	0.30138
43	0.84736	0.40954
44	0.86441	0.34658
45	0.85084	0.34567

Table 12.4: The values of E and X^{3L} for typical TPA molecules studied here. E is calculated from the experimental values of E_{10} and E_{20}. X^{3L} is calculated by using it as a floating parameter when fitting the TPA cross-section data to the three-level model as restricted by the sum-rules.

the resonant term of the three-level model yields a result that correlates well with our exactly rigorous results. A logarithmic relationship is proposed that can be used to convert the off-resonance extrapolation result to the exact one to within an accuracy of about ±20%. This relationship is much easier to apply than the full rigorous result and should be useful to researchers who are interested in assessing the TPA performance ratio of a molecule.

The TPA cross-sections of existing molecules are found to be far from the fundamental limit; so, there is room for improvement. To reach the fundamental limit would require precise control of the energy-level spacing, independently of the transition dipole moments – a task that does not appear possible using today's synthetic approaches. To make the task within reach, we present an analysis of how a molecule can be maximized for a given energy ratio, so, researchers only need to focus on adjusting the oscillator strength to the first excited state. While this approach will not result in molecules with TPA cross-sections at the fundamental limit, it can yield a factor of ten improvements in the largest TPA cross-sections measured.

Clearly it is best to normalize TPA measurements to the fundamental limits when comparing molecules; but, we have shown that simply dividing by the square of the number of electrons per molecule yields a good metric for comparison. Such a simple performance metric is most attractive for cases where the transition moments and energy levels of a molecule are unknown, which is often the case.

Bibliography

[1] J. Pérez-Moreno, "Quantum limits of the nonlinear optical response", *M.S. Thesis* , Washington State University, Department of Physics. August 2004.

[2] J. Pérez-Moreno and M. G. Kuzyk, J. Chem. Phys. **123**, 194101 (2005).

[3] W. Kaiser and C. G. B. Garrett, Phys. Rev. Lett. **7**, 229 (1961).

[4] M. Goeppert-Mayer, Ann. Physik **9**, 273 (1931).

[5] B. H. Cumpstom, S. P. Ananthavel and S. Barlow *et al.*, Nature (London) **398**, 51 (1999).

[6] J. D. Bhawalkar, N. D. Kumar, C. F. Zhao and P. N. Prasad, J. Clin. Laser Med. Sur. **15**, 201 (1997).

[7] D. A. Partenopoulos, P. M. Rentzepis, Science **245**, 843 (1989).

[8] G. S. He, G. C. Xu, P. N. Prasad, B. A. Reinhardt, J. C. Bhatt, and A. G. Dillard, Opt. Lett. **20**, 435 (1995).

[9] M. G. Kuzyk, J. Chem. Phys. **119**, 8327 (2003).

[10] B. J. Orr and J. F. Ward, Mol. Phys. **20**, 513 (1971).

[11] M. G. Kuzyk, Opt. Lett. **25**, 1183 (2000); M. G. Kuzyk, Opt. Lett. **28**, 135 (2003).

[12] M. G. Kuzyk, Phys. Rev. Lett. **85**, 1218 (2000); M. G. Kuzyk, Phys. Rev. Lett. **90**, 039902 (2003).

[13] M. G. Kuzyk, J. Nonlin. Opt. Phys. Mat. **13**, 461 (2004).

[14] Champagne and Kirtman, Phys. Rev. Lett. **95**, 109401 (2005); M. G. Kuzyk, Phys. Rev. Lett. **95**, 109402 (2005).

[15] M. Rumi, J. E. Ehrlich, A. A. Heikal, J. W. Perry, S. Barlow, Z. Hu, D. McCord-Maughon, T. C. Parker, H. Röckel, S. Thayumanavan, S. R. Marder, D. Beljonne and J. L. Brédas, J. Am. Chem. Soc. **122**, 9500 (2000).

[16] M. Albota, D. Beljonne, J. L. Bredas, J. E. Ehrlich, J. Y. Fu, A. A. Heikal, S. E. Hess, T. Kogej, M. D. Levin, S. R. Marder, D. McCord-Maughon, J. W. Perry, H. Röckel, M. Rumi, G. Subramaniam, W. W. Webb, X. L. Wu and C. Xu, Science **281**, 1653 (1998).

[17] M. Drobizhev, A. Karotki, A. Rebane, and C. W. Spangler, Opt. Lett. **26**, 1081 (2001).

[18] J. D. Jackson, *Classical Electrodynamics*, 3rd Edition, John Wiley & Sons Canada, Ltd, (1998).

Chapter 13

Conclusions

In this dissertation we have developed a set of tools and analysis techniques to analyze the nonlinear molecular response that produces reliable results (which do not conflict with semiempirical theoretical calculations or molecular modelling results). These set of techniques can also be used as a guide towards the optimal design of molecules that interact strongly in the nonlinear regime.

We have also developed "rules of thumb" that can be easily used by experimentalist to interpret experimental data. In fact, the quantum limits analysis has helped us to get a better interpretation of the experimental results in each of the study cases presented in this work.

The existence of the quantum limits allows us to describe quantitatively the nonlinear performance of real molecules. Given a set of N delocalized electrons, the quantum limit tell us what would be the value of the first hyperpolarizability for the best "ideal" molecule that is allowed by the generalized Thomas-Kuhn sum rules. When we compare the first hyperpolarizability of a real molecule with the best "ideal" one, we are quantifying the nonlinear performance of real molecules.

The quantum limits are calculated using the "three level ansatz". The "three-level ansatz" is supported by the experimental evidence, at least for all the systems and molecules considered in this dissertation. This is very fortunate, since it allows to obtain simple expressions for the quantum limits. Finding the conditions under which the "three level ansatz" is valid is one of

our priorities, but so far, a justification for the "three level ansatz" that relies only in general principles has not been found.

However, it is important to notice that even if the "three level ansatz" is violated, most of our general conclusions will still hold. For example, the scaling of the molecular polarizabilities as a function of the number of delocalized electrons and the wavelength of maximum absorption are level-independent results.

We have also used the quantum limit analysis to understand the mechanism behind nonlinear response enhancement and to propose different strategies that could improve the performance of nonlinear molecules, even in the presence of resonances.

In conclusion, we have shown how the study of nonlinear optical effects, both at the experimental and at theoretical level, gains clarity if we use quantum limits analysis. We have also developed some of the techniques that will help us towards the goal of setting up a global framework that classifies the elements behind the nonlinear optical response in the most intuitive possible way.

Chapter 14

Perspectives

In this dissertation we have set the first steps towards setting up a global framework that combines experimental and theoretical techniques and helps us to characterize the underlying principles behind nonlinear optical enhancement of molecules. In order to extend our analysis to more general situations we must review some of our assumptions and investigate new scenarios.

The validity of the "three level ansatz" from the theoretical perspective has to be established. Finding out the general conditions under which the "three level ansatz" holds would allow us to determine the range of application of some of the "rules of thumbs" we have presented. Also, if under some circumstances the "three level ansatz" is violated, we would like to determine how does it affect the calculations of the quantum limits.

The dipole-free expression for the diagonal component of the first hyperpolarizability was used by M. G. Kuzyk to calculate the quantum limits of the first hyperpolarizability in the on-resonance regime.[1] In Chapter 7 we have introduced the dipole-free expression for the diagonal component of the second hyperpolarizability, so our next step will be to calculate the quantum limits of the second hyperpolarizability also in the on-resonance regime. The current calculations show promising good agreement with the particular results that were described in Chapter 12. Also, in the same manner as B. Champagne and B. Kirtman did in the case of the first hyperpolarizability,[2] we should study how the traditional sum-over-states expression and the dipole free expression change when the infinite sums are truncated for the second hyperpolarizability.

In the study presented in this dissertation, we have used the Lorentz-Lorenz local field model (Eq. 5.23) A better modelling of the local field could eliminate possible systematic errors in the characterization of the first hyperpolarizability (which are of typically 20% in the nonlinear response).[3]

A better understanding of the interaction between guest and host in the amylose inclusions is needed in order to asses the underlying nature of the nonlinear enhance. We must investigate if the amylose participates passively in the nonlinear process (i.e. it dos not participate in the response but forces the chromophore to adopt optimal configuration) or plays a more active role ("donating" some delocalized electrons, for example).

Some of the approximations used in the calculations of vibrational effects (Chapter 10) could be reviewed or relaxed. More elaborate treatments show that vibrational contributions could contribute up to 18% of the electronic contribution.[4]

Finally, we could investigate if the same techniques and all the body of knowledge that we have gained in the study of molecular susceptibilities can be used to characterize the behavior of other quantities that can also be expressed as a sum-over-states.

Bibliography

[1] M. G. Kuzyk, J. Chem. Phys. **125**, 154108 (2006).

[2] B. Champagne and B. Kirtman, J. Chem. Phys. **125**, 24101 (2006).

[3] D. M. Bishop and B. Kirtman, J. Chem. Phys. **95**, 2646 (1991).

[4] D. M. Bishop and S. P. A. Sauer, J. Chem. Phys. **107** 8502 (1997).

Chapter 15

Epilogue: Modulated conjugation as a means for attaining a record high intrinsic hyperpolarizability

By the time the first draft of this dissertation was getting ready to be sent to the members of the jury, the results of our most recent work were published in an issue of Optics Letters. [1] For completeness, we include a copy of this new result as an epilogue.

15.1 Modulated conjugation as a means for attaining a record high intrinsic hyperpolarizability

Over the last 3 decades, many novel molecules have been designed and synthesized to improve the nonlinear response for a variety of applications. Quantum calculations using sum rules have been used to place an upper-bound on the molecular susceptibilities; [2, 3, 4, 5] but, the largest nonlinear susceptibilities of the best molecules fall short of the fundamental limit by a factor of $10^{3/2}$.[5, 6]

Molecule	λ_{MAX} (nm)	N	β_0 $10^{-30}\,(esu)$	$\frac{\beta_0}{\beta_{MAX}}$
1	551	18	110	0.0208
2	540	20	110	0.0190
3	602	18	240	0.0332
4	567	26	340	0.0334
5	695	18	280	0.0234
6	691	24	735	0.0408
7	677	24	800	0.0477

Table 15.1: Molecular Properties. Uncertainty in hyperpolarizability measurements is about 10%.

A thorough analysis shows that there is no reason why the molecular hyperpolarizability can not exceed this apparent limit.[7] In this letter, we report on a novel set of molecules where the one with modulated conjugation[8] is found to have a hyperpolarizability that breaches the apparent limit of all previously-measured molecules.

Past work has shown that the polarizability is largest when the potential energy function oscillates in a way that localizes the eigenfunctions on different parts of the molecule.[8] This type of oscillation can be designed into a bridge that separates the donor and acceptor ends of a chromophore by varying the degree of conjugation. Our approach is based on the well-known difference in aromatic stabilization energy between benzene and heterpentacyclics, such as thiophene rings.[9]

Figure 15.1 shows the series of molecules under study. The synthesis and the details of the linear and nonlinear optical characterization of this series of compounds will be published elsewhere.[10]

The hyperpolarizability, β, was determined at $800\,nm$ using Hyper-Rayleigh scattering. The zero-frequency hyperpolarizability, β_0 was determined using the two-level model. Table 15.1 shows the measured molecular properties and Figure 15.2 shows a plot of β_0, normalized to the fundamental limit of the hyperpolarizability (this ratio is called the intrinsic hyperpolarizability, which is scale-invariant), where the fundamental limit, β_{MAX}, is given by

$$\beta_{MAX} = \sqrt[4]{3}\left(\frac{e\hbar}{\sqrt{m}}\right)^3 \cdot \frac{N^{3/2}}{E_{10}^{7/2}}, \tag{15.1}$$

where N is the number of electrons (N is determined by counting methods

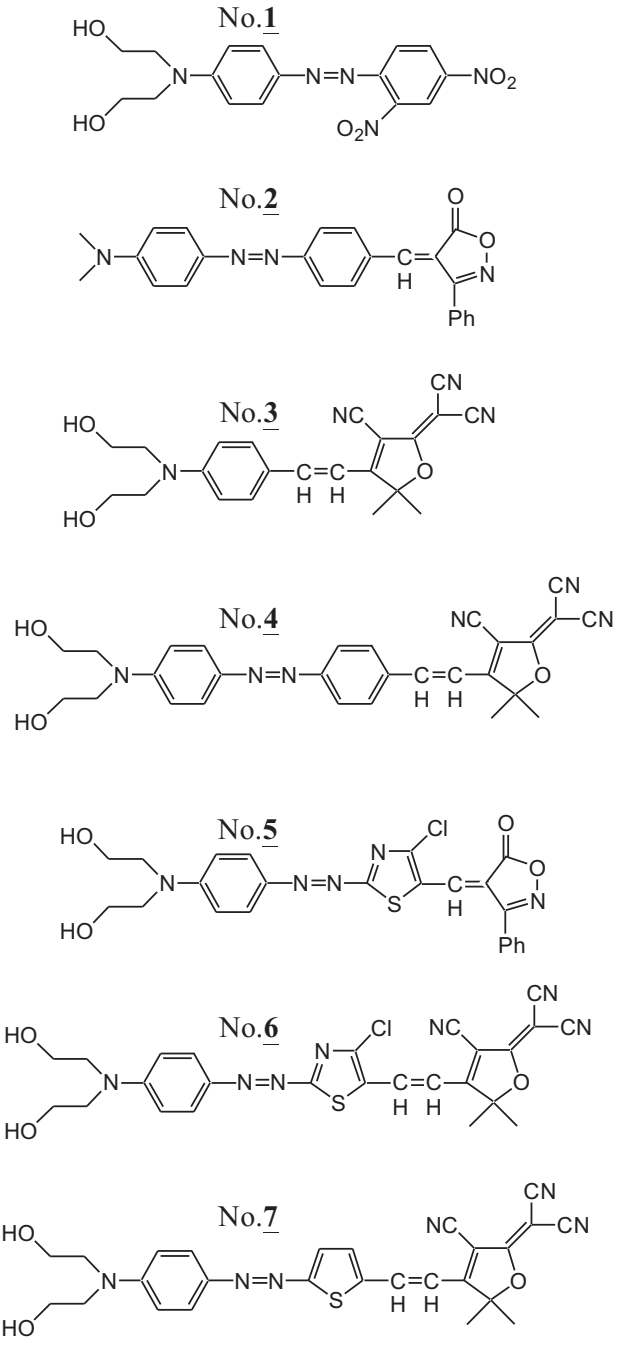

Fig. 15.1: Molecular structure of the chromophores considered in this study.

described in the literature[11, 12]), E_{10} the energy difference between state 1 and 0, e is the electron charge, $\hbar$ Planck's constant and m the mass of the electron. The horizontal line in Figure 15.2 represents the apparent limit defined by the

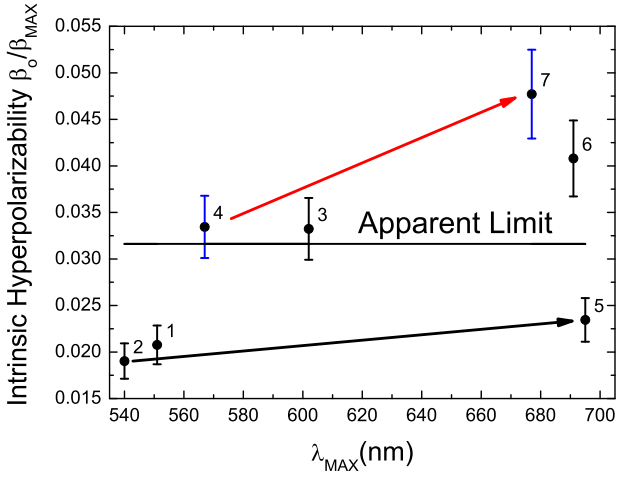

Fig. 15.2: Zero-frequency hyperpolarizability normalized to the fundamental limit, as a function of wavelength of maximum absorption.

best past measurements, which is a factor of $10^{3/2}$ below the fundamental limit.

No single molecule has ever been reported to breach the apparent limit, though some have come close. For example, May and coworkers have shown the the second hyperpolarizability gets within a factor of 2 of the apparent limit.[13] Wang and coworkers, on the other hand, have reported breaking through the apparent limit.[14] However, a close analysis shows that their chromophores, being part of a cross-linked system, were strongly interacting – leading to an under-counting of the number of electrons. So, we believe our reported values to be the first example of single chromophores that breach the limit with record intrinsic hyperpolarizability.

Our molecular design focuses on modulating the amount of aromatic stabilization energy along the conjugated bridge between the donor and the acceptor. To induce the desired modulation, aromatic moieties with a different degree of aromaticity make up the asymmetrically substituted π-bridge. As an example, molecules 4 and 7 are both azo dyes, but while molecule 4 has 2 benzene moieties with identical (36 kcal/mol, or 1.57 eV) aromatic stabilization energy, molecule 7 has a benzene and a thiophene moiety. The latter is well known to have a reduced aromatic stabilization energy (29 kcal/mol, or 1.25 eV). This results in a significant variation of the degree of aromaticity for molecule 7, or in a modulation of the conjugation between the donor and acceptor. This degree of

conjugation modulation yields an enhancement in the hyperpolarizability that breaches the apparent limit well outside the range of experimental uncertainty of 10%. Note that a demodulation technique is used to eliminate the background contribution from two-photon fluorescence,[15, 16, 17] insuring that the measured values are not overestimated due to this known source of systematic error.

Molecule 6 is isoelectronic to molecule 7, but due to the additional Cl atom in molecule 6, steric hindrance induces a twist in the conjugation path, resulting in a decreased hyperpolarizability. Molecules 2 and 5 are homologues of 4 and 7; and show a similar enhancement. However, the larger and more geometrically linear molecules show a more dramatic effect, which is predicted by the theory (steric hindrance caused by the chlorine atom suppresses the enhancement of molecule 5.).[8] In particular, the best molecules are ones that are long with many undulations in the potential energy function, which allows for the electron densities of the eigenstates to be well separated. So, future design strategies should focus on longer molecules with stronger modulation of conjugation.

In addition to increased length, future efforts must also focus on keeping the chain linear. Special attention should be devoted to mimic the optimal undulation[8] by making use of not only benzene and thiophene, but also of other aromatic moieties that exhibit an even wider range of stabilization energies (like pyrrole and furan with aromatic stabilization energy values of 22 and 16 kcal/mol, or 0.98 and 0.69 eV, respectively).

While our best measured values of the hyperpolarizability are still more than an order of magnitude from the fundamental limit, our design strategy appears to be a promising new paradigm for making better molecules.

Bibliography

[1] J. Pérez-Moreno, Y. Zhao, K. Clays and M. G. Kuzyk, Opt. Lett. **32**, 59 (2007).

[2] M. G. Kuzyk, Opt. Lett. **25**, 1183 (2000).

[3] M. G. Kuzyk, Phys. Rev. Lett. **85**, 1218 (2000).

[4] M. G. Kuzyk, Opt. Lett. **28**, 135 (2003).

[5] M. G. Kuzyk, Phys. Rev. Lett. **90** 039902 (2003).

[6] M. G. Kuzyk, Optics & Photonics News **14**, 26 (2003).

[7] K. Tripathi, J. Pérez-Moreno, M. G. Kuzyk, B. J. Coe, K. Clays, and A. M. Kelley, J. Chem. Phys. **121** 7932 (2004).

[8] J. Zhou, M. G. Kuzyk, and D. S. Watkins, Opt. Lett. **31** 2891 (2006).

[9] L. T. Cheng, W. Tam, S. R. Marder, A. E. Stiegman, G. Rikken, and C. W. Spangler, J. Phys. Chem. **95** 10643 (1991).

[10] Y. Shen, L. Qiu, J. Hao, Y. Zhao, J. Pérez-Moreno, M. G. Kuzyk and K. Clays, manuscript in preparation.

[11] M. G. Kuzyk, J. Chem. Phys. **119**, 8327 (2003).

[12] J. Pérez-Moreno and M. G. Kuzyk, J. Chem. Phys. **121**, 194101 (2003).

[13] J. C. May, J. H. Lim, I. Biaggio, N. N. P. Moonen, T. Michinobu, and F. Diederich, Opt. Lett. **30**, 3057 (2005).

[14] Q. Y. Chen, L. Kuang, Z. Y. Wang, and E. H. Sargent, Nano. Lett. **4**, 1673 (2004).

[15] K. Clays and A. Persoons, Phys. Rev. Lett. **66**, 2980 (1991).

[16] K. Clays and A. Persoons, Rev. Sci. Instrum. **63**, 3285-3289 (1992).

[17] G. Olbrechts, R. Strobbe, K. Clays, and A. Persoons, Rev. Sci. Instrum. **69**, 2233-2241 (1998).

Chapter 16

Conclusions

In this dissertation we have developed a set of tools and analysis techniques to analyze the nonlinear molecular response that produces reliable results (which do not conflict with semiempirical theoretical calculations or molecular modelling results). These set of techniques can also be used as a guide towards the optimal design of molecules that interact strongly in the nonlinear regime.

We have also developed "rules of thumb" that can be easily used by experimentalist to interpret experimental data. In fact, the quantum limits analysis has helped us to get a better interpretation of the experimental results in each of the study cases presented in this work.

The existence of the quantum limits allows us to describe quantitatively the nonlinear performance of real molecules. Given a set of N delocalized electrons, the quantum limit tell us what would be the value of the first hyperpolarizability for the best "ideal" molecule that is allowed by the generalized Thomas-Kuhn sum rules. When we compare the first hyperpolarizability of a real molecule with the best "ideal" one, we are quantifying the nonlinear performance of real molecules.

The quantum limits are calculated using the "three level ansatz". The "three-level ansatz" is supported by the experimental evidence, at least for all the systems and molecules considered in this dissertation. This is very fortunate, since it allows to obtain simple expressions for the quantum limits. Finding the conditions under which the "three level ansatz" is valid is one of

our priorities, but so far, a justification for the "three level ansatz" that relies only in general principles has not been found.

However, it is important to notice that even if the "three level ansatz" is violated, most of our general conclusions will still hold. For example, the scaling of the molecular polarizabilities as a function of the number of delocalized electrons and the wavelength of maximum absorption are level-independent results.

We have also used the quantum limit analysis to understand the mechanism behind nonlinear response enhancement and to propose different strategies that could improve the performance of nonlinear molecules, even in the presence of resonances.

In conclusion, we have shown how the study of nonlinear optical effects, both at the experimental and at theoretical level, gains clarity if we use quantum limits analysis. We have also developed some of the techniques that will help us towards the goal of setting up a global framework that classifies the elements behind the nonlinear optical response in the most intuitive possible way.

Appendix A

Time-reversal invariance and the reality of the transition dipole moments

The Thomas-Kuhn sum rules are derived under the assumption that the unperturbed Hamiltonian is conservative (Eq. 6.6):

$$H = \sum_{i}^{N} \frac{(\vec{p}^{\,i})^2}{2m} + V(\vec{r}^{\,1}, \vec{r}^{\,2}, \cdots, \vec{r}^{\,N}). \tag{A.1}$$

This implies that the unperturbed hamiltonian is invariant under the time-reversal operator, Θ, and we can apply the following theorem, as stated by *Sakurai* [1]:

Theorem.

> "Suppose the Hamiltonian is invariant under time reversal and the energy eigenket $|n\rangle$ is nondegenerate; then the corresponding energy eigenfunction are real."

Since:

$$\Theta \vec{r} \Theta^{-1} \quad = \quad \vec{r}, \tag{A.2}$$

(A.3)

and

$$\Theta\vec{p}\Theta^{-1} \quad = \quad -\vec{p}, \tag{A.4}$$

where Θ is the time reversal operator, the unperturbed Hamiltonian, Eq. (A.1), is invariant under the time reversal operator, and if we assume that the system is non degenerate we conclude that the energy eigenfunctions can be chosen to be real. Since the position operator, $r_x \equiv x$, is also real, the transition dipole moments, $x_{nm} = \langle n|x|m\rangle$, must be real.

Bibliography

[1] J. J. Sakurai, *Modern Quantum Mechanics*, Addison-Wesley, 1994.

Appendix B

Evaluating integrals for the clipped harmonic oscillator

In order to calculate transition moments it is necessary to evaluate integrals of the form:

$$\int_0^\infty \psi_n^{CHO}(x)\ x\ \psi_m^{CHO}(x)\ dx. \tag{B.1}$$

Recalling the form of the wavefunctions,

$$\psi_n^{CHO}(x) = \begin{cases} 0 & x < 0 \\ (2^{(n-1)}n!)^{-1/2} \left(\frac{m\omega}{\pi\hbar}\right)^{1/4} \exp(-x^2/2) H_n(x). & x \geq 0, \end{cases} \tag{B.2}$$

we see that the problem reduces to the evaluation of integrals of the form:

$$\int_0^\infty H_n(x)\ x\ H_m(x)\ \exp(-x^2) dx. \tag{B.3}$$

Because of broken symmetry, we can not use the results from the regular harmonic oscillator, but we still can make use of the recursion relations of the Hermite polynomials:

$$H_{n+1}(x) = 2xH_n(x) - 2nH_{n-1}(x) \qquad n \geq 1, \tag{B.4}$$

$$H_n'(x) = 2nH_{n-1}(x) \qquad n \geq 1, \tag{B.5}$$

$$\tag{B.6}$$

and

$$H_n''(x) - 2xH_n'(x) + 2nH_n(x) = 0 \qquad n \geq 0. \tag{B.7}$$

In the following we will not show the explicit dependence of the Hermite polynomials on x.

Using (Eq. B.5) we can transform the integral,

$$\int_0^\infty H_n \; x \; H_m \; e^{-x^2} dx = \frac{1}{2(n+1)} \int_0^\infty H_{n+1}' \; x \; H_m e^{-x^2} dx. \tag{B.8}$$

Now using (Eq. B.7),

$$\begin{aligned} \int_0^\infty H_n \; x \; H_m \; e^{-x^2} dx &= \\ \frac{1}{4(n+1)} \int_0^\infty H_{n+1}'' \; H_m \; e^{-x^2} dx &+ \frac{1}{2} \int_0^\infty H_{n+1} \; H_m \; e^{-x^2} dx. \end{aligned} \tag{B.9}$$

Let us integrate by parts the first integral on the right hand side,

$$\begin{aligned} \int_0^\infty H_{n+1}'' H_m e^{-x^2} dx &= \\ \Big[H_m(x) e^{-x^2} 2(n+1) H_n(x)\Big]_0^\infty &- \int_0^\infty H_{n+1}' 2(mH_{m-1} - xH_m) e^{x^2} dx, \\ . & \end{aligned} \tag{B.10}$$

where we have also used the recursion relationships (Eqs. B.4, B.5 and B.7).

At infinity, the exponential goes to zero fast enough to overcome the infinity of any polynomial, and at zero, the Hermite polynomials can be written in terms of the Gamma function ($H_n(0) = \Gamma(\frac{1-n}{2})$),

$$\begin{aligned} \int_0^\infty H_{n+1}'' H_m e^{-x^2} dx &= -\frac{2^{1+m+n}(1+n)\pi}{\Gamma(\frac{1-m}{2})\Gamma(\frac{1-n}{2})} \\ -2m \int_0^\infty H_{n+1}' H_{m-1} e^{-x^2} dx &+ 2 \int_0^\infty H_{n+1}' x H_m e^{-x^2} dx. \end{aligned} \tag{B.11}$$

Now, using (Eq. B.5),

$$\begin{aligned}\int_0^\infty H''_{n+1} H_m e^{-x^2} dx &= -\frac{2^{1+m+n}(1+n)\pi}{\Gamma(\frac{1-m}{2})\Gamma(\frac{1-n}{2})} \\ -4m(n+1)\int_0^\infty H_n H_{m-1} e^{-x^2} dx &+ 4(n+1)\int_0^\infty H'_n x H_m e^{-x^2} dx \end{aligned} \quad \text{(B.12)}$$

Substituting back onto (Eq. B.9), we find the following useful relation:

$$\begin{aligned}\int_0^\infty H_{n+1} H_m e^{-x^2} dx &= \\ \frac{2^{(m+n)}\pi}{\Gamma(\frac{1-m}{2})\Gamma(\frac{1-n}{2})} &+ 2m\int_0^\infty H_n H_{m-1} e^{-x^2} dx. \end{aligned} \quad \text{(B.13)}$$

The above expression can be written in a more convenient way, by relabeling $(n \to n-1)$,

$$\begin{aligned}\int_0^\infty H_n H_m e^{-x^2} dx &= \\ \frac{2^{(m+n-1)}\pi}{\Gamma(\frac{1-m}{2})\Gamma(\frac{2-n}{2})} &+ 2m\int_0^\infty H_{n-1} H_{m-1} e^{-x^2} dx. \end{aligned} \quad \text{(B.14)}$$

Now we interchange m and n in the above (Eq. B.14) and subtract from the original, we find:

$$\begin{aligned}(2m-2n)\int_0^\infty H_{n-1} H_{m-1} e^{-x^2} dx &= \\ 2^{(m+n-1)}\pi\left\{\frac{1}{\Gamma(\frac{1-n}{2})\Gamma(\frac{2-m}{2})} - \frac{1}{\Gamma(\frac{1-m}{2})\Gamma(\frac{2-n}{2})}\right\}. \end{aligned} \quad \text{(B.15)}$$

In the case when $n \neq m$, by relabeling $(n \to n-1, m \to m-1)$, we find:

$$\int_0^\infty H_n H_m e^{-x^2} dx = \frac{2^{(m+n)}\pi}{(m-n)}\left\{\frac{1}{\Gamma(\frac{-n}{2})\Gamma(\frac{1-m}{2})} - \frac{1}{\Gamma(\frac{-m}{2})\Gamma(\frac{1-n}{2})}\right\}. \quad \text{(B.16)}$$

When n=m we use the normalization condition for the Hermite Polynomials

(dividing by 2, since we integrate for half the domain). That is:

$$\int_0^\infty H_n(x)H_m(x)e^{-x^2}dx = \begin{cases} \sqrt{\pi}2^{(n-1)}n!, & m=n \\ \frac{2^{(m+n)}\pi}{(m-n)}\left(\frac{1}{\Gamma(\frac{-n}{2})\Gamma(\frac{1-m}{2})} - \frac{1}{\Gamma(\frac{-m}{2})\Gamma(\frac{1-n}{2})}\right), & m \neq n. \end{cases} \tag{B.17}$$

The original integral we wanted to evaluate, Eq. (B.4), becomes:

$$\int_0^\infty H_n x H_m e^{-x^2}dx = \frac{1}{2}\int_0^\infty H_{n+1}H_m e^{-x^2}dx + n\int_0^\infty H_{n-1}H_m e^{-x^2}dx. \tag{B.18}$$

We can get a "symmetric" expression in terms of n and m, by using the result from Eq. (B.13):

$$\begin{aligned} \int_0^\infty H_n x H_m e^{-x^2}dx &= \frac{2^{(m+n-1)}\pi}{\Gamma(\frac{1-m}{2})\Gamma(\frac{1-n}{2})} \\ +m\int_0^\infty H_n H_{m-1} e^{-x^2}dx &+ n\int_0^\infty H_{n-1}H_m e^{-x^2}dx. \end{aligned} \tag{B.19}$$

Eq. B.19, together with Eq. B.17 allow us to calculate any transition moment, since:

$$x_{mn} = \sqrt{\frac{\hbar}{\pi m\omega}}g_{mn}, \tag{B.20}$$

with,

$$g_{mn} = (2^{(n-1)}n!)^{-1/2}(2^{(m-1)}m!)^{-1/2}\int_0^\infty H_m(\xi)\xi H_n(\xi)e^{-\xi^2}d\xi. \tag{B.21}$$

Appendix C

List of publications

1. "Why hyperpolarizabilities fall short of the fundamental quantum limits", Kakoli Tripathy, Javier Pérez-Moreno, Mark G. Kuzyk, Benjamin J. Coe, Koen Clays and Anne Myers Kelley. *The Journal of Chemical Physics*, Vol. **121**, Issue 16, pp. 7932-7945 (2004).

2. "Combined molecular and supramolecular bottom-up engineering for enhanced nonlinear response", Javier Pérez-Moreno et al., *Proc. SPIE*, Vol **5935**, pp. 84-95, Linear and Nonlinear Optics of Organic Materials V; Manfred Eich; Ed. August 2005.

3. "Why experimental hyperpolarizabilities fall short of the fundamental limits and new approaches for breaking this barrier" M. G. Kuzyk et al. (secondary author), *Proc. SPIE*, Vol **5935**, pp. 62-66, Linear and Nonlinear Optics of Organic Materials V; Manfred Eich; Ed. August 2005.

4. "Fundamental Limits of the Dispersion of the Two-Photon Absorption Cross-Section", Javier Pérez-Moreno and Mark G. Kuzyk, *The Journal of Chemical Physics* Vol. **123**, pp. 194101-194114 (2005).

5. "Erratum: Why hyperpolarizabilities fall short of the fundamental quantum limit", Kakoli Tripathy, Javier Pérez-Moreno, Mark G. Kuzyk, Benjamin J. Coe, Koen Clays and Anne Myers Kelley. *The Journal of Chemical Physics* Vol. **125**, pp. 79905-79906 (2006).

6. "Characterization techniques of nonlinear optical materials: an introduction to experimental nonlinear optical techniques" (book chapter), Inge Asselberghs, Javier Pérez-Moreno and Koen Clays, (57 pages), *Characterization techniques of nonlinear optical materials: From molecules to condensed phases*, G. Papadopoulos, Andrzej J. Sadlej and J. Leszczynski (Eds). Springer-Verlag New York, LLC (2006).

7. "Synthesis, Crystal Structure, and Second-Order Nonlinear Optical Properties of Ruthenium(II) Complexes with Substituted Bipyridine and Phenylpyridine Ligands" L. Labat et al., *European Journal of Inorganic Chemistry*, Vol. **2006**, Issue 15, pp. 3105 - 3113 (2006).

8. "Modulated conjugation as a means for attaining a record high intrinsic hyperpolarizability", Javier Pérez-Moreno, Yuxia Zhao, Koen Clays, and Mark G. Kuzyk. *Optics Letters*, Vol. **32**, Issue 1, pp. 59-61 (2007).

9. "Combined molecular and supramolecular bottom-up nano-engineering for enhanced nonlinear optical response: Experiments, modeling and approaching the fundamental limit", Javier Pérez-Moreno et al. *The Journal of Chemical Physics* **126**, 074705 (2007).